UNIVERSITY OF SOUTHAMPTON

A Geochemical Study of Hydrothermal Signals in Marine Sediments: The Rainbow Hydrothermal Area, 36°N on the Mid-Atlantic Ridge

Rachel R. Cave

Thesis submitted in partial fulfillment of the requirements for the degree of Doctor of Philosophy

School of Ocean and Earth Science

Faculty of Science

January 2002

UNIVERSITY OF SOUTHAMPTON

ABSTRACT

FACULTY OF SCIENCE, SCHOOL OF OCEAN & EARTH SCIENCE

Doctor of Philosophy

A Geochemical Study of Hydrothermal Signals in Marine Sediments: The Rainbow Hydrothermal Area, 36°N on the Mid-Atlantic Ridge

by

Rachel Rosemary Cave

The geochemistry of a suite of cores accumulating at increasing distance downstream of a major hydrothermal vent site has been characterized for the first time, in order to examine the changing chemistry of particles being deposited from the plume with distance from the vent, to try to establish the different processes operating in the plume, particularly with regard to scavenging of elements from seawater, and to quantify the fluxes from seawater to the sediments as a result of venting, for a wide range of major and trace elements (Mg, Fe, V, Mn, Co, Cu, Zn, REE, PGE, Os isotopes).

Sediment cores were collected at 2-25km downplume of the Rainbow hydrothermal vent site at 36°14'N on the Mid-Atlantic Ridge, a known site of vigorous high-temperature venting. Samples from long-term sediment traps located 0.5-2km from this vent site were also studied. All samples showed similar bulk chemistry, with an overprint of hydrothermally derived material. Sedimentation rates of 40-60mg.m^2.d^{-1} for the cores were established using bulk radiocarbon dating of the carbonate material, and were found to be of the same order as the sediment traps, 11-25mg.m^2.d^{-1}. The maximum age of the core samples ranged from 8-26 x 10^3 radiocarbon years.

For many elements, particularly the PGEs, the element to iron ratios in plume derived material were found to be up to an order of magnitude higher than those found globally in metalliferous sediments of hydrogenous origin. Burial fluxes to the Rainbow sediments have been calculated for hydrothermally derived elements - Mn (16-37μmol.cm^{-2}.kyr^{-1}), Fe (368-718μmol.cm^{-2}.kyr^{-1}), Co (0.3-0.5μmol.cm^{-2}.kyr^{-1}), Cu (3.5-12μmol.cm^{-2}.kyr^{-1}), Zn (0.2-0.6μmol.cm^{-2}.kyr^{-1}), - and elements scavenged from seawater by hydrothermal Fe-oxyhydroxides - P (36-64μmol.cm^{-2}.kyr^{-1}), V (3-5μmol.cm^{-2}.kyr^{-1}), As (0.6-1.4μmol.cm^{-2}.kyr^{-1}), Pd (20-53pmol.cm^{-2}.kyr^{-1}), Os (1.0-2.3pmol.cm^{-2}.kyr^{-1}), Ir (0.2-0.6pmol.cm^{-2}.kyr^{-1}), Pt (6.5 -18.5pmol.cm^{-2}.kyr^{-1}). Magnesium from seawater appears to co-precipitate with Fe in the vent plume at this site, and Mg burial fluxes are calculated to be 73-146μmol.cm^{-2}.kyr^{-1}. Burial fluxes of the hydrothermally derived elements represent only a fraction of the estimated vent output, implying that vent products are dispersed over long distances. Element/Fe ratios for scavenged elements are high compared to other metalliferous sediments, indicating enhanced scavenging efficiency at this site.

Contents

List of Figures

List of Tables

List of Acronyms

ADCP	Acoustic Doppler Current Profiler
AMAR	ALVIN Mid-Atlantic Ridge
BOFS	Biogeochemical Ocean Flux Study
BRIDGE	British Mid-Ocean Ridge Programme
BRIDGET	BRIDGE instrument platform for plume research
EPR	East Pacific Rise
FLAME	Fluxes at AMAR Experiment
ICP-AES	Inductively-coupled Plasma Atomic Emission Spectroscopy
ICP-MS	Inductively-coupled Plasma Mass Spectroscopy
LOI	Loss on ignition
MAP	Madeira Abyssal Plain
MAR	Mid-Atlantic Ridge
MORB	Mid-ocean ridge basalt
NAP	Nares Abyssal Plain
NEADW	North east Atlantic Deep Water
NTD	Non-transform discontinuity
PGE	Platinum-group element(s)
REE	Rare-earth element(s)
SAP	Stand-alone Pump
SML	Surface Mixed Layer
SOC	Southampton Oceanography Centre
TOBI	Towed Ocean Bottom Instrument (sidescan sonar)
XRF	X-ray Fluorescence

Acknowledgements

I would like to thank the following people for all their support over the last few years. Many others are not mentioned here, but should be.

My three wise men:- Chris German who rescued me from geophysics and has almost managed to turn me into a geochemist, and who first took me to sea; John Thomson for keeping my feet firmly on the ground while my head remained (and remains) firmly in the clouds, and both of them for always making time for me when I knocked on their doors; Bob Nesbitt for signing the cheques, and for teaching me rude words in French for those bad hair days. Thanks to Ian Harding and Steve Roberts for being on my advisory panel.

Anthony Moran, love of my life, who warms my toes when they are cold (often), and who has never complained while I spent all our weekends scribbling away at this work. Thank you for teaching me the rudiments of LaTeX, with which I wrote this thesis.

Philippe Blondel, friend (or is that fiend?) who has instigated and shared so many stray thoughts while slaving over our respective hot computers. On les aura!, the battle-cry resounds along the corridors, may its echoes never grow silent.

Elizabeth, Sarah, Vera and Richard Cave, my long-suffering family, who have supported me in so many ways since the day I decided to give up the day job and go to university, all those years ago.

Kirsty Campbell, for great conversation, and much laughter on the doorstep of 'the cottages', and to librarians of her ilk everywhere, without whom we could not pursue our science to anything like such good effect.

Rachel 'Moose' Maddison, who comes like a fairy godmother to take me out to dinner and drag me off for weekends in the mountains as often as I let her. Veit Huehnerbach, phantom housemate and purveyor of fine breadmakers to the nation, for many delicious dinners and desserts, may we have many more together. Jill Schwarz, for music, good things to eat, and fun things to do, through whose tender care I have even been persuaded to like olives.

Bill Jenkins, for setting up the WHOI exchange programme, Greg Ravizza for hosting me at WHOI, for introducing me to osmium, and for lending me his car when I had visitors. Bernhard Peucker-Ehrenbrink, Tracy Abrusezze, Jurek Bluthzain, Larry Ball and Rindy Ostermann at WHOI for all their help during my 4 months there.

Posy Boella, who has taught me almost everything I know of what goes on inside a chemistry lab, Darryl Green and Sharon Nixon for teaching me the rest.

Lindsay Parson, who along with Chris German hired me as a student to work for the BRIDGE group, fostered my interest in all things hydrothermal, and bought me many beers over the years. Germain Bayon, office mate and fellow sufferer, who taught Bob many of the rude words mentioned above. Guy Rothwell and Dave Gunn for helping me to augment my studentship income with work for the British Ocean Sediment Core Repository, Dave again for all those Burns Nights, and Mark Lee for time on Shoreham Beach, watching the shingle roll by and getting paid for it.

Finally I would like to thank the NERC for the studentship that provided my financial support (GT4/97/2661), the SOC for the excellent facilities I was provided with during my thesis work, Ian Croudace, Darryl Green, Andy Milton and Rex Taylor who keep all the equipment running that provided the bulk of my data, Pauline Simpson and all the staff of the National Oceanographic Library, Tim Jickells and Julian Andrews at UEA for their patience during the last few months, the 'Jickell's Group' for all those Tuesday nights and office teas, and all those societies and organisations who foster marine science students, particularly the Society for Underwater Technology, the Challenger Society for Marine Science, the UNESCO Training Through Research cruise programme, and the Mercator (now Socrates) EU student exchange programme.

This thesis is dedicated to all those who, like me, have passed through the Challenger Division and moved on, and who have added so much to my time there. Susana, Veronique, Laurence, Hedy and Todd, Ingo, Tim, Eulalia and Raimon, Emilio and Roberta (honorary members of this club), Philippe, Kate, Barbara, Doris, to mention but a few. To the rest of the Challenger Division, thank you for making me so welcome, and for putting so many opportunities my way during my various incarnations there.

Chapter 1

Introduction

The overall purpose of this work is to examine the pelagic sediments accumulating along a part of the ridge axis of the Mid-Atlantic Ridge influenced by the Rainbow hydrothermal plume, in order to determine the fluxes of a wide range of major and trace elements to these sediments resulting from hydrothermal plume fallout. The fluxes are studied on the temporal and spatial scale, and the findings compared with other metalliferous sediments accumulating along ridge crests and ridge flanks. The principal objectives of the thesis are:

- to establish sedimentation rates for core material collected downplume of the Rainbow hydrothermal vent;

- to analyse sediment core and sediment trap material, collected in the vicinity of the Rainbow hydrothermal vent, for a wide range of elements using readily available techniques;

- to calculate fluxes of plume-derived material (both vented and scavenged) to the sediments downstream of the Rainbow hydrothermal vent site, and to determine whether there is evidence of a geochemical gradient in plume fallout downstream;

- to compare and contrast the geochemistry of material collected above and within the neutrally buoyant plume with sediment core tops;

- to describe the geochemical 'fingerprint' of the Rainbow hydrothermal plume on the surrounding pelagic sediments and to relate it to that of pelagic sediments containing hydrothermal fallout from other vent sources;

- to compare element accumulation rates in hydrothermal sediments with those in hydrogenous sediments.

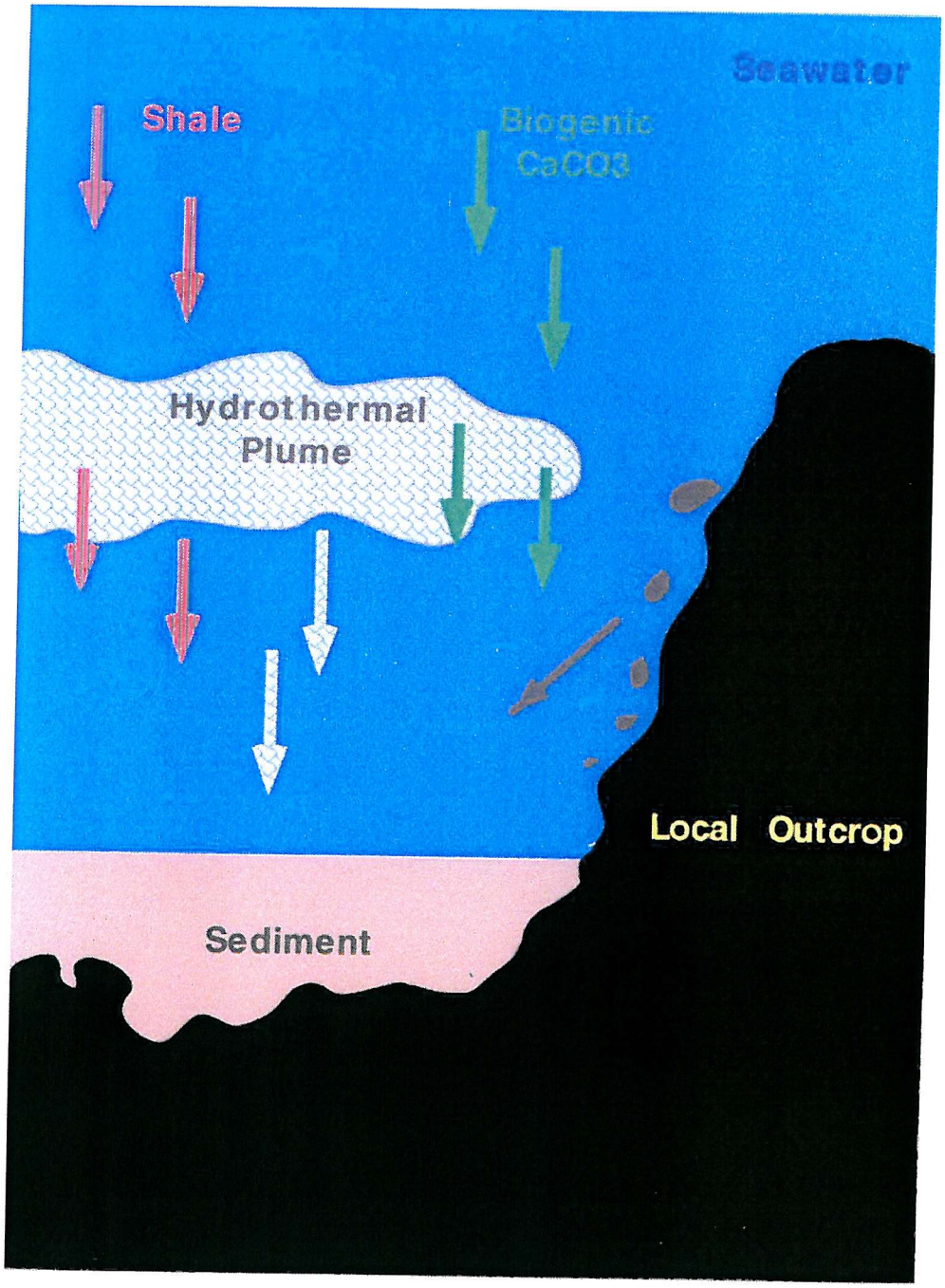

Figure 1.1: Schematic diagram of potential sources of material to the Rainbow sediments accumulating beyond the confines of the vent-field.
Not to scale.

The initial objective of the study was to collect a series of sediment cores downplume of a known hydrothermal vent site. The Rainbow hydrothermal vent site was chosen for the following reasons:

1. it is the most vigorous vent field so far discovered along the Mid-Atlantic Ridge, producing a particle-rich hydrothermal plume;
2. it has a well characterised plume path, and the local hydrography is known;
3. high-resolution sidescan sonar data of the AMAR and S. AMAR segments of the Mid-Atlantic Ridge were available, which was vital for the successful recovery of core material, particularly given the overall paucity of sediment cover in the area surrounding the Rainbow vent site;
4. a cruise was already planned to go to the area to recover long-term moorings, some of the material from which was then made available for this study.

1.1 The nature of the problem

Metalliferous sediments blanket large areas of the deep sea floor along spreading plate boundaries. Mapping of such ridge sediments pre-dated the first discovery of hydrothermal venting in the mid-1970s (e.g. Bostrom and Peterson, 1969, Bostrom et al, 1969), but that discovery of warm springs of metal-rich water diffusing out of the seabed of the Galapagos Rift (Weiss *et al.*, 1977; Corliss *et al.*, 1979), followed by the first sightings of hot particle-rich 'smokers' on the East Pacific Rise (Spiess *et al.*, 1980) seemed to confirm the provenance of the excess metals in the sediments. In the 30 years or so since the first sighting, high-temperature hydrothermal vents, or evidence for their presence, have been found on all active spreading ridges, whether fast or slow-spreading, and at most other oceanic plate boundaries.

Geochemical studies of massive sulfides accumulating as chimneys and mounds in the immediate surroundings of individual vents have been made along the Mid-Atlantic Ridge (Rona *et al.*, 1986; Thompson *et al.*, 1988), along the East Pacific Rise (Edmond *et al.*, 1982) and the Juan da Fuca Ridge, on the heavily sedimented Gorda Ridge (Koski *et al.*, 1994; Zierenberg and Shanks, 1994) and more recently in the Indian Ocean (Kuhn *et al.*, 2000). Comparisons have been drawn between modern vent sites and sites in the geological record such as ophiolites, and commercially mined volcanogenic massive sulfide deposits on land. Biological studies of the often highly adapted fauna living

around vents have been made, with species new to science regularly being found e.g. Juniper and Tebo (1995). The optical and hydrological properties of the vent plumes have been used as an aid to finding vent sites (Feely *et al.*, 1992), and several studies have been made of the chemistry of the vent fluids (von Damm *et al.*, 1985; Campbell *et al.*, 1988; Campbell *et al.*, 1994; Kadko, 1993; James *et al.*, 1995; Bau and Dulski, 1999) and plumes (Trocine and Trefry, 1988; Cowen *et al.*, 1990; German and Sparks, 1993; Feely *et al.*, 1994; Field and Sherrell, 2000). Several major programmes of mid-ocean ridge studies have been run by interested countries, under the umbrella of the co-ordinating body InterRidge.

Pelagic sediments affected by hydrothermal plume fallout, which first gave the clue to the existence of vents, have been largely neglected since the discovery of the vents themselves. Their areal extent is very great, both on the modern seafloor and in the geological record, and they act not only as sinks for material being input to seawater from vent fluid, but also as sinks for material in seawater scavenged by vent plume particles (Dymond, 1981; Dymond and Roth, 1988; Mills and Elderfield, 1995b; Mills and Elderfield, 1995a; German *et al.*, 1997; German *et al.*, 1999). Understanding the nature of these sinks, their relationship to the source vents, and their variability, is therefore important for our understanding of the fluxes of a range of elements into and out of seawater.

Metalliferous sediments also accumulate in other areas of the deep sea, apparently unaffected by venting, and such sediments are described as hydrogenous. The point at which a hydrothermal sediment, say along a ridge flank close to the crest, becomes a hydrogenous one, is unclear, and the different mechanisms and the timescales associated with the accumulation of metals and oxyanions from seawater are not well understood. Hydrothermal plumes can influence the composition of ocean waters hundreds and perhaps thousands of kilometres away from the venting area, as is evidenced by the work on Mn (e.g. Klinkhammer et al., 1985, Klinkhammer and Hudson, 1986, Aballea et al., 1998, Radford-Knoery et al., 1998) and He isotope ratios (e.g. Lupton and Craig, 1981). For metalliferous sediments, it is not known, for instance, how much of a part is played by the substrate, e.g. clay versus carbonate material, in the removal of metals from seawater at the sediment surface, nor what part is played by micro-organisms. What is known is that in the vicinity of hydrothermal vents, some of the mechanisms are very fast - metalliferous crusts will accumulate on instruments in a matter of days. Microbial mechanisms are believed to be involved in the oxidation of manganese in seawater, for example, but iron in hydrothermal plumes is assumed to

oxidise abiotically. The oxidation rate of Fe(II) in seawater increases with pH, oxygen content and temperature, and decreases with increasing salinity (Lilley *et al.*, 1995). The relative abundance of sulfide minerals in the hydrothermal plume largely depends on the metal and H_2S concentration in the vent fluid. If the H_2S is > Fe and other metals in the plume, sulfide mineral phases tend to dominate (Lilley *et al.*, 1995). However, in the case of Rainbow, Fe is an order of magnitude greater in the plume than H_2S (Douville *et al.*, 2002), so much more of the Fe is likely to be entering the oxide phase in this plume than is common at other hydrothermal vent sites.

The problem being addressed here is that while widespread observations of vent output imply a clear link between the metal-rich vent fluids and the accumulation of surrounding metalliferous sediments, direct comparisons of the output from a particular vent with seafloor accumulation of vent-derived products have not until now been made. In the following chapters, sediment samples from cores collected directly beneath the known path of a hydrothermal plume, at increasing distances from the Rainbow vent site, are compared both with each other, and with sediment trap samples taken close to the vent site from within and below the plume. Further comparisons are made between the estimated flux of a range of elements previously measured in the vent fluid by other workers, and the flux of these elements to the seafloor as measured in the sediment traps and cores. Making these comparisons should lead us to a better understanding of how hydrothermal vent activity directly affects both ocean sediments and seawater.

1.2 Metalliferous sediments and global hydrothermal activity

A surprisingly small percentage of the deep sea floor has been mapped other than at very low resolution. Surface sediments have been mapped for their carbonate and clay content over large areas of the Atlantic (e.g. Lisitzin 1996), but little attention has been paid to their metal content. Only along the East Pacific Rise (Bostrom and Fisher, 1969) and on the Nazca Plate (Dymond, 1981) have large scale studies of the areal extent of metalliferous sediments been carried out. Some of the earliest geochemical work on metalliferous sediment distribution was done by Bostrom and co-workers in the 1960s in the Pacific (Bostrom and Fisher, 1969; Bostrom and Peterson, 1969). They proposed a sedimentary concentration index of $Alx10^2/(Al+Fe+Mn)$, where the smaller the index, the more metalliferous the sediment, and used this index to infer the presence of hydrothermal venting of metal-enriched fluids along the ridge crests.

Aluminium content can be used as a measure of the detrital 'shale' component of a sediment, and in general the Fe and Mn content of a sediment depends on the shale component, as the amount of Fe and Mn derived from the detritus of primary production is negligible. The index is therefore almost constant for marine sediments from a given region, but if a local source of Fe and Mn is introduced to the sediment, such as fallout from hydrothermal activity, the index will decrease. Metalliferous sediments were found along several sections of the MAR during the 1970s (Bostrom et al, 1972, Cronan, 1972, Horowitz and Cronan, 1976, Hoffert et al 1978) and 1980s (Rona et al, 1984, Rona et al., 1986, Thompson et al, 1988), both within the rift valley, and on the ridge flanks. A summary of information on Fe and Mn rich sediments throughout the world's oceans can be found in Hannington and Jonasson, (1992).

1.2.1 Hydrothermal activity in the oceans

The first active hydrothermal vents were discovered in the Pacific Ocean, on the Galapagos Rift (Weiss *et al.*, 1977; Corliss *et al.*, 1979), where a series of warm springs diffuse out of the seabed. Following this, observations were made of black smokers on the East Pacific Rise at 21^o (Spiess *et al.*, 1980), and at 13^oN (Hekinian *et al.*, 1983), and on its northerly extension through the Guaymas Basin (Lonsdale *et al.*, 1980). Throughout the 1980's, several vent sites were identified along the Juan de Fuca Ridge in the North Pacific e.g. (USGS, 1986; Baker *et al.*, 1995) and on its eastern flank (e.g. Wheat and Mottl, 2000). In the Indian Ocean, evidence of venting was observed on the Central Indian Ridge (CIR) (Pluger *et al.*, 1990), and metalliferous sediments from the Red Sea indicated a hydrothermal influence (e.g. Cocherie *et al.* 1994). Vents have been found on the Valu Fa Ridge in the Lau Basin (von Stackelberg and Party, 1988) and in the Manus Basin, north-west of Papua New Guinea (Gamo *et al.*, 1993). A listing of the 30 or so vent sites from a range of geological settings discovered during the 1980's can be found in Seyfried and Mottl, (1995). Since then, investigations along the South-West Indian Ridge (German *et al.*, 1998b), the Scotia Ridge (German *et al.*, 2000) and Bransfield Basin in the Southern Ocean (Bohrmann *et al.*, 1999; Klinkhammer *et al.*, 2001), and the Mediterranean Sea (reviewed in Dando *et al.* (1999) have discovered hydrothermal plumes, while recent expeditions to the Gakkel Ridge in the Arctic Ocean (Edmonds *et al.*, 2001) have also yielded evidence of venting. Soon after the first discoveries of venting on the EPR, hydrothermal vents were discovered on the Mid-Atlantic Ridge in the N. Atlantic, and these are detailed in the next section. In short, hydrothermal activity is now known to be rife at all oceanic plate bound-

aries, with more than 100 documented vent sites worldwide. Biological investigations at these sites have yielded hundreds of new species, many of which exist in distinct biogeographical provinces (van Dover *et al.*, 2002), while vent fluids have been shown to transport significant quantities of heat and chemicals out of the seafloor and into the oceans (Elderfield and Schultz, 1996).

1.2.2 Hydrothermal activity along the Mid-Atlantic Ridge in the N. Atlantic

Some of the earliest indications of hydrothermal activity in the N. Atlantic were noted by Bonatti et al, (1975), when dredging carried out by the R/V Pillsburg brought up serpentinites and meta-serpentinites from the lower slopes of the east wall of the MAR at 06^{o}N. These rocks appeared to have been hydrothermally altered before being emplaced at the surface. A cruise carried out between 12^{o}N and 26^{o}N on the MAR in 1984 (NOAA Vents Program), established the presence of several CH_4 and Mn anomalies at depths below 2000m in the water column, at different sites along the crest and rift valley of the MAR (Klinkhammer *et al.*, 1985). A repeat survey carried out in 1985 carried out detailed plume work above the seafloor at TAG (Klinkhammer *et al.*, 1985; Nelsen *et al.*, 1986) and resulted in the first video footage of vents on the MAR (Rona *et al.*, 1986), at TAG, 26^{o}08'N. First indications of hydrothermal activity at TAG had been found in 1972 (Scott et al, 1974), but not until 1985 was actual video taken of actively venting black smokers (Rona *et al.*, 1986; Detrick *et al.*, 1986; Campbell *et al.*, 1988; Seyfried and Mottl, 1995). Following the discovery of TAG, the Ocean Drilling program (ODP) relocated to another of the areas where Mn anomalies had been noted by Klinkhammer *et al.*, (1985) and discovered the Snakepit (or MARK) site (Detrick *et al.*, 1986) at 23^{o}22'N. Further cruises were carried out in 1988 (Ridelente cruise, MAR/88 cruise) (Charlou *et al.*, 1993). The water column chemistry at these sites was compared with that of samples taken above the two now known hydrothermal vent sites in this section of the MAR, which indicated that at least 5 of these anomalies resulted from hydrothermal activity, while others may have resulted from seafloor serpentinisation. Activity was found to be most intense close to the Kane and Fifteen-Twenty fracture zones. A systematic survey between 27^{o}N to 30^{o}N on the MAR in March 1993 dredged hydrothermal sulfides (Murton et al, 1994) and detected the presence of a hydrothermal plume. The Broken Spur hydrothermal vent site at 29^{o}10'N was identified during 2 Alvin dives in June 1993, with at least 3 active vents.

Some exploration between 30°N to 36°N on the ridge was carried out in 1992 on the FAZAR cruises, a joint French American project (Charlou *et al.*, 1993). Hydrothermal plume signals were detected in the South Oceanographer segment around 34°50'N but bad weather and time constraints prevented further work in this area. A plume was also identified at the northern end of the South AMAR segment, around 36°N , and at the southern end of the AMAR segment. This segment of the ridge, between 36°N and 38°N, was extensively surveyed during cruises in 1994, both for geological studies and for water column anomalies. At least seven discrete hydrothermal plumes were identified both within the rift valley segments and at the segment ends (German et al, 1996a). One of these was subsequently found to be coming from the Rainbow hydrothermal vent site at 36°15'N (German et al, 1996b), located on the western side of an ultramafic block at the southern end of the AMAR segment (Fouquet et al, 1997). The sediment-covered Saldanha vent site was discovered in July 1998 in the axial discontinuity between the FAMOUS and AMAR segments. Earlier cruises had identified the Lucky Strike vent site, at 37°18'N (Langmuir et al, 1993) and the Menez Gwen vent site at 37°50'N (Fouquet et al, 1994), but the sources of the intervening plumes remain unidentified to date.

The Azores islands are located to the east of the MAR, scattered along the failed arm of a triple junction, at about 39°N. Some studies of shallow submarine hydrothermal activity observed around some of the islands have been carried out by biologists, (e.g. Nunes et al, 1992), but otherwise this segment of the MAR remains unexplored for hydrothermal activity. North of the Azores, Cronan (1972) reported excesses of Hg, As and Fe, all elements associated with hydrothermal activity, on the eastern flanks of the MAR at 45-46°N. Box cores from this area, and along the MAR crest from 45°N south to the Azores, were studied by Grousset and Donard (1984), who confirmed the strong enrichment in Hg on the flank and some enrichment along the crest between 40°N and 45°N. They also reported Cd and As enrichments in the high-carbonate ridge crest sediments (up to 87ppm As on a carbonate-free basis). No venting has yet been reported from this section of the MAR, but Melkert et al (1992) reported that the Mn/Fe ratios for coatings on pteropod shells indicate that these elements are derived from hydrothermal activity.

In 1993, a cruise was mounted to survey the Reykjanes Ridge for hydrothermal activity between 57°N (the Bight Fracture Zone) and 63°N (German et al, 1994). Despite detailed sampling, of the order of 4-5km intervals in several areas, no anomalies indicative of hydrothermal activity were found until arrival at Steinaholl, at 63°06'N, in

about 350m water depth, just south of Iceland. This site had previously been surveyed in 1990, following an earthquake swarm (Olafsson *et al.*, 1991), and Mn anomalies indicated the presence of hydrothermal venting in the area, though it was not known whether this had been initiated by the earthquakes. The 1993 sampling measured both CH_4 and Mn water column anomalies, but sediment loads in the water column hampered plume identification by light attenuation methods. The apparent lack of venting along the Reykjanes Ridge may be an artefact however. The Reykjanes Ridge is relatively shallow, which is now known to lead to phase separation in hydrothermal fluids, and thus a sampling strategy which takes into account the different chemical content of vented phase-separated fluids may need to be adopted here.

1.3 Summary and thesis outline

Hydrothermal activity is widespread along active ocean ridges. Global estimates of hydrothermal heat and chemical fluxes to the oceans have been made from geophysical data, and from geochemical mass balance data, and a summary of the estimates from a range of methods is given in Elderfield and Schultz (1996) . However, vent sites so far studied represent a very small proportion of the estimated total number, and have been found to span a huge range of fluid temperatures and chemistries. This study is the first to attempt to fully characterise the effects of a particular vent plume on the surrounding seawater and sediments. Some of the results are applicable to all high-temperature vent sites, while others may be applicable only to ultramafic-hosted sites. The range of measurements described here will contribute to a much better understanding of the effects of high-temperature venting on the chemistry of the oceans and ocean sediments.

The sample collection for the study was very successful, recovering a suite of four sediment box cores at increasing distance from the vent site, under the path of the plume, as well as recovering long-term sediment trap samples. Sample collection and analytical methods are described in Chapter 2. The first objective, to establish sedimentation rates, was achieved by radiocarbon dating, and the results are presented in Chapter 3 (see Cave *et al.*, 2002) together with analyses of the core samples for major and trace elements, carried out by XRF. Chapter 4 gives the results of major, trace and rare-earth element analyses for the sediment trap samples, carried out using ICP-MS and ICP-AES techniques, and compares the results with surficial samples from the cores, analysed using the same methods. Core samples were further analysed for platinum-group elements, including osmium isotopes, and these results are described

in Chapter 5. Each of these three data chapters includes an overview of the literature pertaining to the studies being carried out. The conclusions of the thesis are outlined in Chapter 6, together with a discussion on future work needed in this area to address unanswered questions. Full data sets are given in the Appendices.

Chapter 2

Methods

2.1 Sample Collection

2.1.1 Cruise Objectives

The purpose of cruise RV Poseidon 240 (FLAME II) to the Rainbow area of the MAR (36°14'N, Fig. 2.1) in June/July 1998 was fourfold - to recover a number of long-term current meters deployed on the Fluxes at AMAR Experiment (FLAME) cruise to the area in 1997; to recover 3 sediment trap moorings deployed at varying distances from the vent site for biological studies; to occupy a number of CTD/nephelometer stations to both confirm the continuing propagation of the plume in this area, and to better constrain the local physical oceanography; to acquire a series of boxcores from sedimented areas around the Rainbow site for geochemical studies of sedimentation beneath the neutrally buoyant plume. Samples from the cores and the sediment traps have been used in this study.

2.1.2 Box coring

The box coring sites were planned so that sediment would be recovered from beneath the path of the spreading, non-buoyant hydrothermal plume at varying distances from the Rainbow hydrothermal vent site. An approximate trajectory of the plume had been previously determined from a combination of water column transmissometer and nephelometer anomalies measured during CTD casts and BRIDGET tows, together with lowered ADCP data for the area (German *et al.*, 1998). CTD stations carried out at the beginning of the cruise confirmed the continuing presence of the plume and its trajectory. The plume appears to achieve neutral buoyancy at between 2000 and 2200m water depth, and follows the ~2300m contour around the northern end of the Rainbow Ridge, then south and east still following this contour into the bottom of

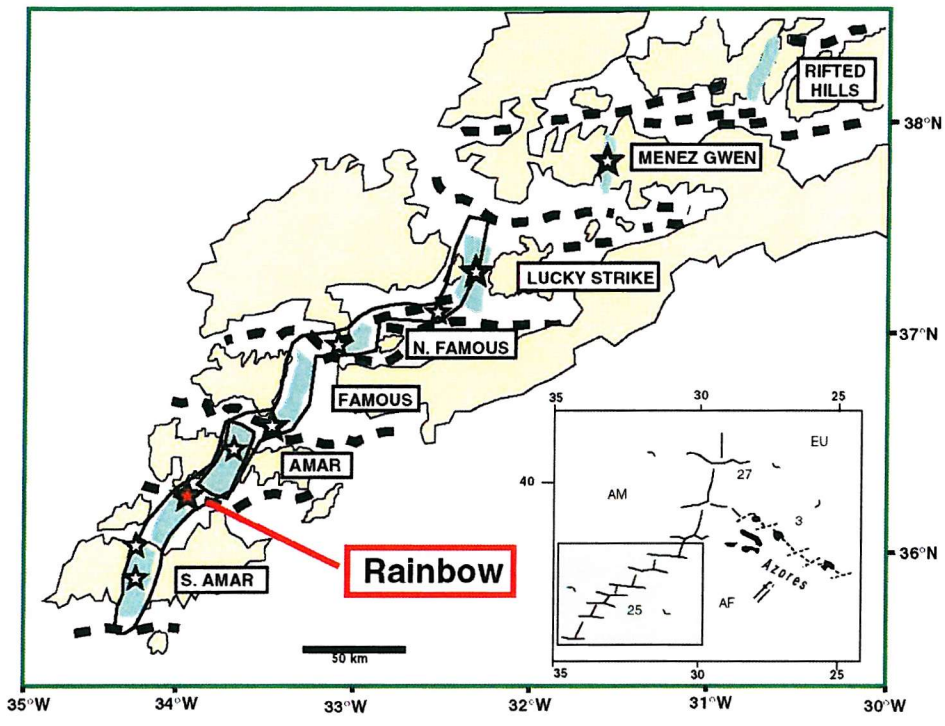

Figure 2.1: The Mid-Atlantic Ridge, south of the Azores.
The ridge has several segments (named), separated by non-transform discontinuities (NTDs). The outlined section of the rift valley shows the area of TOBI sidescan sonar coverage. Inset shows the area in relation to the Azores.

the AMAR segment before being forced north-east by the topography (Fig. 2.2). A number of Stand Alone Pump (SAP) stations had acquired plume particulate material on the FLAME 1 cruise and, accordingly, the coring sites were chosen as close to some of the SAP station coordinates as sedimentary cover permitted, so that comparative studies could be carried out between plume particulate material in the water column, and sediment accumulating below the plume . Plume height may vary over time, due to variations in the temperature and content of the hydrothermal fluid, and plume spreading direction may be affected in the short and long term by variations in current direction and speed over the local area.

Box coring stations were selected using a combination of processed TOBI sidescan sonar imagery, co-registered with Simrad bathymetry, (Fig. 2.3), and CTD and BRIDGET nephelometer (optical backscatter) data from the beginning of this and previous cruises, to identify areas of sediment underlying the already established trajectory of the neutrally buoyant plume (German *et al.*, 1996b; German *et al.*, 1998c). Potential coring areas were few due to the largely unsedimented nature of the terrain (Cave and

German, 1998a). For each box core, the ship's bridge was given a 'footprint' of 500m to 1000m square, within which TOBI data indicated sufficient sediment cover for coring to be feasible. Box coring was carried out using a 50cm x 50cm x 60cm (height) box-corer provided by courtesy of Prof. Peter Stoffers, Kiel University, Germany, and was successful in retrieving sediment at each of the four stations chosen (Fig. 2.2). The shortest core recovered was 18cm, the longest 43cm, and all cores appeared to have undisturbed surfaces.

The sediments recovered were all brownish-yellow foraminiferal/coccolith ooze. On board ship, 11cm diameter subcores were taken from each of the boxcores, capped and stored upright at 4°C for return to port (Fig. 2.4).

Core	Lat°N	Long°W	Depth	Length
343	36°14.8'	33°54.3'	2540m	41cm
316	36°15.5'	33°52.8'	2322m	25cm
325	36°12.8'	33°50.6'	2363m	18cm
329	36°17.5'	33°42.2'	2519m	18cm
22#6	32°53.5'	19°16.4'	3830m	
23#12	32°33.3'	20°20.9'	4660m	

Table 2.1: Locations of the Rainbow and background cores.
Rainbow cores are 2-20km from vent site. Background cores are from well to the east of the MAR, taken during an earlier cruise (Shimmield, 1990).

2.1.3 Sediment Trap Samples

Three sediment trap moorings were deployed during the MARVEL cruise in August 1997 and retrieved during the FLAME II cruise in June 1998 (Fig. 2.5). Mooring 1 had a single trap and was deployed to the south-east of the Rainbow vent field, on top of the Rainbow Ridge, in 1950m water depth, 200m above bottom (ridge-top trap). Mooring 2 was deployed at c. 500m north of the vent field in 2300m water depth, with 2 traps, one at 150m above bottom and one at 300m above bottom (near-field traps). Mooring 3 was deployed c. 1300m north-east of the vent field, in 2250m water depth, again with two traps, at 150m and 300m above bottom (far-field traps). The traps were cone-shaped type Technicap PPS5, with 22 collection bottles, rotating at periods of 14 days, and the moorings were in place for 304 days. Prior to deployment, the sampling

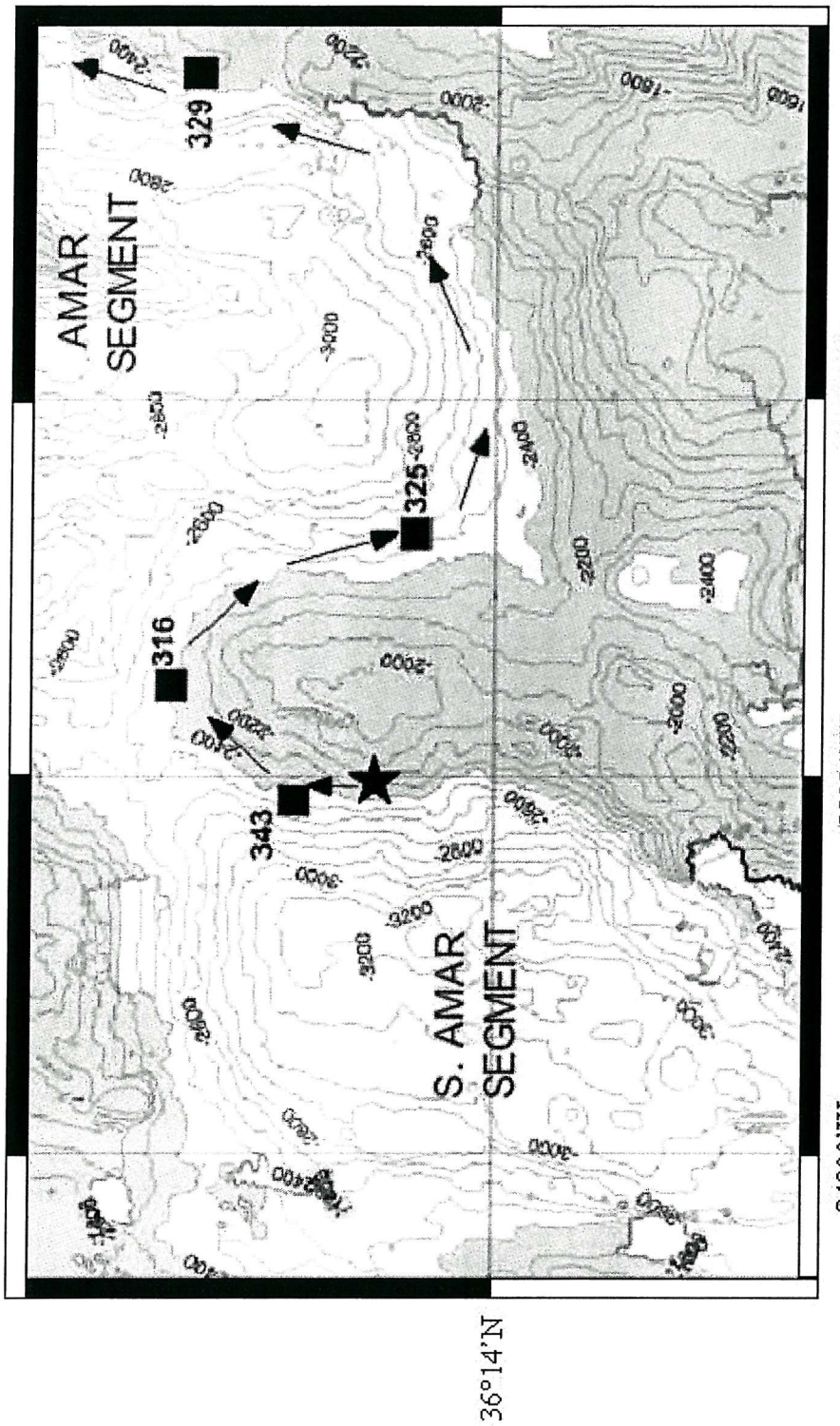

Figure 2.2: Location of cores and Rainbow vent site
Cores (squares) are located 2km (343), 5km (316), 10km (325) and 25km (329) downplume of the vent site. Star indicates location of vent site. Arrows indicate plume path (after Thurnherr and Richards, 2001). Contours are at 100m intervals, shaded area is shallower than 2400m water depth.

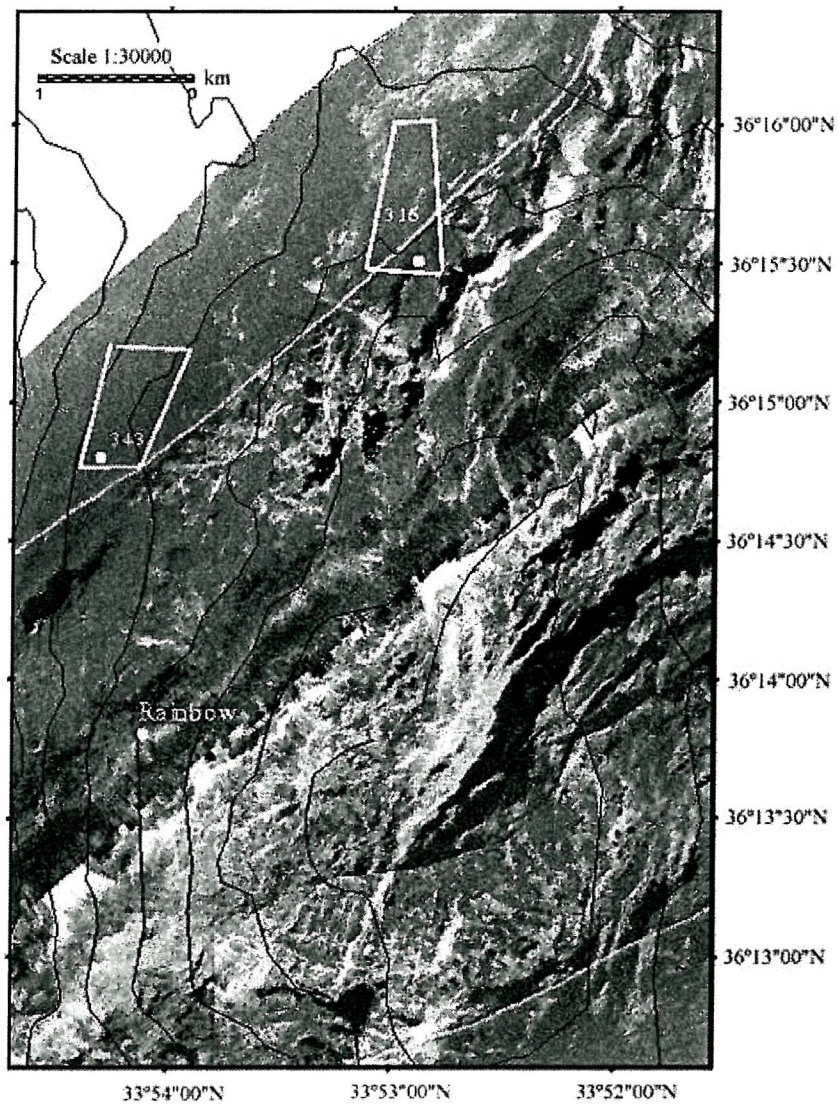

Figure 2.3: TOBI sidescan sonar data over the Rainbow Ridge. White areas indicate high backscatter i.e. bare rock, grey areas indicate some sediment cover, black areas are shadows. White dot marks the Rainbow vent site. White polygons indicate co-ordinates of areas given to the ship's bridge in which to core. White numbers and dots refer to the locations of the two core sites most proximal to the vent site, at 2km (core 343) and 5km (core 316) distance respectively.

Figure 2.4: Boxcore on deck with subcoring tubes inserted
Subcore tubes were inserted and pushed vertically into the sediment before the side of the box was removed. Tube diameter is 11.4cm. Box has a 50cm x 50cm footprint and is 60cm high.

bottles were filled with filtered seawater containing sodium borate buffered formalin to give a final concentration of 3%. Before drying, the particles collected were rinsed twice with distilled water (A. Khripounoff, pers. comm). Mooring 1 was placed away from the known plume path and above known plume rise height in order to collect the background pelagic flux. Mooring 2 was expected to be in the path of the buoyant plume, and Mooring 3 in the path of the neutrally buoyant plume.

On recovery, the traps located below plume depth along the path of the spreading plume were found to be coated with orange-coloured sediment (Fig. 2.6), while the traps located above plume height had a much paler coating. The off-axis trap did not have a noticeable coating. For the work being presented here, a selection of sample material from the traps was kindly provided by Dr. Alexis Khripounoff from IFREMER (Table 2.3).

Trap	Lat^{o}N	Long^{o}W	Depth
Near-field(u)	36^{o}14.0'	33^{o}54.0'	2000m
Near-field(l)	36^{o}14.0'	33^{o}54.0'	2150m
Far-field(u)	36^{o}14.2'	33^{o}54.0'	1950m
Far-field(l)	36^{o}14.2'	33^{o}54.0'	2150m
Ridge-top	36^{o}13.3'	33^{o}54.0'	1750m

Table 2.2: Locations of the Rainbow sediment traps.
Near-field traps were 500m north of vent site, far-field traps were 1.3km north-east of vent site, ridge-top trap was 2km east of vent-site, on top of the Rainbow Ridge. Near-field and far-field traps were in the direct path of the plume.

2.1.4 Ancillary Data

Sidescan sonar data

Extensive high-resolution side-scan sonar data of the southern AMAR segment was collected during cruise CD89 of the R.V. Charles Darwin in 1993, as part of the MARFLUX/AJJ programme (Parson *et al.*, 2000). It was during this cruise that the Rainbow hydrothermal plume was first mapped, using a transmissometer mounted on the SOC's TOBI sidescan sonar system (German *et al.*, 1996a; Cave and German, 1998b). The sidescan sonar data was processed at IOSDL by the author during 1993/94

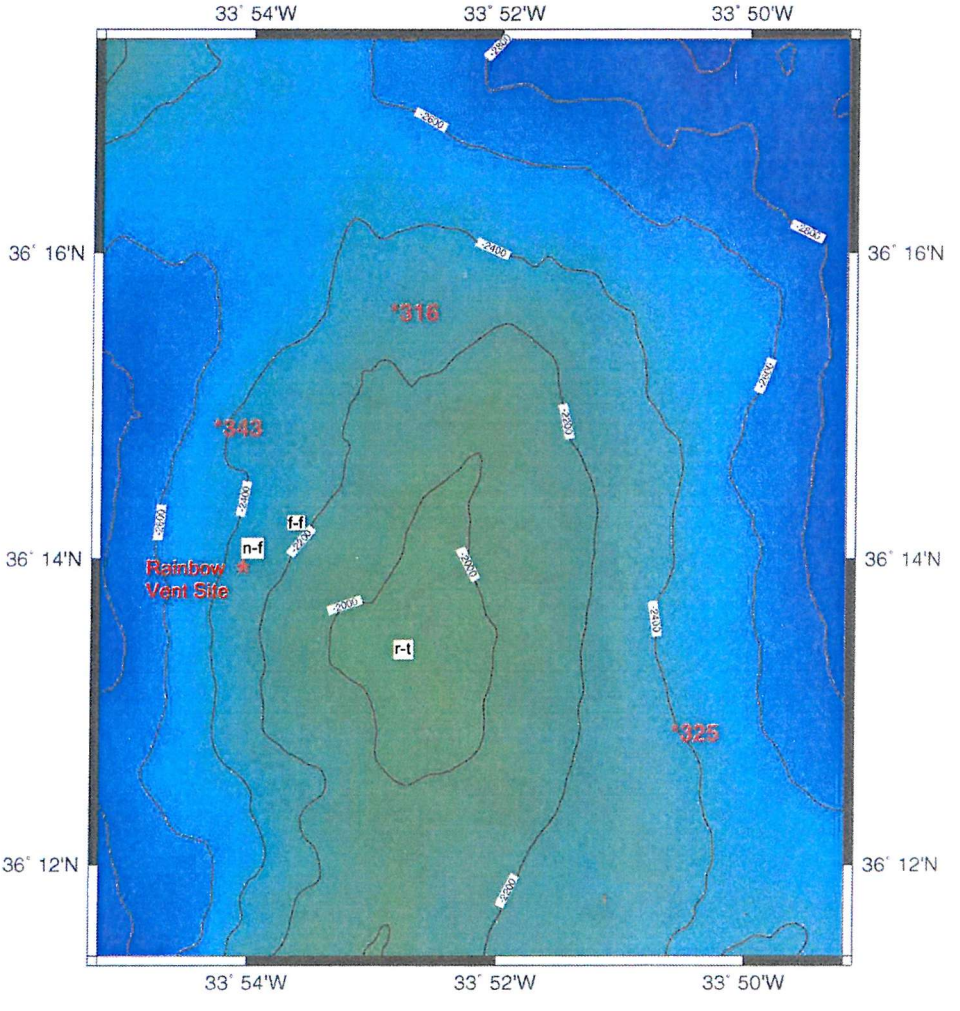

Figure 2.5: Sediment trap locations near the Rainbow vent site. Traps are near-field (n-f, 500m from vent site), far-field (f-f, 1300m from vent site) and ridge-top (r-t, *circa* 2km from the vent site, away from the plume path, and above nominal plume height. Red stars mark Rainbow vent site, and three of the four core locations. Contours are in metres below sea-surface.

Figure 2.6: Sediment trap coated in orange-coloured sediment.
This trap was one of the pair on the near-field mooring, located 500m from the vent site. The traps on the distal moorings did not have this coloured coating of sediment on recovery.

dist/ht	near-field	near-field	far-field	far-field	Pelagic
Period 1997-98	150m a.b.	300m a.b.	150m a.b.	300m a.b.	200m a.b.
10/9-24/9	Am1	Am5	Am9	Am13	Am17
22/10-5/11	Am2	Am6	Am10	Am14	Am18
17/12-31/12	Am3	-	-	-	-
31/12-14/1	Am4	Am7	Am12	Am16	Am20
25/2-11/3	-	Am8	-	-	Am19
17/6-26/6	-	-	Am11	Am15	-

Table 2.3: Sampling periods of the Rainbow sediment trap samples. Samples from other periods were used up in earlier studies (Khripounoff *et al.*, 2001).

and subsequently geographically registered by Dr. P. Blondel at the Southampton Oceanography Centre (Blondel, 1997). This dataset was used during the FLAME II cruise in June 1997 to identify areas around Rainbow Ridge where sedimentary cover was sufficient to allow box coring to take place (Cave and German, 1998a). Much of this area of the MAR rift valley is almost bare rock, generally pillow lavas and sheet flows, with only a few centimetres of sediment cover, or rocky talus from local outcrops of ultramfic seafloor (Fig. 2.3).

Optical data

During several cruises to the southern end of the AMAR segment from 1993 onward, the vertical and lateral extent of the Rainbow hydrothermal plume was mapped using nephelometers and transmissometers attached to CTDs, to BRIDGET (SOCs towed instrument for plume detection) and to TOBI (SOCs sidescan sonar system). Vertical casts and tow-yo's were made through the plume at several locations to determine the rise height of the plume and its prevailing direction (German *et al.*, 1998c; Thurnherr and Richards, 2001). ADCPs were deployed on long-term moorings to determine the movement of currents in the area.

2.2 Analytical Methods

Sediment cores were removed from 4°C storage and placed in an upright position in an extrusion assembly which incorporated a precision screw device (Fig. 2.7). The cores were extruded and sliced at 1 cm intervals, and weighed. These slices were then freeze dried and reweighed. Each slice was then ground to a fine powder, in an agate mortar to minimise metal contamination.

2.2.1 Calcium Carbonate and organic Carbon determination

$CaCO_3$

$CaCO_3$ measurements were made using a UIC Model 5012 Carbon Dioxide Coulometer. $CaCO_3$ content was determined from CO_2 liberated by 10% phosphoric acid, using ~25mg of sample. Reference standard sediment 10549#1K was run approximately every 6th sample to check the calibration of the instrument, followed by a blank.

Organic Carbon (Corg)

Total carbon was measured by Total Combustion Coulometer using ~25mg of sample. Reference standard sediment 10549#1K was run approximately every 6th sample to check the calibration of the instrument, followed by a blank. Corg was determined by subtracting the carbon measured by the carbon dioxide method above, from the combusted carbon content.

2.2.2 Radiocarbon dating

Samples of bulk sediment from the Rainbow cores were taken approximately every 5cm downcore, and sent to the NERC Radiocarbon Laboratory for analysis (allocation no. 791.0599). Details of the radiocarbon ages are given in Table 2.4.

The 'conventional radiocarbon (or ^{14}C) age' given for any material is quoted with reference to the 0.95 (specific) activity of the NBS oxalic radiocarbon standard, which equals the natural activity of a fictitious wood from A.D. 1950. The activity of the fictitious 1950 wood has been calculated from measurements of actual A.D. 1890 wood, allowing for radioactive decay, as anthropogenic effects on natural ^{14}C preclude di-

Figure 2.7: SOC's precision core extruder
Core endcaps are removed and core is clamped upright on a block which exactly fits the inner diameter of the core casing. Each turn of the screw advances the core 0.1cm. Slices of sediment are cut off at desired intervals using a cheese wire or fishing line.

rect measurement of its natural activity in 1950's material (Olsson *et al.*, 1974). Radiocarbon dating was initially developed for aging of plants or animals that take up atmospherically-derived carbon in their 'food'. It works on the principle that all living things take up a proportion of ^{14}C as part of their total carbon intake. The carbon is at equilibrium until the organism dies, when the ^{14}C begins to decay at a known rate. Knowing the decay rate and the equilibrium value allows the time of death of the organism to be calculated (within error) by measuring its current ^{14}C activity and total carbon content. However, comparisons with dendrochronology (tree-ring dating) has shown that the atmospheric ^{14}C reservoir has altered over the last 6500 years, so a correction must be applied if converting ^{14}C dating to calendar years. ^{14}C dating of organic carbonate material in marine sediments is also complicated by the existence of different amounts of ^{14}C in different oceanic reservoirs, and by the length of the oceanic mixing time, requiring further corrections. Finally, bioturbation of the top few centimetres of marine sediments creates a 'mixed' layer within which the ^{14}C ages will be homogenised, so that the top of the sediment will appear older, and the bottom of the mixed layer younger, than their actual ages.

Depth	core343	core316	core325	core329
5.5	3145±50	4610±55	4185±50	3715±50
10.5	4490±55	5580±55	4925±55	4055±50
14.5	5955±50	7060±55	5990±55	4815±55
17.5	6715±55	7650±55	7615±55	5950±55
24.5	11540±55	10785±55		
30.5	17380±60			
40.5	25975±120			

Table 2.4: Radiocarbon dating of the Rainbow cores.
The top sample was taken from within the mixed layer, as defined by ^{210}Pb excess profile, other samples were from below the mixed layer. Radiocarbon dating was carried out on bulk samples by the NERC Radiocarbon Laboratory.

2.2.3 ^{210}Pb determination and the surface mixed layer

^{210}Pb measurements were made by gamma-ray detection for each cm of the top 10cm of each core. 20gm of dried ground sediment from each 1cm core slice was made into

a pellet by pressing at 10 tons for 90 seconds on a hand press. No PVA binder was required as the pellets were sufficiently robust without it. The pellets were placed inside plastic petri dishes, sealed with Araldite, and stored for 20 days to allow secular equilibrium between ^{226}Ra and its radioactive daughters to develop. Samples were then counted for 3 days on a low background, high resolution Ge detector with a good low energy gamma response.

Assuming that bioturbation is relatively rapid, an estimate of the depth of the surface mixed layer can be made using a short-lived naturally occurring radio-nuclide such as ^{210}Pb. ^{210}Pb is part of the ^{238}U decay series, produced by the decay of ^{222}Rn, which is largely derived from weathering of continental material. It enters the seawater system both as an aerosol and in river-borne particulate material. It is also produced in-situ by the decay of dissolved ^{226}Ra, and in deep waters (2-4km) this can greatly exceed the atmospheric input. It is quickly removed from seawater by the rain of particulate material to the seafloor (Cochran, 1992).

2.2.4 Major element determination by XRF

Major elements were measured on a Philips PW1400 fully automatic Wavelength Dispersive XRF. All four cores had major elements measured for the top 3cm, and every other cm downcore. A large piece of serpentinite recovered from core 343 was also crushed and ground for analysis. Major elements measured were Si, Ti, Al, Fe, Mn, Mg, Ca, K, P, and S.

Major element bead preparation

For cores 343, 325 and 329, approximately 2gm of sediment from each sample depth were ignited overnight at 970^{o}C in clean ceramic crucibles. The crucibles and samples were weighed before and after ignition in order to calculate the loss-on-ignition (LOI) values. 0.8gm of ignited sediment was weighed out into an acid-cleaned Pt crucible for each bead for major element measurements, and then mixed in proportion of 1:5 with Spectraflux 100 lithium tetraborate flux. In order to test the effects of ignition on major elements, core 316 used oven-dried samples, which were not ignited prior to beading, with (100-Sum) taken to be the LOI (de Jongh, 1979). Two samples from core 316 were ignited following the procedure for the other 3 cores, in order to check the validity of the results from the unignited sediment. These were found to agree within $\pm$ 5%, with the exception of the elements Na, K and S. Na and K were found

to be present in an order of magnitude greater concentration in the beads made from unignited sediment, while S was about half its concentration compared to the ignited sediment. A bead of unignited sample from core 329 was also made up, and the results agreed to within ±5% of the ignited bead results, within the exceptions of Na, K and S, as above. It seems therefore that the ignition process causes significant loss of Na and K, probably from loosely bound species present in the sea salt, but the beading process retains these elements in unignited sediment. S becomes more tightly bound during the ignition process, and so is retained during beading, but is lost during beading of unignited sediment.

Major element standards

A bead of international standard BRR-1 was used for each set of major elements run in order to be able to check the consistency of the results, as although all the beads for any one core were measured during the same XRF run, different cores were measured on different days. As the cores were known to have a high $CaCO_3$ content, and BRR-1 $CaCO_3$ content is only moderate, another standard bead was made up using JDo-1 (dolomite) which has a high carbonate content, and this was also run. Repeat runs agreed to within 1% or better for both standards.

2.2.5 Trace element determination by XRF

Trace elements were measured on a Philips PW1400 fully automatic Wavelength Dispersive XRF. All four cores had trace elements measured for the top 3cm, and every other cm downcore, as for the major elements (see above). Trace element analyses were also carried on the serpentinite piece from core 343.

Trace element pellet preparation

Approximately 8gm of sediment per sample was pressed into pellets with a 12 ton automatic press for trace element measurements. Binder was not used as the sediment was sufficiently cohesive for the pellets not to crack.

Trace element detection limits

Table 2.5 shows XRF detection limits for trace elements of interest. Elements for which results are quantifiable are indicated by (1). Elements which were determinable but may not be quantifiable with confidence by this method are indicated by (2). Elements whose measured concentrations were close to or below detection limits are indicated by (3). Major elements occur in % concentrations so they are all quantifiable using XRF. LLD = detection limit. Limit of determination = 3 x LLD, Limit of Quantitation = 10 x LLD.

Element	LLD (ppm)	Core 343	Core 316	Core 325	Core 329
As[1]	6	8-28	26-38	33-42	8 - 30
Ba[1]	10	98-194	86-182	151-271	13 - 132
Ce[1]	10	36-76	43-86	40-85	38 - 85
Cr[1]	4	12-47	8-16	8-20	10 - 139
Ga[2]	1.5	0-4	1.7-4	0-4	0.7 - 4.5
La[2]	5	7-16	6-20	10-20	n.a.
Ni[1]	1.5	14-41	9-13	11-16	11-85
Nb[2]	1.5	4-6	4-6.5	5-7	3.5-6.3
Pb[2]	1.5	5-10	6-11	7-10	5-11.5
Rb[3]	1.5	0.3-2	1.2-2.5	1-3	0.8-5
Sr[1]	1.5	1287-1524	1524-1650	1540-1643	1200-1600
Th[3]	2	0-1.4	0-1.9	0-1.1	0-1.7
U[3]	3	0-0.88	0-0.75	0-0.15	0-0.88
V[1]	4	41-97	89-116	105-131	31-97
Y[2]	1.5	5-8	7-10	8-11	6-13
Zn[1]	1.5	24-30	18-26	19-25	23-31

Table 2.5: XRF Trace Element detection limits.
Results for Rainbow cores are indicated by ([1]) = quantifiable, ([2]) determinable but may not be quantifiable with confidence ([3]) = close to or below detection limits.

Trace Element Standards

No suitable standards for high-carbonate metal-rich sediments were available, so a series of standards were prepared using laboratory standard $CaCO_3$ powder, to which was added various amounts of rock standards BEN, JSl-1, JSd-1, JSd-2, JSd-3 and SCo-1. This latter standard was used in a range of concentrations in order to provide calibration curves for the trace elements of interest (see next section).

Trace Element Calibration

Due to the very high carbonate content of the samples, it was decided to make a set of pellets to check the linearity of response of the XRF for the trace elements to be measured. Five pellets were made using laboratory standard $CaCO_3$ mixed with international shale standard SCo-1, as follows: (a) 100% $CaCO_3$, (b) 80% $CaCO_3$ + 20% SCo-1, (c) 60%$CaCO_3$ + 40%SCo-1, (d) 40%$CaCO_3$ + 60% SCo-1, and (e) 20%$CaCO_3$ + 80% SCo-1. Expected values for each trace element of interest were calculated from the international standard reference values for SCo-1. The 100% $CaCO_3$ pellet was measured for the presence of trace elements impurities, and the results were included in the calculations. The XRF showed a very linear response to increasing proportions of $CaCO_3$ in the samples, and good agreement with expected values, with the exception of Nb, which measured higher than expected, and Th, which was close to detection limits. See Appendix 1 for calibration graphs.

Copper Calibration

Some copper is produced by the rhodium XRF tube itself, which must be corrected for when measuring copper as a trace element in a sample. A calibration of the XRF using a set of pure reference standards containing no Cu was made (Table 2.6, Fig. 2.8), by measuring the intensity of Cu from the tube over a range of Rh intensities. This provided a regression line to allow calculation of the amount of Cu produced by the tube for any Rh intensity, yielding m=0.3997, c=0.0942 for these sample runs.

Following this, reference standards containing a range of known Cu concentrations were used to check Rh output of the XRF. Copper concentration was plotted against Cu/Rh ratio to yield a second regression line equation which was then used to calculate the true Cu concentration in the unknown samples (Table 2.7, Fig. 2.9).

Pure Stds	Rh intensity cps	Cu intensity cps
$Al2O_3$	8.8380	0.4460
$Fe2O_3$	0.8054	0.1273
SiO_2	7.5746	0.3994
$CaCO_3$	3.3026	0.2243

Table 2.6: Copper-rhodium calibration.
See text for details.

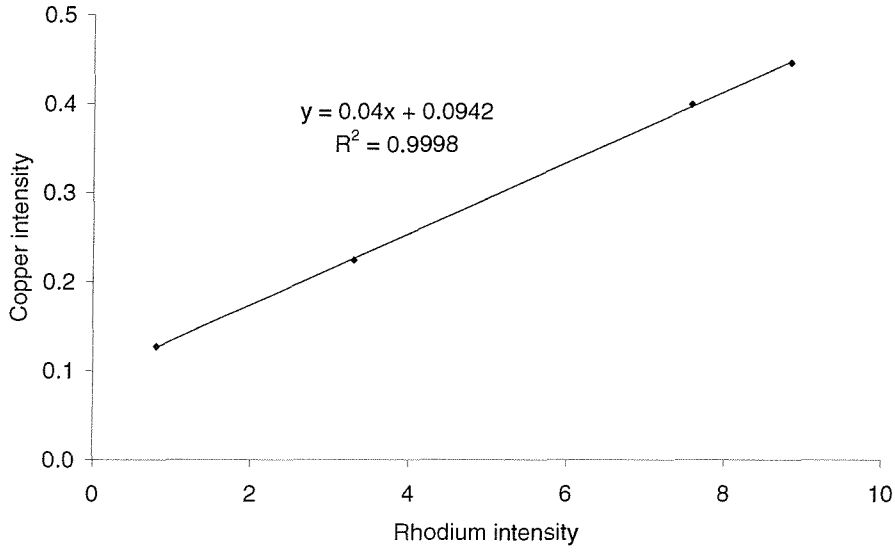

Figure 2.8: Correction for copper from XRF rhodium tube.
See text for details.

Reference Standard	Rh cps	Tot Cu cps	Cu Tube cps	Cu Sample cps	Cu/Rh	Cu conc. ppm
$Al2O_3$	8.8380	0.4460	0.4475	-0.0015	-0.0002	0
$Fe2O_3$	0.8054	0.1273	0.1264	0.0009	0.0011	0
SiO_2	7.5746	0.3994	0.3970	0.0024	0.0003	0
$CaCO_3$	3.3026	0.2243	0.2262	-0.0019	-0.0006	0
Ben	3.0179	0.4910	0.2148	0.2762	0.0915	72
BCR	3.2890	0.3478	0.2257	0.1221	0.0371	19
JLk1	5.0640	0.6149	0.2966	0.3183	0.0629	59.8
JDo1	4.8110	0.2416	0.2865	-0.0449	-0.0093	1.4
TS	4.5234	2.3896	0.2750	2.1146	0.4675	493
Jsd2	3.7803	4.8750	0.2453	4.6297	1.2247	1114
Jsd3	5.4810	2.7916	0.3133	2.4783	0.4522	426

Table 2.7: Copper-standard calibration.
See text for details.

Seasalt correction

Sediment slices were freeze-dried after slicing and weighing, but without any rinsing. The dried sediment was therefore assumed to contain an amount of seasalt, remaining after the pore-waters had evaporated during the drying process. Calculation of the salt content of the sediment was made by subtracting the dry weight of the sample from its wet weight before drying, and calculating the salt content of the water lost if all the water was seawater at 35 parts per thousand. The sodium and magnesium content of the sediments was also measured as major elements by the XRF (see previous section) and are further discussed here.

Sodium (Na) The Na contributions from seasalt calculated for core 316 are found to closely follow the Na curve from the XRF data down to 20cm, but are about 20% lower (Fig. 2.10). The difference should be the contribution from the detrital component of the sediment. Average ultramafic rock concentration of Na is ~0.4% (Note - the Na concentration in local serpentinite was below detection limits), average shale concentration of Na is ~0.9%, and average basalt about twice shale at 1.8% (Turekian and Wedepohl, 1961). The detrital component makes up ~20% of these sediments, so

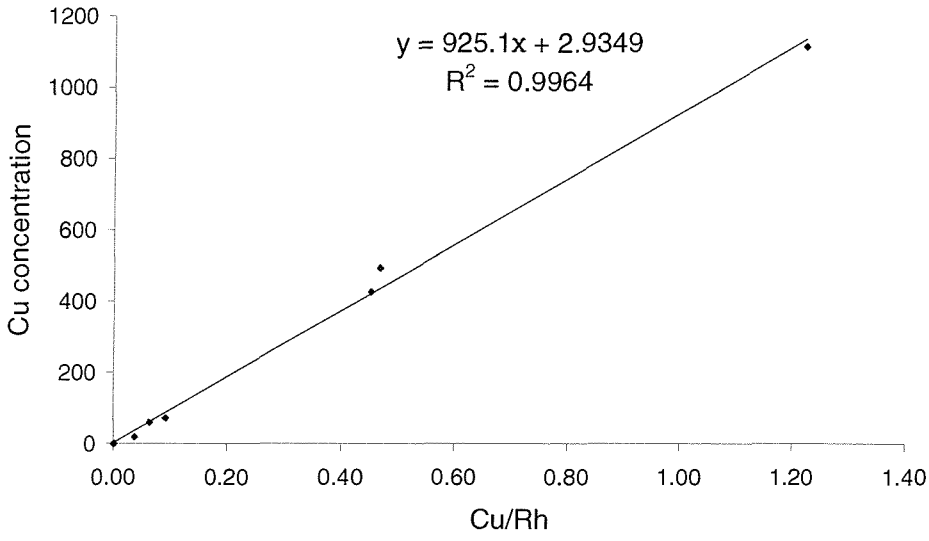

Figure 2.9: Copper standard calibration.
The regression equation is used to calculate the true copper content of unknown samples.

an Na contribution to the bulk sediment of between 0.08% (ultramafic only) and 0.36% (basalt only) might be expected. The actual difference measured is 0.2 - 0.3%, indicating that shale is the likely contributor. The separation of the curves below 20cm depth could indicate either increasing salinity of the porewaters, or reflect the greater proportion of weathered material in the sediments below this depth. An increase in the average concentration of Mg in the sediments below 20cm depth would seem to indicate the presence of more weathered material, as it is too great to result from increased porewater salinity. As cores 343, 325 and 329 had major elements measured on ignited sediments, the Na measured by the XRF is not a true representation of the concentration in those cores (see earlier section) and so this calculation can only be made for core 316 at present.

Magnesium (Mg) About 1000 - 1500μg g^{-1} of the Mg measured in the Rainbow core sediments has come from salt in the pore waters (Fig. 2.11). The Mg concentration in average shale is 1.5%, while Mg concentration measured in local serpentinite is 22.5%, and 4-5.5% in local basalts. (Mg in average ultramafic rock is 20.4%, 4.6% in average basalt). Sediments from core 343 and 316 average a salt-free Mg concentration of

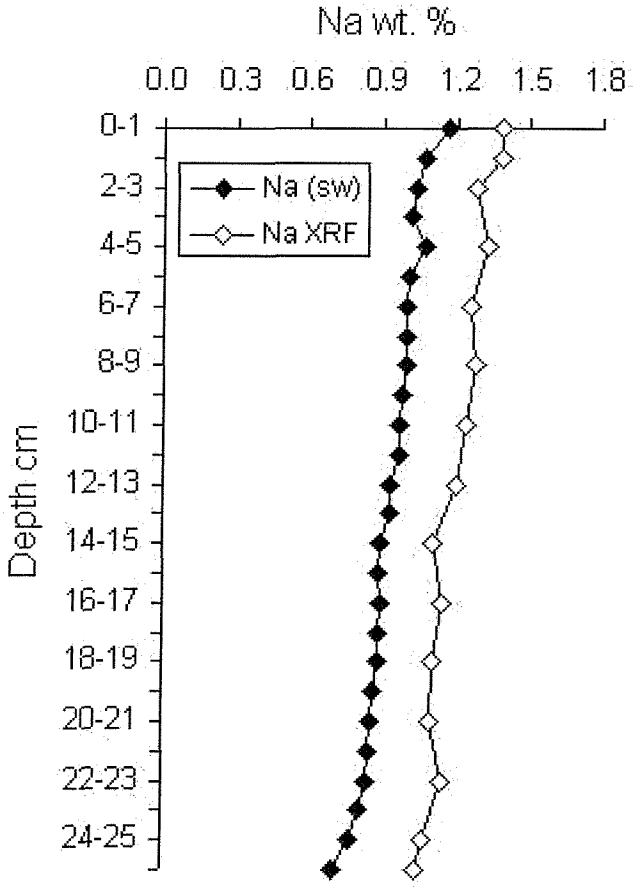

Figure 2.10: Sodium in core 316.
The contribution of Na from seasalt to the total Na of the sample has been calculated from the pore water content of each sample, assuming a pore-water salinity of 35ppt, and an Na content of 10.773g kg^{-1} (Libes, 1992) p.36.

4000ppm in the upper part of the core, and 5000ppm in the lower part. Values for core 325 average 3000ppm, and for core 329 are slightly higher at 3400 ppm. The maximum possible shale contribution to the sediments is 20% , which would provide only 3000ppm of Mg to the sediments. It is clear therefore that Stations 316 and 343 have a significant input of Mg from another source.

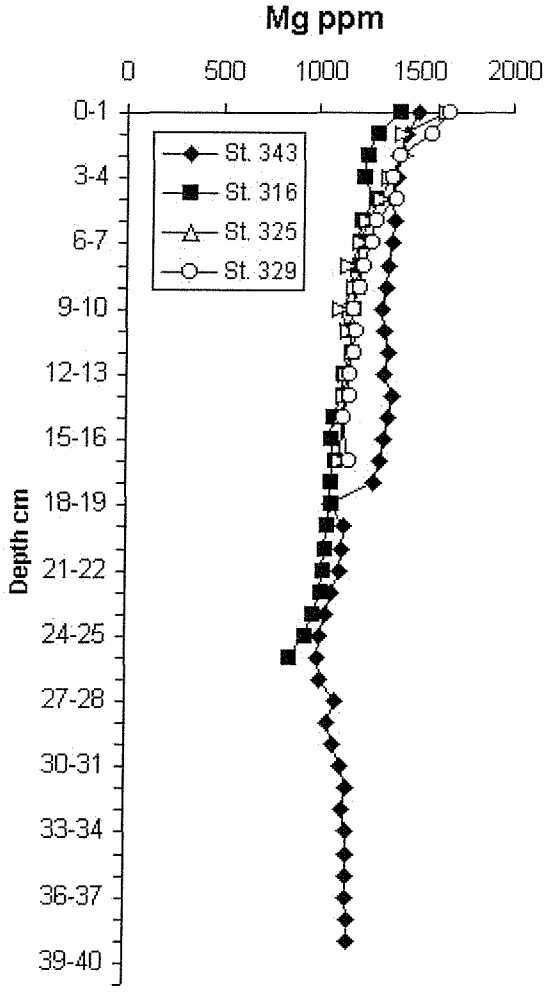

Figure 2.11: Contribution of Magnesium from seasalt in Rainbow cores. Salt content is calculated from the water content for each core slice, assuming pore waters to be at 35ppt salinity, with a Mg content of 1.294g kg^{-1} (Libes, 1992) p.36.

2.2.6 Major and trace element determination by ICP-AES

A collection of sediment trap samples were made available for this study by Dr. Alexis Khripounoff, IFREMER. Only a few hundred milligrammes of each sample was available so it was not possible to analyse them by the XRF methods used for the core samples. Consequently, sediment trap samples were analysed on the ICP-AES for major and trace elements. Samples from the tops of each of the four cores were also analysed in this way in order to have directly comparable results between core top and sediment trap samples (see Chapter 4).

Samples of 100-200mg of sediment trap and core sample material were first treated with a few ml of 6M HCl to dissolve carbonate and allow Ca to be separated from the residue by centrifuging, to prevent formation of insoluble fluorides during later HF dissolution. The residue was then treated with a combination of HF/HNO_3 followed by dissolution in 6M HCl. The residue and supernatant were then recombined and made up into a x300 dilution in 6M HCl.

Major elements (Mg, Al, Ca, Ti, Fe, Mn) and high-level trace elements (V, Cr, Cu, Zn, Ni) were measured on a Phillips PV8060 ICP-AES for sediment trap and core top samples, by standard additions.

2.2.7 Rare-earth element determination by ICP-MS

Rare-earth elements from the sediment trap samples and a selection of core samples were measured on a VG Elemental PlasmaQuad PQ2+ ICP-MS, by comparison with matrix-matched SGR-1 (Green River Shale) and synthetic standards. Interferences of Ba and LREE on Eu and Gd were corrected for by running dilutions of single element standards of Ba, La, Ce, and Pr, and applying a correction factor to the counts for the affected elements. Repeat measurements of SGR-1 agreed within 5%.

2.2.8 Osmium isotope and platinum group element (PGE) determination

A selection of samples from each of the four cores was taken to the Woods Hole Oceanographic Institution for PGE analysis. Samples were first pre-concentrated by the NiS fire assay method of Ravizza and Pyle, (1997). Samples of 3g of dried ground sediment

were placed in clean ceramic crucibles, spiked with ~0.03g of an in-house calibrated mixed solution standard of ^{194}Pt, ^{105}Pd, ^{191}Ir, ^{190}Os, ^{99}Ru and left to dry overnight. 5g of borate flux was mixed with 0.6g Ni and 0.3g S and then stirred into each sample. Crucibles were then covered with lids and placed in a 1000°C furnace for an hour to melt. After removal from the furnace, the melt was allowed to cool, and the crucible cracked open with a hammer, to reveal a glassy material containing one or more NiS beads. The beads were recovered and dissolved in a glass conical flask with 6.2M distilled HCl (Fig. 2.12). Once dissolution was complete, the solution was filtered through a Millipore 0.45μm type HA filter paper. The filter paper was placed in a cleaned Teflon screwtop pot with 1ml concentrated Seastar HNO_3 and left to dissolve on a hotplate. Following dissolution, samples were diluted with ~5ml MilliQ water and analysed for Os concentration and isotopic composition by sparging to a magnetic sector ICP-MS, using the method described in Hassler *et al.*, (2000). This involves bubbling Ar as a carrier gas through the solution , carrying volatile OsO_4 into the ICP. Following Os analysis, an aliquot of 0.4ml of the residual solution was made up to 2ml in MilliQ water, before being analysed for complementary PGE on the ICP-MS using a microconcentric nebulizer (Ravizza and Pyle, 1997; Hassler *et al.*, 2000).

Figure 2.12: Dissolution of NiS beads for Os and PGE analysis

2.2.9 Calculation of the hydrothermal component

Four components have been identified in the Rainbow cores: (a) a biogenic $CaCO_3$ component (b) a continentally-derived detrital component (c) a hydrothermal component, and (d) a locally derived ultramafic component that is present at certain levels

in cores 343 and 316 only. The $CaCO_3$ component of the sediments has been measured directly (Appendix 2), and is assumed to make a negligible contribution to the range of metals of interest. The hydrothermal component is calculated by subtracting the contributions of the other different components (b) and (d) identified above, from the bulk composition. The detrital component of each element is calculated from the mean element/Al ratios of the BOFS cores (Table 3.1) and the individual Al contents of the Rainbow cores:

$$[\mathrm{X}]_{detrital} = (\mathrm{X/Al})_{BOFS} \times [\mathrm{Al}]_{total} \quad \text{(Eq. 1)}$$

Subtraction of the detrital component $[X]_{detrital}$ from the bulk composition $[X]_{total}$ yields an excess that represents either the hydrothermal input (cores 325 and 329) or the combined ultramafic and hydrothermal inputs (certain horizons of cores 343 and 316):

$$[\mathrm{X}]_{excess} = [\mathrm{X}]_{total} - [\mathrm{X}]_{detrital} \quad \text{(Eq. 2)}$$

Nickel rather than Cr is used to estimate the ultramafic component because the Cr content of MAR ultramafic rocks varies over almost an order of magnitude in whole-rock analyses (e.g. GERM database, http: //www.EarthRef.org), whereas Ni varies by only a factor of 2 for the same samples. Once the Ni contribution from shale has been calculated and subtracted, the ultramafic component of the excess fraction is extracted by multiplying the $[Ni]_{excess}$ content of each sample by the element/Ni ratio of the serpentinite fragment recovered from core 343 (Table 3.1). Thus,

$$[\mathrm{X}]_{ultramafic} = [\mathrm{X/Ni}]_{serpentinite} \times [\mathrm{Ni}]_{excess} \quad \text{(Eq. 3)}$$

and the hydrothermal component of each element is then:

$$[\mathrm{X}]_{hydrothermal} = [\mathrm{X}]_{total} - [\mathrm{X}]_{detrital} - [\mathrm{X}]_{ultramafic} \quad \text{(Eq. 4)}$$

A hydrothermal contribution is estimated in this way for one set of elements precipitated directly from vent fluids (Mn, Fe, Co, Cu and Zn) and for another set (V, P and As) scavenged from seawater by those hydrothermal precipitates.

Chapter 3

Hydrothermal Sediments at Rainbow

Abstract

A geochemical investigation has been conducted of a suite of 4 sediment cores collected from directly beneath the hydrothermal plume at distances of 2-25km from the Rainbow hydrothermal field. As well as a large biogenic component (>80% $CaCO_3$) these sediments record clear enrichments of the elements Fe, Cu, Mn, V, P and As from hydrothermal plume fallout but only minor detrital background material. Systematic variations in the abundances of "hydrothermal" elements are observed at increasing distance from the vent site, consistent with chemical evolution of the dispersing plume. Further, pronounced Ni and Cr enrichments at specific levels within each of the two cores collected from closest to the vent site are indicative of discrete episodes of additional input of ultramafic material at these two near-field locations. Radiocarbon dating reveals mean Holocene accumulation rates for all four cores of 2.7-3.7 cm.kyr^{-1}, with surface mixed layers 7-10+ cm thick, from which a history of deposition from the Rainbow hydrothermal plume can be deduced. Deposition from the plume supplies elements to the underlying sediments that are either directly hydrothermally sourced (e.g. Fe, Mn, Cu) or scavenged from seawater via the hydrothermal plume (e.g. V, P, As). Holocene fluxes into to the cores' surface mixed layers are presented which, typically, are an order of magnitude greater than "background" authigenic fluxes from the open N. Atlantic. One core, collected closest to the vent-site, indicates that both the concentration and flux of hydrothermally-derived material increased significantly at some point between 8 and 12 ^{14}C kyr ago; the preferred explanation is that this variation reflects the initiation/intensification of hydrothermal venting at the Rainbow hydrothermal field at this time - perhaps linked to some specific tectonic event in this fault-controlled hydrothermal setting.

3.1 Introduction

The existence of hydrothermal systems was postulated to provide the additional sources and sinks needed to balance the budgets of elements entering the ocean from rivers and being removed to sediments (e.g. Conway, 1943), and subsequently such systems have been shown to play an important role in the recycling of elements between seawater and crust (e.g. Kadko et al., 1995). Initial searches for modern submarine venting focused on restricted areas of sediments with high Fe and Mn contents discovered along mid-ocean ridge crests (Arrhenius and Bonatti, 1965; Bostrom and Peterson, 1966). The discovery of active vents on the Galapagos Rift (Corliss *et al.*, 1979), and of black smokers at 21^{o}N on the East Pacific Rise (EPR) (Spiess *et al.*, 1980), then turned attention from broad-scale studies of ridge sediments to more localized studies of sediments within vent fields (German *et al.*, 1993; German *et al.*, 1999; Lalou *et al.*, 1986; Metz *et al.*, 1988; Mills *et al.*, 1993) and of hydrothermal plumes themselves (Feely *et al.*, 1991; Field and Sherrell, 2000; German *et al.*, 1991; Metz and Trefry, 1993; Trefry and Metz, 1989; Trocine and Trefry, 1988). Detailed studies have also been undertaken on individual ridge-flank cores (German *et al.*, 1997; Olivarez and Owen, 1989) and on the sedimentation from hydrothermal plumes using sediment traps (Dymond and Roth, 1988; Feely *et al.*, 1994; Khripounoff *et al.*, 2000; German *et al.*, in press). A gap nevertheless remains in our knowledge of how vent signals are imprinted on sediments accumulating beyond vent fields, because no systematic study has been undertaken on sediments at progressive distance under a specific plume.

The Rainbow vent field on the Mid-Atlantic Ridge (MAR) was discovered in 1994 (German *et al.*, 1996a). Between 1994 and 1999, water column studies provided data on local hydrographic conditions, water column chemistry, plume path (German *et al.*, 1998a; Thurnherr and Richards, 2001; Thurnherr *et al.*, in press) and plume composition (Edmonds *et al.*, 1998; Khripounoff *et al.*, 2001; Radford-Knoery *et al.*, 1998; Radford-Knoery *et al.*, 2001). Direct investigations of the vent field by the submersible Nautile in 1997 (Fouquet *et al.*, 1997) revealed that the Rainbow field comprises at least 10 groups of active black smokers, with vent fluid exit temperatures up to 360^{o}C. The outputs of these black smokers coalesce to form the most particle-rich hydrothermal plume so far observed on the MAR (German *et al.*, 1996b). A suite of 4 cores was collected in 1998 from sites located downstream from the vent field and directly under the plume trajectory (Cave and German, 1998a; German *et al.*, 1998c). Here geochemical data are presented from this series of cores in order to characterize the deposition of discharge from the Rainbow hydrothermal field, and its history.

3.2 Sampling and Methods

The Rainbow vent field is situated at 36°14'N in the N.E. corner of the S. AMAR segment of the MAR. It lies on a westward-facing fault scarp, near the intersection with the adjacent non-transform discontinuity (NTD) that exposes ultramafic rock (Fouquet *et al.*, 1997)(Fig. 2.3). The vent field complex is at a depth of 2300m, and its plume reaches neutral buoyancy at ~ 2100m water depth. Prior to core collection, it had already been ascertained that plume dispersion at Rainbow is predictable, but complex: due to a combination of Coriolis effects and "topographic steering" (German *et al.*, 1998a; Thurnherr and Richards, 2001) the neutrally-buoyant hydrothermal plume at Rainbow (at 2100m depth) initially spreads to an across-plume width of ca. 2km, in accordance with the Rossby radius (l=3km) and then disperses down-plume, closely following the path of the underlying 2300m isobath - the depth at which hydrothermal fluid is first injected into the base of the water column (Fouquet *et al.*, 1997). A more detailed discussion of the subject is presented by Thurnherr and Richards (2001) but for this study, the key observation is that the "topographically controlled" path of the neutrally-buoyant hydrothermal plume is first to the north and east, around Rainbow Ridge, then south and east around the non-transform discontinuity (NTD) before continuing north following the eastern wall of the AMAR segment (German *et al.*, 1998a). Current speeds in the area are up to 20cm s^{-1} at plume height (Thurnherr and Richards, 2001), and the vigorous venting ensures that a strong plume signal is observed at least 50 km from the vent complex. High-resolution sidescan sonar data for the area (German *et al.*, 1996a; Gracia *et al.*, 2000; Parson *et al.*, 2000) show that the upper ~200m of the ridge is bare rock, and that sediment cover in the area is sparse with many bare rock outcrops (Fig. 2.3).

All areas which had sufficient sediment cover for box coring, and which occurred close to the appropriate beneath-plume depth of ca. 2300m, were identified on FS Poseidon cruise 240 in 1998, using sidescan sonar data co-registered with bathymetry from previous cruises (Cave and German, 1998b; German *et al.*, 1996a). CTD stations carried out at the beginning of the cruise confirmed the continuing presence of the plume and its trajectory. Four cores were then taken at sites beneath the spreading plume (Fig. 2.2), at water depths between 2322m and 2540m and at distances from 2-25 km downstream from the vent site (Table 2.1). On board ship, 11cm diameter sub-cores were taken from each box core, capped and stored upright at 4°C for return to the shore laboratory. The sediments were all pale-brown carbonate oozes, but layers containing rock fragments were noted in the two cores closest to the vent site, at ~20-30cm in core

343, and at ~16cm and ~26cm in core 316.

Cores were extruded using a precision screw device and sliced at 1cm intervals (Fig. 2.7). Slices were weighed, freeze-dried and re-weighed in order to calculate water content and bulk density. Any visible rock fragments were removed and the samples were ground in an agate mortar. Total carbon and $CaCO_3$ were determined by UIC Model 5012 Carbon Dioxide Coulometer, with Corg calculated as the difference between the total carbon and inorganic carbon contents. Elemental analyses were made with a Philips PW1400 Wavelength Dispersive XRF; ~2g samples were ignited at 970°C and fused into glass beads using Spectraflux 100 lithium metaborate flux for major element determination, while 10g samples were pressed as pellets for trace element determination. A fragment of serpentinite a few cm in diameter from core 343 was also ground and analyzed by XRF for major and trace elements. To ensure accuracy of response of the XRF for trace elements in these $CaCO_3$-rich sediments, a set of 5 pellets was made up from pure $CaCO_3$ mixed with varying amounts of international shale standard SCo-1. The XRF showed a linear response to increasing proportions of $CaCO_3$ in the samples for all trace elements of interest, within 1% of expected values (Appendix 1). Other international standards run simultaneously with the samples were BEN, JDo-1 and BRR-1.

To determine sediment accumulation rates, radiometric radiocarbon dating was undertaken on the CO_2 released from the bulk carbonate of 30g samples at 5cm spacing from each Rainbow core (Table 2.4). The uppermost 10cm of each core was analyzed by gamma-spectrometry in 1cm increments to determine $^{210}Pb_{excess}$ (= total ^{210}Pb measured minus ^{226}Ra measured (Thomson *et al.*, 2000)) to determine the depths of mixing achieved by active bioturbation.

In order to determine the hydrothermal component in the Rainbow core sediments, sediment of a similar provenance and composition to the detrital component was required to define background elemental levels. Cores collected during the Biogeochemical Ocean Flux Study (BOFS) were selected to represent this background material (cores 22#6M and 23#12M in Table 2.1; Shimmield, 1990) and analysed in the same manner as the Rainbow core samples. These background core sites are a few degrees south of the latitude of Rainbow and several degrees to the east of the MAR, and had been previously analyzed for $^{210}Pb_{excess}$ and radiocarbon dated (Thomson *et al.*, 1993).

3.3 Results and Discussion

3.3.1 Sediment accumulation rates and the surface mixed layer

^{210}Pb is a relatively short-lived radioisotope ($t_{1/2}$ = 22.7yrs) so that it persists in surficial sediments for only about 100 years after deposition from the water column. In the absence of bioturbation, all $^{210}Pb_{excess}$ present would therefore be expected to be present in the upper few millimetres of deep-sea sediments since they accumulate at rates of cm.ky^{-1} (Cochran, 1992). In fact, bioturbation has mixed $^{210}Pb_{excess}$ down to -7cm in Rainbow cores 343 and 316 closest to the vent site, and to >10 cm in cores 325 and 329 (Fig. 3.1). These must be considered minimum estimates of the surface mixed layer (SML) depth in these cores, because intercomparisons have shown that longer-lived radionuclides like ^{14}C generally indicate deeper SMLs than $^{210}Pb_{excess}$ (Thomson *et al.*, 2000). In core 329 for example, a live echiuran with a full sac of faecal pellets was recovered at about 12cm depth. Burrows at this level and above tended to be green, likely due to decomposing organic matter brought down by burrowing organisms, while burrows deeper in the sediment were white, indicating that oxidation had taken place at these deeper levels and that burrowing no longer operated.

Mean sediment accumulation rates for the Rainbow cores were calculated using the ^{14}C dates reported in Table 2.4 and by assuming that the 5 cm sample in each case provides a suitable estimate of the SML age. Mixed layer ages varied from 3.1-4.6 ^{14}C kyr (Fig. 3.2 a-d), and below the SML mean sediment accumulation rates are calculated that range from 2.7-3.8 cm.kyr^{-1} during the Holocene (Fig. 3.2 a-d). This range is consistent with other N. Atlantic cores at this latitude both inside and outside the MAR rift valley (Balsam, 1988; Dennielou *et al.*, 1999; Nozaki *et al.*, 1977). The BOFS cores display slightly lower Holocene accumulation rates of 1.5-1.9 cm.kyr^{-1} (Fig. 3.2 e,f). The bottom 10cm of sediment in the longest core (343) was paler in colour than the other sediments recovered, and a lower pre-Holocene accumulation rate of 1.1cm.kyr^{-1} is estimated for this section (Fig. 3.2 a).

Taken together, the $^{210}Pb_{excess}$ and ^{14}C data indicate that all four Rainbow cores are slowly accumulated with well-developed SMLs. The combination of bioturbation and slow accumulation means that it is not possible to discern rapid fluctuations in hydrothermal input through changes in sediment composition in these cores.

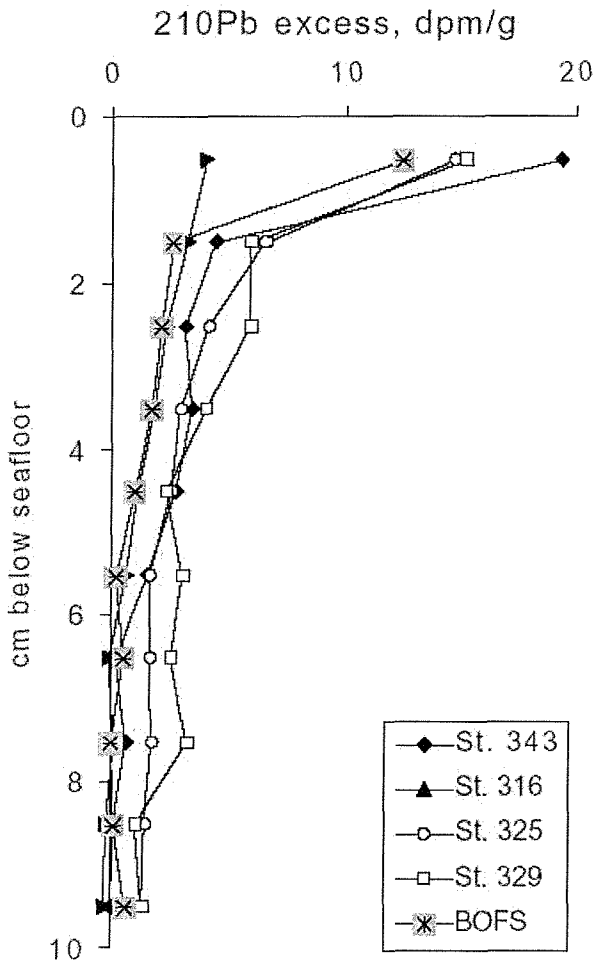

Figure 3.1: ^{210}Pb in Rainbow cores defining bioturbational mixing depth. Apparent mixing depth ($^{210}Pb_{excess} = 0$) is ~7cm in the two proximal cores (343 and 316), but increases to ¿10cm in the more distal cores (325 and 329). BOFS core 23#12M is shown for comparison (data from Thomson et al., 1993).

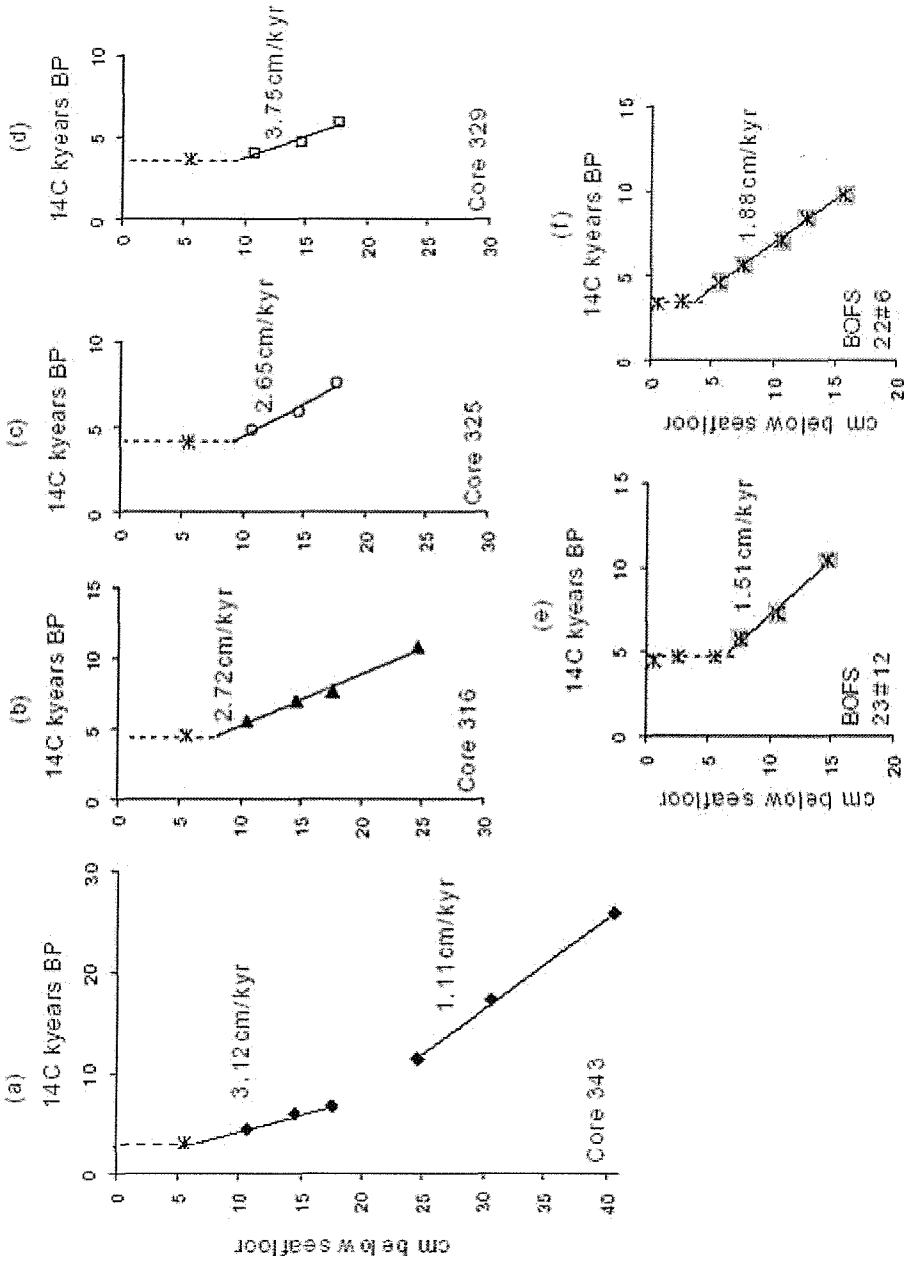

Figure 3.2: Sediment accumulation rates for Rainbow and BOFS cores, from bulk radiocarbon dating.

Asterisks indicate the samples from the surface sediment mixed layer; dashed lines indicate the apparent depth of the mixed layer. BOFS data are from Thomson et al., (1993).

3.3.2 Composition of the Rainbow cores

The compositional data for the cores (Appendix 2) reveal that the Rainbow cores consistently contain 80-87% $CaCO_3$, (Fig. 3.3 a), a value typical for Holocene sediments on the MAR and over most of the central N. Atlantic (Balsam and McCoy, 1987; Cremer *et al.*, 1992; Lisitzin, 1996). The Corg content is less than 0.5% in all samples, reflecting the low sedimentation rate and oxic bottom water conditions. Aluminium concentrations vary from 0.5-0.8%, Fe contents from 1%-2%, and Ti/Al ratios for all samples lie between 0.07 and 0.12 with the lowest values in the deepest section of the longest core (Fig. 3.3b). The $CaCO_3$ content of the BOFS core sediments varies from 80-83% (Fig. 3.3 a), with an Al concentration of 1.2-1.4%, and Fe from 0.8-0.9%. Aluminium is generally taken to be 8-10% of the total detrital input (Lambert *et al.*, 1984; Taylor and McLennan, 1985). The BOFS cores are assumed to be a simple mix of biogenic $CaCO_3$ and continental detritus, and their Ti/Al ratios vary between 0.08 and 0.10, similar to the Rainbow cores (Fig. 3.3 b).

The input of continental detrital material at Rainbow is low. The area lies beneath the Azores-Bermuda high-pressure system, at the northernmost edge of the summer east-west transport path for N. African dust (Arimoto *et al.*, 1995; Kuss and Kremling, 1999b; Perry *et al.*, 1997). Numerous studies have documented the aeolian flux of particulate material, primarily Saharan dust, from the N. African continent across the N. Atlantic from measurements made on Barbados and Bermuda (Arimoto *et al.*, 1995; Delany *et al.*, 1967), in the continental USA (Perry *et al.*, 1997; Prospero, 1999) and from satellite data (Prospero *et al.*, 1999; Li *et al.*, 1996)(Fig. 3.4). Studies of sediments lying under the path of the North-East Trades also indicate that the bulk of the detrital component in the sediments from the E. Atlantic and across the Mid-Atlantic Ridge between 5-35^{o}N has N. African sources (Balsam *et al.*, 1995; Chester, 1982; Jickells *et al.*, 1998; Zimmermann, 1981). The Rainbow area lies within the MAR rift valley and is protected by the valley walls from continental turbidite inputs, so that the bulk of the detrital input to the sediments can be expected to be from this aeolian source. The background BOFS samples are also from the northern part of the region covered by the dust envelope and similarly have high carbonate contents (>75%) and low sedimentation rates (<2 cm.kyr^{-1}). A comparison of Ti/Al ratios in published core data from similar north-east Atlantic latitudes (Fig. 3.5) reveals that the continental material in the Rainbow and BOFS cores is most likely derived from the same sources, because north-western Atlantic cores from a similar latitude display much lower Ti/Al ratios (< 0.05; Carpenter *et al.*, 1983). Consistent with this, physical oceanographic

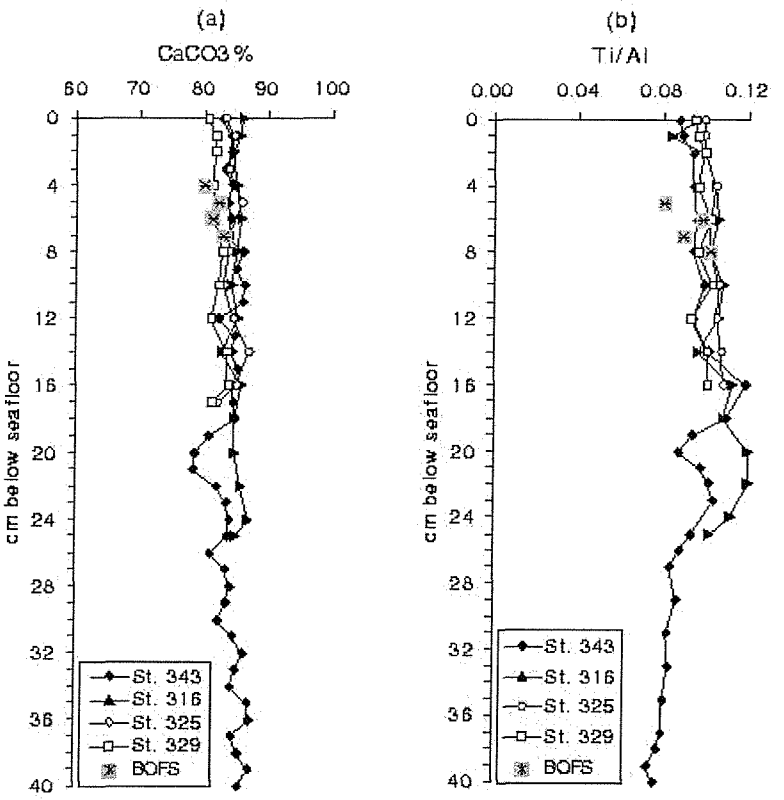

Figure 3.3: (a)%$CaCO_3$, and (b)Ti/Al in Rainbow and BOFS cores. The carbonate content is similar in all the cores. Note the expanded scale for $CaCO_3$ on the x-axis. Ti/Al ratios fall within a narrow range throughout all the cores, indicating similar provenance through time for the continental detrital component, but are lowest in the deeper section of core 343.

data for deep-waters within the rift-valley at Rainbow are also indicative of deep-water inflow from the NE Atlantic rather than from the NW Atlantic (Thurnherr and Richards, 2001; Thurnherr *et al.*, in press). For this study, therefore, it is assumed that the carbonate-free data for the BOFS cores can be taken as representative of the continentally-derived detritus contributing to the bulk composition of the Rainbow cores.

Bostrom *et al.*, (1969) proposed the index $100 * Al/(Al + Fe + Mn)$ to enable discrimination between metalliferous and non-metalliferous pelagic sediments. This index assumes that Al in pelagic sediments is derived wholly from continental sources, and that Fe/Al and Mn/Al ratios for continental detritus have a narrow range of values. Pelagic sediments composed solely of a mixture of biogenic and detrital material have an index of >50, as seen in the index of ~60 for the BOFS sediments (Fig. 3.6). Sediments with a large hydrothermal component exhibit much lower index values, and the index

Fig. 3.4 Saharan dust over the N. Atlantic.
Composite image from the SeaWIFS satellite, courtesy of NASA's Visible Earth website, http://visibleearth.nasa.gov/browse.html. Star marks the approximate location of the Rainbow vent site. Large dust plumes from N. Africa regularly sweep across the Atlantic and are sampled by monitoring stations on the western side of the Atlantic located on Barbados and Bermuda.

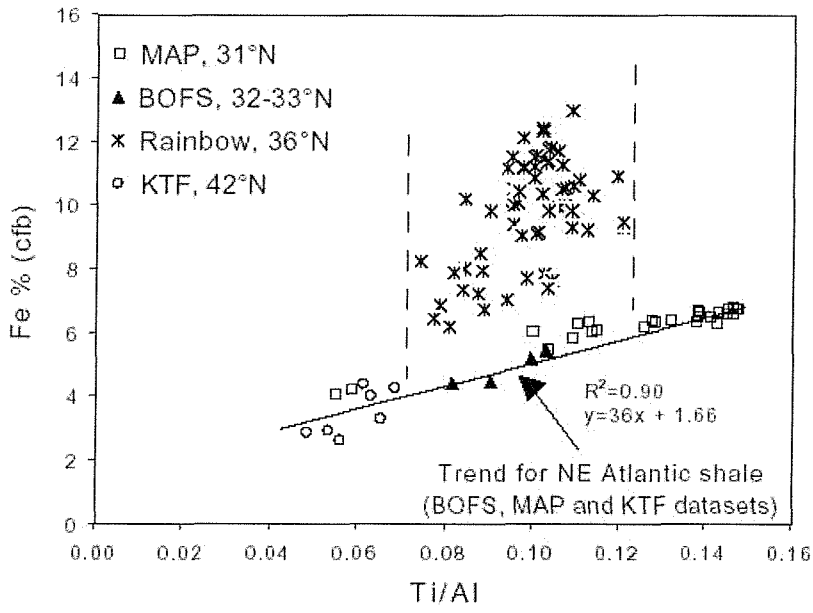

Figure 3.5: %Fe (carbonate-free basis [cfb]) vs. Ti/Al for Rainbow and other N. Atlantic cores.
Rainbow and BOFS data (this work); MAP = Madeira Abyssal Plain turbidites a and b (Pearce and Jarvis, 1992; Pearce and Jarvis, 1995); KTF = core 10708# from the King's Trough Flank (Booty, 1985). All the Rainbow data fall within the Ti/Al range for eastern N. Atlantic sediments, indicating a similar provenance for their continental detrital component, but show excess Fe over N. Atlantic background, consistent with a hydrothermal overprint.

is 20-25 for the upper (Holocene) parts of all the Rainbow cores, although in the longer cores (316 and 343) it rises to values of 35-37 at depths >20cm (Fig. 3.6). The index data therefore indicate a significant hydrothermal component in the Holocene sediments of the Rainbow cores, with a lesser hydrothermal component in the older sediments that are present only in the two longer cores.

When the average compositions of elements from the SML of the Rainbow cores are compared with N. Atlantic background values derived from the BOFS samples, consistent enrichments of P, V, Mn, Fe, Cu (Fig. 3.7) and As (not shown in Fig. 3.7) are evident. All of these elements are commonly enriched in hydrothermal plume particulates (e.g. German *et al.*, 1991). Examination of the downcore profiles of Cr/Al and Ni/Al in the four cores (Fig. 3.8), however, reveals evidence for highly-localized enrichments in Cr and Ni at specific horizons in cores 343 and 316 only, coincident with depths at which rock fragments were found at the time of sampling. Ultrabasic rocks are enriched in both Cr and Ni compared to continental crust (Turekian and

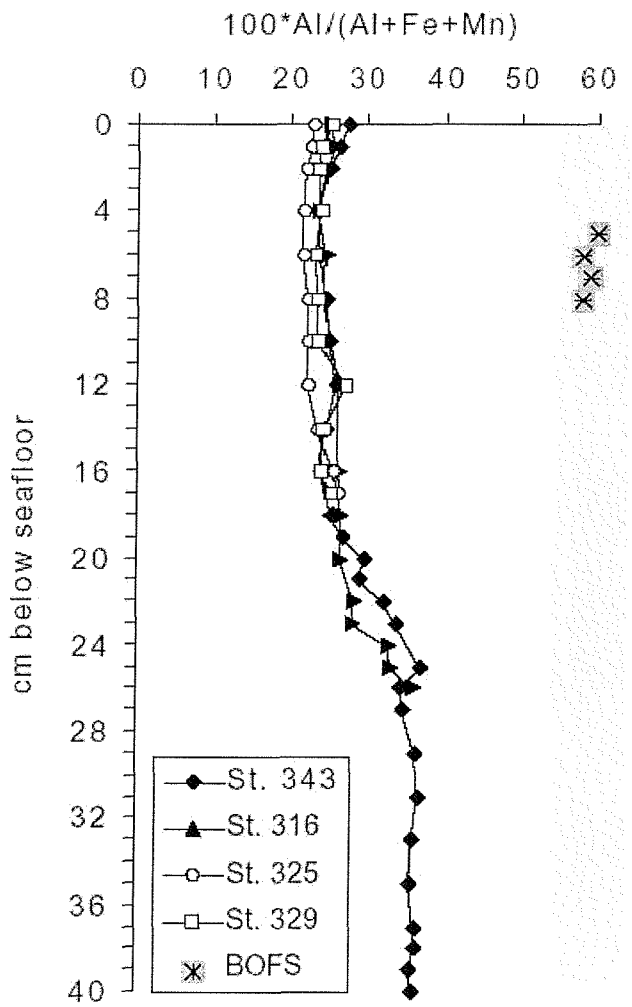

Figure 3.6: Metalliferous sediment index (Bostrom and Peterson, 1969c) for Rainbow and N. Atlantic core samples.
The shaded area represents the range observed worldwide for detrital material. Highly metalliferous sediments such as are found immediately surrounding hydrothermal vents would have and index <10. Note the shift towards more detrital values below 20cm in cores 316 and 343.

Wedepohl, 1961), and it appears that the ultramafic material that outcrops around the Rainbow vent site has delivered significant enrichments of Ni and Cr to the near-field cores, without noticeably affecting their Ti or Al content. Consistent with this, the fragments recovered from cores 343 and 316 were all serpentinised ultramafic rocks.

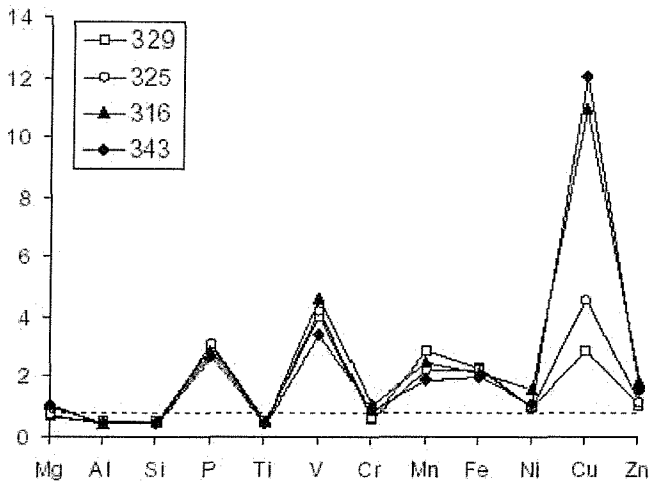

Figure 3.7: Mean concentrations of surface mixed layer (SML) samples from each of the Rainbow cores, normalised to mean concentrations of the BOFS sediments. Peaks at P, V, Mn, Fe and Cu are due to enrichments in the sediments caused by fallout from the hydrothermal plume. Arsenic enrichments (not shown) are of the order of x 40. elements are shown in order of increasing atomic number.

3.3.3 Estimation of the different sedimentary components

Four components have been identified in the Rainbow cores: (a) a biogenic $CaCO_3$ component (b) a continentally-derived detrital component (c) a hydrothermal component, and (d) a locally derived ultramafic component that is present at certain levels in cores 343 and 316 only. The $CaCO_3$ component of the sediments has been measured directly (Appendix 2), and is assumed to make a negligible contribution to the range of metals of interest. The hydrothermal component is calculated by subtracting the contributions of the other different components identified above from the bulk composition. The elemental ratios used to calculate the continental detrital and ultramafic contributions for each element of interest are shown in Table 3.1. See Methods chapter, section 2.2.9, for equations.

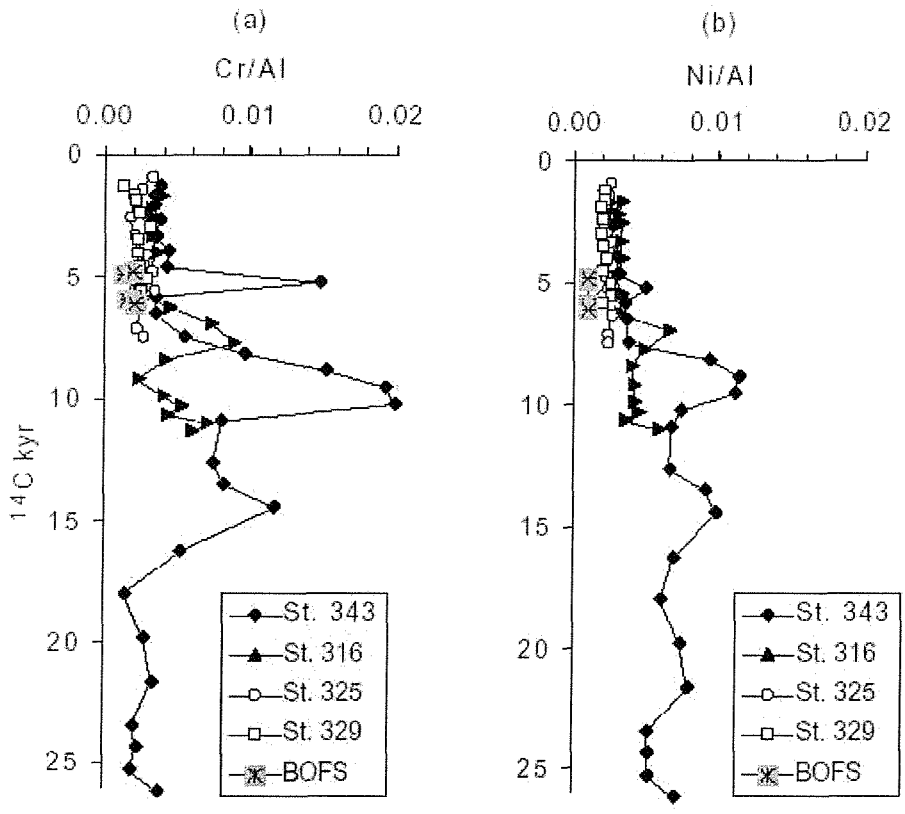

Figure 3.8: The contribution of ultramafic detritus in the Rainbow cores. Departures from the baseline values of ~0.002 for Cr/Al and Ni/Al indicate the localised presence of ultramafic rock fragments at these levels.

3.3.4 Hydrothermally sourced elements Fe, Cu, and Mn

The hydrothermal Fe component is at constant concentrations back to 8 ^{14}C ky in the longer cores 343 and 316 that are located nearer the vent field, and then decreases with depth from 8-12 ky (Fig. 3.9a). Cores 325 and 329 are too short for any corresponding change with time to be seen and hydrothermal Fe levels are constant throughout.

Like Fe, hydrothermal Cu shows a marked increase up-core between 12 and 8 ^{14}C kyr in the two near-field cores (Fig. 3.9b). Earlier than 12 ky, hydrothermal Cu is present in core 343 at concentrations similar to those found in the Holocene sediments in cores 325 and 329. Trocine and Trefry (1988) collected suspended particles from the TAG hydrothermal area (26^{o}N on the MAR) and found that particulate Cu, Zn and Cd decreased dramatically with distance from the vent site compared with Fe. They attributed this to the rapid removal of Cu, Zn and Cd from the plume in sulfide-bearing phases. A similar explanation fits the observations in the Rainbow cores, where

Ratio	BOFS	Ratio	Serp.
Fe/Al	0.6700	Fe/Ni	59.0000
Cu/Al	0.0035	Cu/Ni	0.0780
Mn/Al	0.0260	Mn/Ni	0.9200
V/Al	0.0023	V/Ni	0.0360
P/Al	0.0250	P/Ni	0.0520
As/Al	0	As/Ni	0.0087
Cr/Al	0.0020		
Ni/Al	0.0010		

Table 3.1: Elemental ratios for calculation of sediment components. Element to Al ratios from the BOFS core samples have been averaged and are used to calculate the continental detrital component of the Rainbow sediments. Element to Ni ratios from the serpentinite piece recovered from core 343 are used to calculate the component derived from local outcrops.

Cu concentrations decrease rapidly with distance from the vent site (Fig. 3.9b) while Fe concentrations remain similar or even increase (Fig. 3.9a). The hydrothermal Cu contents are 4 times higher at the most proximal compared to the most distal core site (Fig. 3.9b). Zinc, which is present in Rainbow fluid at similar molar concentrations to Cu (Douville *et al.*, 2002), is present at an order of magnitude lower concentration than Cu in the Rainbow core series. This indicates that, by comparison with Cu and Fe, Zn must be preferentially precipitated as sulfides closer to the vent site.

The hydrothermal Mn component is present at similar levels in cores 343, 316 and 325, but the most distal core, 329, has significantly higher Mn concentrations (Fig. 3.9c). The concentration of hydrothermal Fe is also highest in this core, but the difference in Fe content between the cores is much less marked than for Mn. Near-surface Mn enrichments formed by early diagenesis are common in deep-sea sediments. They are caused by the reduction of oxic forms of Mn once they are buried into reducing conditions at depth. This reductive mobilisation then allows a diffusion of Mn^{2+} back upwards into oxic conditions where it is re-precipitated as Mn oxyhydroxides. By this mechanism, solid-phase Mn enrichments may be formed in the oxic SML or as peaks a few centimeters in width tens of centimeters below the sediment/water interface. In particular, such peaks can form at or below the glacial/Holocene boundary (Thomson *et al.*, 1996; Wallace *et al.*, 1988; Wilson *et al.*, 1986). In order for reducing conditions

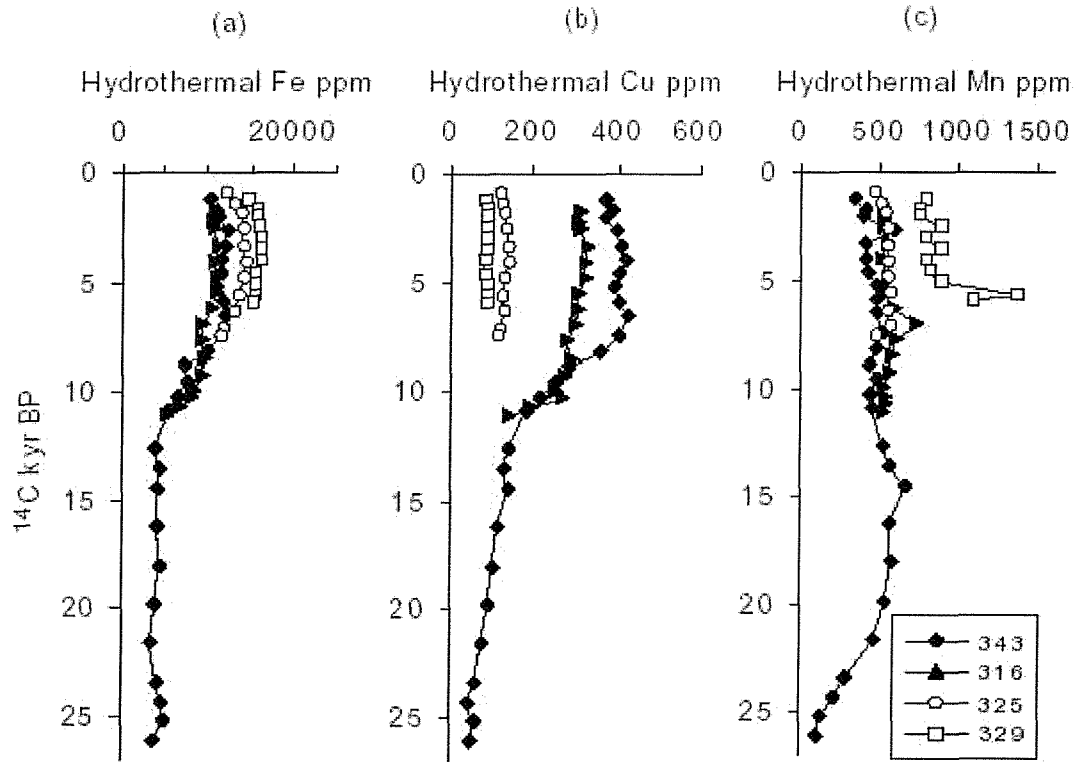

Figure 3.9: (a) Fe, (b) Cu, and (c) Mn in Rainbow sediments. Hydrothermal concentrations have been calculated by subtracting the detrital and ultramafic components from the total values. See Table 3.1 and Methods chapter for details of calculations. Cores listed in order from proximal (core 343) to distal (core 329). Error is +/−5%.

to develop, however, sedimentation rates must be high enough to bury organic matter below the zone of oxygen penetration before it can be oxidized (Wilson *et al.*, 1985), so that relatively organic-rich, rapidly-deposited sediments favor formation of diagenetic Mn peaks. The Rainbow sediments are accumulating at 2.6-3.7cm kyr^{-1}, under oxic bottom water conditions, and have a uniformly low organic carbon content (Appendix 2). The excess Mn in cores 343, 316 and 325 is uniform over several centimeters down-core (Fig. 3.9c), and it seems most likely, therefore, that the excess Mn in these cores is from a hydrothermal rather than a diagenetic source. Core 329 does have a narrow peak in the excess Mn at the bottom of the core (17cm depth), and it is possible that some of the hydrothermal Mn at this level in this core has been remobilized and redeposited in a small peak. No pore water data is available for these cores, but the other evidence points to the excess Mn in these cores being of hydrothermal rather than diagenetic origin, at least at the depths of sediment that were obtained in this study. The larger overall excess Mn in core 329, 25km downstream from the vent site, compared to the near-field cores is therefore likely to be a result of the slower oxidation kinetics of hydrothermal Mn in seawater compared with Fe (Cowen *et al.*, 1990), leading to increased fallout of Mn from the plume with distance from the vent site.

3.3.5 Element/Fe molar ratios for vent-derived Cu and Mn

Over the last 8 ^{14}C kyr, both the hydrothermal Cu/Fe ratios (Fig. 3.10) and Cu concentrations (Fig. 3.9b) are higher in the proximal Rainbow cores 343 and 316 than in the distal cores 325 and 329. This indicates that sulfidic plume particles are transported at least 5 km from the vent site. Although concentrations of both Cu and Fe in Rainbow vent fluids are very high compared to other MAR vents, the Cu/Fe ratio of the Rainbow fluids is two to five times lower than that measured at other MAR sites (Douville *et al.*, 1997; Douville *et al.*, 2002). The Fe concentration of 24mM in Rainbow fluid is an order of magnitude greater than at any other site so far studied on the MAR, which with a concentration of Cu of 140μM, gives a Cu/Fe ratio in the fluid of ~$5.8x10^{-3}$. The Fe/H_2S ratio is also much higher in Rainbow fluids than at other MAR sites (Donval *et al.*, 1997), which is likely to increase the amount of Fe precipitated as oxide rather than sulfide phases in the plume by comparison with other MAR vent sites. The molar hydrothermal Cu/Fe ratios of the core tops closest to the vent site are 5 times higher than in the fluids, diminishing to more fluid-like values at the most distal site, 329 (Fig. 3.10a). This indicates that while Cu rapidly falls out of

the plume, presumably as sulfides, a large proportion of the Fe remains in suspension.

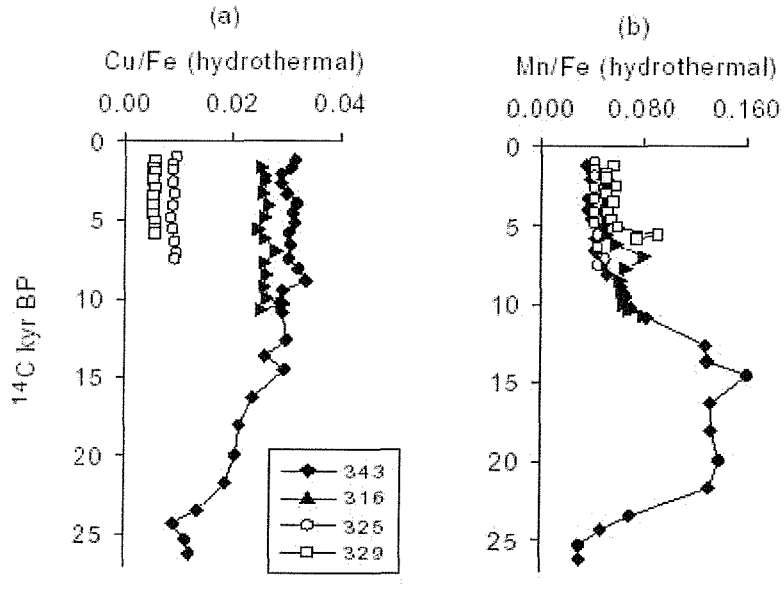

Figure 3.10: (a) Cu/Fe, and (b) Mn/Fe in Rainbow cores. Hydrothermal values have been calculated by subtracting detrital and ultramafic components from the total values. See Table 3.1 and Methods chapter for details of calculations. Cores listed in order from proximal (core 343) to distal (core 329).

In the Rainbow core SMLs, molar ratios of hydrothermal Mn/Fe lie between 0.03 in the near-field cores and 0.05 in the far-field cores (Fig. 3.10b). Manganese has slower oxidation kinetics in seawater than Fe (e.g. Cowen *et al.*, 1990), so that in hydrothermal plumes the Mn/Fe ratio of deposited particles is expected to increase with distance from the source. The Mn/Fe ratio of the Rainbow vent fluids is ~0.08 (Chiba *et al.*, 1999) so the indication is that even at ~25km downstream, only a small proportion of the Mn has had time to oxidize and precipitate. This is borne out by the consistently high dissolved Mn values measured in the water column of the axial valley north of the Rainbow vent site (Aballea *et al.*, 1998; Radford-Knoery *et al.*, 1998) and is also consistent with the short time (order 4 days) estimated for plume waters to reach this corner of the Rainbow NTD near 36°20'N (German *et al.*, 1998a).

For the deeper samples in core 343, the hydrothermal Cu/Fe decreases and Mn/Fe increases in sediments older than 12 ^{14}C kyr, both indicating a more distal source for the hydrothermal component in this core prior to the Holocene. The lowest Cu/Fe and Mn/Fe values in core 343 are found at the very base, with both ratios exhibiting values similar to those found at the top of core 325. Absolute concentrations of Fe, Cu

and Mn are also much lower at the base of core 343 than at the top, suggesting that high-temperature venting was having less impact at this core site before 25 ^{14}C kyr.

3.3.6 Scavenged elements V, P and As

Total V, P and As concentrations are strongly enhanced in the Rainbow cores compared to the respective mean BOFS core values of 31 ppm, 325 ppm and <1 ppm (see Appendix 2b). However, based on the BOFS core element/Al ratios, the detrital concentrations of these elements in the Rainbow cores should only be ~50% of the mean BOFS values. The estimated V, P and As hydrothermal components all show very similar trends to their total concentrations (Fig. 3.11 a-c).

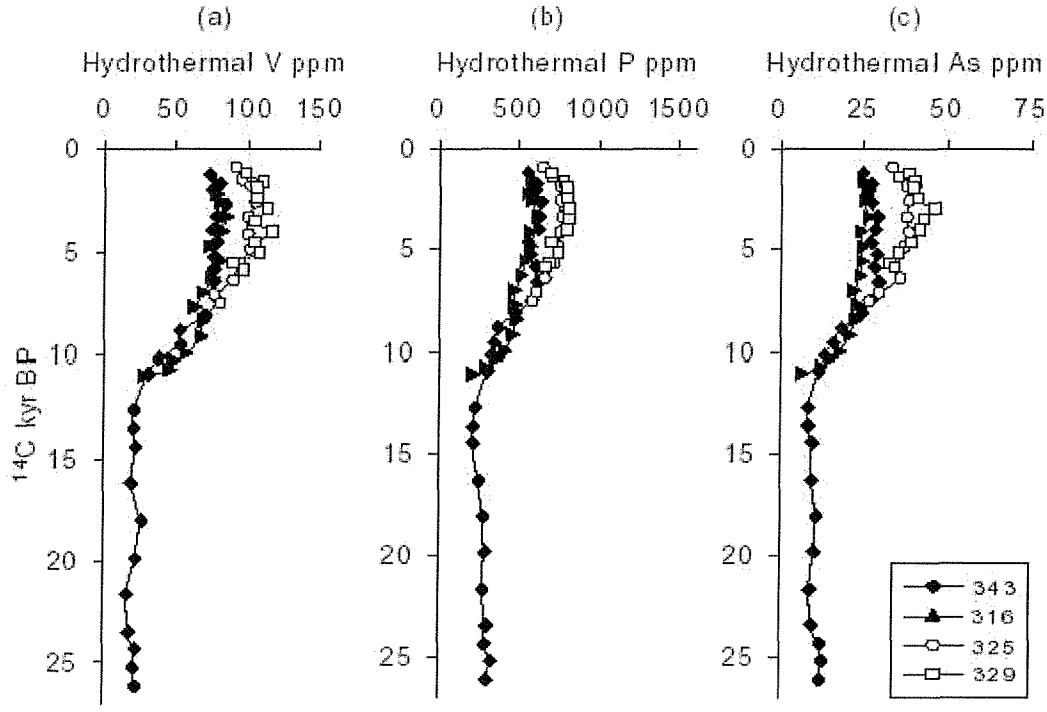

Figure 3.11: (a) V, (b)P, and (c) As in Rainbow cores. Hydrothermal values have been calculated by subtracting detrital and ultramafic components from the total values. See Table 3.1 and Methods chapter for details of calculations. Cores listed in order from proximal (core 343) to distal (core 329). Error is +/−5%

Most of the V in the Holocene sections of the Rainbow cores can be attributed to scavenging of V from seawater by hydrothermal particles. The situation for hydrothermal P is a little more complicated. Most slowly-accumulated marine sediments contain

more P than can be accounted for by the detrital component alone. This 'excess' P was initially attributed to the biogenic carbonate fraction (Froelich *et al.*, 1982), but Sherwood *et al.* (1987) demonstrated that P was not a constituent of the carbonate itself but was rather associated with Fe-Mn coatings on biogenic particles in slowly accumulating sediments. An overview of current hypotheses on the accumulation of P in marine sediments is given by Delaney, (1998). Bulk P/Al in the Rainbow cores is ~0.14, while the BOFS cores and Madeira Abyssal Plain turbidites have a P/Al of 0.02-0.03 (Pearce and Jarvis, 1995). The P/Al ratio in shale is lower at <0.01 (Carpenter *et al.*, 1983; Turekian and Wedepohl, 1961). Calculations of hydrothermal P in the Rainbow sediments have therefore been based on the P/Al ratios of the high carbonate content BOFS samples (Table 3.1). A mean detrital value of P/Al = 0.025 indicates that about two thirds of the P in the Rainbow cores is associated with the hydrothermal component.

Arsenic is present in very low concentrations in most crustal materials, with an average crustal abundance of <2 ppm (Onishi, 1970). Arsenic has been measured in hydrothermal fluids (Douville *et al.*, 1999) and in suspended particles from hydrothermal plumes at a number of sites (German *et al.*, 1991; Feely *et al.*, 1991; Feely *et al.*, 1994) and high As concentrations have been noted in high-carbonate ferruginous sediments from various locations on the MAR (Cronan, 1972; Grousset and Donard, 1984). In this study, As for the BOFS samples was below detection levels (<1 ppm) while As in the Rainbow sediments varied from 7 - 46 ppm. Like V, the As in the Rainbow sediments (Fig. 3.11c) is therefore taken to be entirely derived from hydrothermal scavenging because the contribution of both As and V from ultramafic fragments is negligible.

3.3.7 Element/Fe molar ratios for scavenged V, P and As

The sediments accumulating downstream from the Rainbow vent complex show hydrothermal V/Fe molar ratios of 0.006-0.007, decreasing to values of 0.004-0.005 only in the deeper sediments from core 343 (Fig. 3.12a). By contrast, hydrothermal P/Fe molar ratios increase with depth (0.09-0.14; Fig. 3.12b) and hydrothermal As/Fe ratios (Fig. 3.12c) are very similar at ~0.002 throughout the cores and show no apparent change in trend between modern and pre-Holocene samples. Dissolved V and P in seawater compete for sorption sites on Fe-oxyhydroxides within hydrothermal vent plumes. In a comparative Atlantic/Pacific study, Feely *et al.*, (1998) concluded that differences in dissolved seawater P concentration affect the process, with waters higher in dissolved

P (e.g. Pacific Ocean) leading to higher P/Fe and lower V/Fe ratios in hydrothermal particles due to sorption site competition.

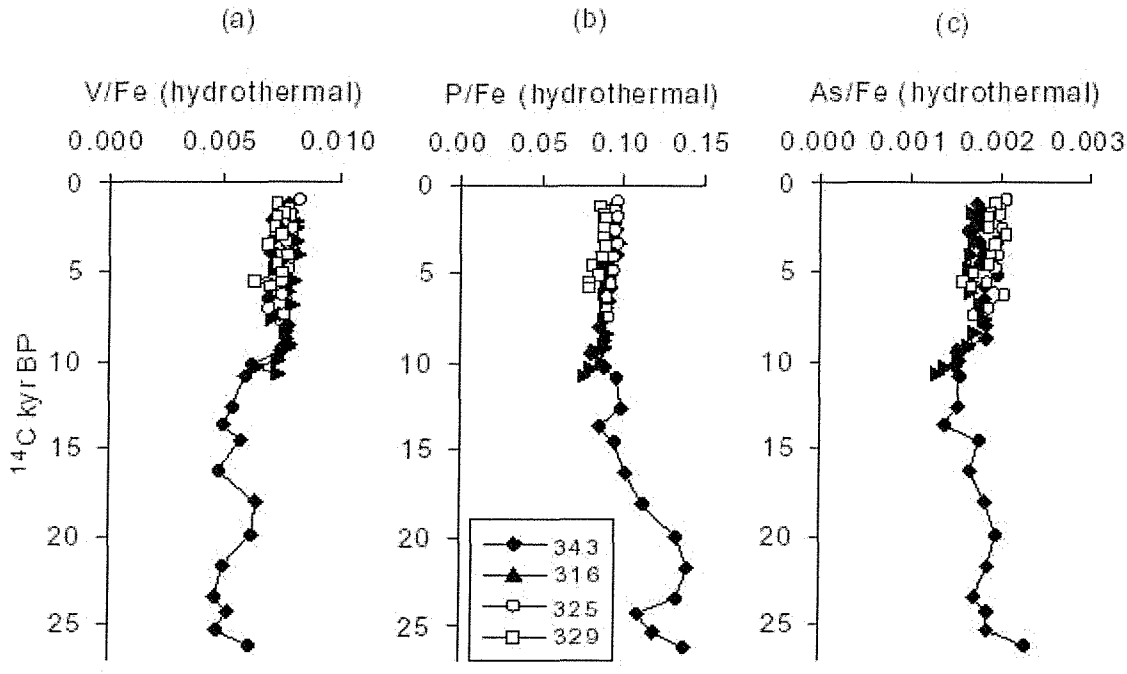

Figure 3.12: (a) V/Fe,. (b) P/Fe and (c) As/Fe molar ratios in Rainbow sediments. Hydrothermal values have been calculated by subtracting detrital and ultramafic components from the total values. See Table 3.1 and Methods chapter for details of calculations. Cores listed in order from proximal (core 343) to distal (core 329).

At the Atlantic TAG hydrothermal site, particulate Fe scavenges V from seawater with an average molar V/Fe ratio of 0.005 (Trocine and Trefry, 1988), and particles in the Rainbow plume have the same average molar V/Fe ratio (Edmonds *et al.*, 1998). Ratios of hydrothermal V/Fe in Atlantic sediments might be expected to reflect these particulate values, but the Rainbow SML sediments have higher hydrothermal V/Fe molar ratios of ~0.007 (Fig. 3.12) and decrease to values of 0.005 only below 10 ^{14}C kyr. Metalliferous sediments from the vicinity of the TAG vent site also show a similar variability in V/Fe ratios compared with plume particles (Metz *et al.*, 1988). Hydrothermal P/Fe in the Rainbow core tops has a molar ratio of 0.08-0.10, which is intermediate between the P/Fe molar ratios of 0.12 found by Feely *et al.*, (1998) for Fe-oxyhydroxide particles from the TAG plume and the values of 0.06 ±0.02 measured in plume particulate material at Rainbow (Edmonds *et al.*, 1998).

Although all calculated V/Fe, P/Fe and As/Fe ratios throughout all the Rainbow cores fall within the range for previously reported MAR plume particulates, the observation that hydrothermal V/Fe and P/Fe ratios are uniform for sediments younger than 10 ^{14}C kyr, but show variations in V/Fe and P/Fe earlier than 10 kyr is intriguing - not least because a) the variation is apparently synchronous and b) dissolved concentrations of P in seawater have been shown to affect the uptake of V into/onto hydrothermal particles (Feely *et al.*, 1998). Taken together, therefore, it is tempting to speculate that these observations could be indicative of some change in the nature of the ambient deep water at this site in pre-Holocene times. Thurnherr and Richards (2001) have shown that the present-day deep water in the Rainbow area of the rift valley is recirculating deepwater from the N.E. Atlantic. A comprehensive analysis of the deep water masses in the mid-latitude N.E. Atlantic by van Aken, (2000) shows that modern N.E. Atlantic deep water (NEADW, below -2000m) is composed of a mixture of four water masses (Labrador Deep Water, Mediterranean Surface Water, Iceland-Scotland Overflow Water and Labrador Surface Water), each with characteristic salinity, dissolved oxygen and nutrient properties. The variation in the concentration of dissolved PO_4 in these water masses is striking: Labrador Deep Water (1.5mmol/kg) contains almost double the Mediterranean Surface Water concentration (0.79mmol/kg) while the remaining two water masses contain 1.02 and 1.12 mmol/kg PO_4 respectively (van Aken, 2000). Over the Madeira Abyssal Plain, at the same latitude as Rainbow, the upper NEADW is estimated to contain 42% Labrador Deep Water (van Aken, 2000). If this proportion were to increase, as may have been the case prior to the Holocene when deep water formation in the N. Atlantic may have moved further to the south (Ganopolski *et al.*, 1998), then - assuming inflow to the MAR rift-valley continued to be sourced from the NE Atlantic - the concentration of dissolved P in the water flowing into the rift valley would also increase, and this would be expected to be reflected in the P/Fe ratio of hydrothermal sediments being deposited at this time.

Concentrations of As vs. total Fe in the Rainbow sediments (Fig. 3.13a) show a similar trend to that reported previously in rift valley sediments (Cronan, 1972). When the detrital Fe component is removed from the Rainbow sediments ((Fig. 3.13b), the Rainbow values then compare well with As/Fe ratios found by German *et al.*, (1991) and Metz and Trefry (1993) for particles in the neutrally buoyant plume at TAG, 26^{o}N on the MAR, providing confirmation that the method used for calculating the hydrothermal component in the Rainbow sediments is valid. Further, because As is present in very low levels in detrital sediments (undetectable in the BOFS samples by XRF in this work) it is also clear that hydrothermal plume-fallout can represent a

significant source of As to sediments close to hydrothermal systems.

3.3.8 Fluxes of elements into Rainbow sediments

Total sediment accumulation fluxes have been calculated using the mean bulk dry density measured (~0.7 g.cm^{-3} for all cores) and the linear accumulation rates estimated above from radiocarbon data. Core 343 has a higher sediment accumulation rate during the Holocene (average 2.17 g.cm^{-2}.kyr^{-1}) than in the pre-Holocene (0.77 g.cm^{-2}.kyr^{-1}). Because bioturbation will have smoothed the sediment record, it is not possible to determine an exact time at which the change in sedimentation rates occurred, or whether this change was abrupt or gradual. The data indicates that it occurred between 8 and 12 ^{14}C kyr (Fig. 3.2a). There is a hint of a similar change in the compositional data from core 316, but the radiocarbon data are insufficiently detailed to confirm this and so a regression line has been drawn assuming the sedimentation rate to be uniform (Fig. 3.2b). While a sedimentation rate of ~2cm kyr^{-1} is typical for the MAR and the N. Atlantic in general during Holocene times (Balsam and McCoy, 1987), the lower sedimentation rate during glacial times indicated in core 343 is the reverse of what is generally observed. In most N. Atlantic cores, an increase in sedimentation rate is observed during the last glacial due to increased fluxes of terrigenous material.

The hydrothermal fluxes for elements with a significant hydrothermal component (Table 3.2) can be compared with authigenic fluxes of the same elements to clays from the Nares Abyssal Plain (NAP; Thomson *et al.*, 1984). The authigenic flux is an order of magnitude less for Fe, Cu, and V, but is comparable for Mn, while authigenic flux data for As and P are not available. Nevertheless, the P_2O_5 content of the NAP clays ranges from 0.15-0.20% (Carpenter *et al.*, 1983) compared to average shale values of 0.16%, indicating a maximum authigenic flux for P that, like V, is 1-2 orders of magnitude less than the modern day hydrothermal flux at Rainbow.

Vent-derived elements: Fe, Cu , Mn

During the Holocene, mean accumulation fluxes of hydrothermal Fe in Rainbow cores vary from 368-718 μmol.cm^{-2}.kyr^{-1} (Table 3.2), with the greatest accumulation in the more distal cores, while accumulation rates of Cu vary between 3.5-12 μmol.cm^{-2}.kyr^{-1} with maximum accumulation rates in the most proximal cores. Hydrothermal Mn is accumulating at 16-37 μmol.cm^{-2}.kyr^{-1}, with a maximum accumulation of about twice that of the other 3 stations occurring in the most distal core 329. Pre-Holocene accu-

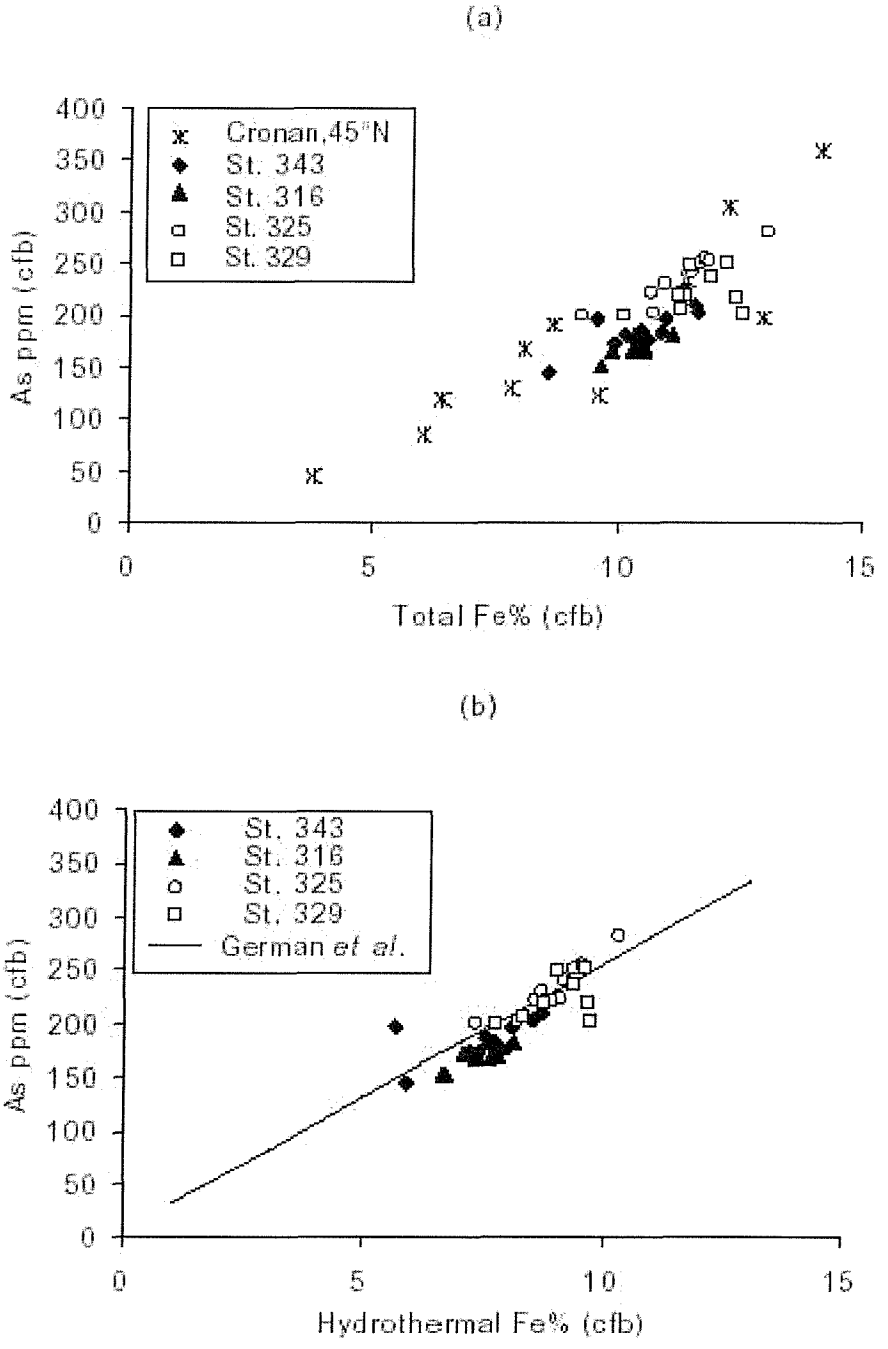

Figure 3.13: As and Fe in MAR sediments and plume particles.
(a) As vs. total Fe (carbonate-free basis) in Rainbow sediments. Bulk data for sediments from the median valley of the MAR at 45°N, described by Cronan (1972), are included for comparison. (b) Once the detrital and ultrabasic components have been subtracted from total Fe, the Rainbow samples fall on the regression line measured by German *et al.*, (1991) in in plume particles from the TAG hydrothermal site at 26°N on the MAR.

μmol.cm^{-2} .kyr^{-1}	Core 343	Core 316	Core 325	Core 329	Core 343>12ky	NAP hydrog.
Fe	410	368	426	718	67	28
Cu	12	9.4	3.7	3.5	1.3	0.4
Mn	16	18	17	37	6.7	22
V	3	3	3.3	5.3	0.3	0.12
P	39	36	41	64	7.6	n.a.
As	0.7	0.6	0.9	1.4	0.1	n.a.

Table 3.2: Element accumulation fluxes.
Average accumulation fluxes of hydrothermally derived elements in the surface mixed layer of the Rainbow cores (80% carbonate sediments) compared with mean pre-Holocene fluxes in core 343, and with authigenic fluxes to clays (<2% carbonate) from the Nares Abyssal Plain (NAP). NAP data are from Thomson *et al.,* 1984.

mulation rates and concentrations (core 343 only) are significantly less than Holocene values for all the elements of interest (Table 3.2): fluxes of Fe are about one sixth of Holocene values; for Cu, fluxes are about one tenth, and for Mn, about one third. Even at these much lower fluxes, however, Fe and Cu accumulation rates in the Rainbow sediments remain ca. 3 times greater than the authigenic flux into the NAP sediments.

Scavenged elements: V, P, As

These three elements are strongly associated with hydrothermal Fe in the Rainbow cores, so that accumulation fluxes for proximal cores 343 and 316 are similar to each other during the last 8ky but are less than the fluxes into more distal cores 325 and, especially, 329 (Table 3.2). The flux of scavenged V into the sediments is 3-5 μmol.cm^{-2}.kyr^{-1} for the upper part of the sediment column, falling to 0.3 μmol.cm^{-2}.kyr^{-1} prior to the Holocene (Table 3.2), but even this pre-Holocene flux exceeds the authigenic flux of V to the NAP clays. Hydrothermal P is accumulating in the Rainbow sediments at between 36-64 μmol.cm^{-2}.kyr^{-1} for the upper part of the sediment column, reducing to ~7 μmol. cm^{-2}.kyr^{-1} in pre-Holocene samples from core 343 (Table 3.2). Hydrothermal As is accumulating at 0.6-1.4 μmol.cm^{-2}.kyr^{-1} in the upper part of the sediment column at Rainbow, reducing to ~0.1 μmol. cm^{-2}.kyr^{-1} in pre-Holocene samples from core 343. NAP hydrogenous fluxes of As and P are not available.

3.3.9 Temporal variation in the Rainbow plume

The Rainbow cores provide the first quantitative flux data from a specific hydrothermal plume to sediments at distances up to 25km downstream from a common source. What is also known, however, is that the present Rainbow plume extends at least 50km to the north-east away from the vent-site, as measured from nephelometry, indicating that hydrothermal plume fall-out actually continues much farther afield than the most distal sites investigated here (German *et al.*, 1998c). Nevertheless, a minimum Fe-flux for the NTD between the Rainbow vent-field and the farthest core-site (329) can be determined by assuming: i) a plume area overlying the seafloor with a minimum width of 2km (German *et al.*, 1998c); ii) an along-flow extent of at least 25km (the distance to core 329) and iii) a representative minimum Fe flux of ca.400 μmol.cm^{-2}.kyr^{-1} (mean of cores 343, 316 and 325). This yields a total potential Fe flux into the sediments of this basin of 200,000 mol.yr^{-1} Fe which represents only about 0.1% of the total Fe flux estimated to be released from the Rainbow hydrothermal field based upon the Fe content of reported Rainbow hydrothermal fluids (ca. 24mM; Douville *et al.*, submitted) and the predicted vent-fluid flux (ca. 500L/sec; Thurnherr and Richards, 2001). Clearly, therefore, the total flux from Rainbow is not well represented by the cores presented here. What is important is the demonstration that these cores do, nevertheless, provide a faithful record of both the intensity and direction of output through the Rainbow hydrothermal plume.

The data from Rainbow suggest that vigorous high-temperature venting has been in operation at the same site for at least 8 ^{14}C ky, but the low sedimentation rates, coupled with bioturbation, do not allow distinction of whether venting has been continuous or episodic over that time. It has been shown that the TAG vent site (26°N on the MAR) has been active for the past 20,000 years or more (Lalou *et al.*, 1990; Lalou *et al.*, 1993) but it has also been suggested that the TAG mound could have been built up in as little as a few hundred years by short powerful bursts of hydrothermal activity and eroded during less active periods (Humphris and Cann, 2000). The Rainbow core data show significantly greater hydrothermal input to the sediments in the last 8 kyr than before 12 ^{14}C kyr. The control exerted by the topography on the local current regime (German *et al.*, 1998a; Thurnherr and Richards, 2001) means that there are two possible causes for this, which are considered in turn, below: (i) a reversal in the dominant current regime in the rift valley at 8-12 ^{14}C ky; (ii) an intensification of vent output, beginning at 8-12 ^{14}C ky.

(i) The high hydrothermal enrichments occur in Holocene sediments, and changes in the N. Atlantic circulation occurred as conditions changed from glacial to interglacial, culminating in the present-day N. Atlantic circulation pattern (Curry, 1996; Curry *et al.*, 1988; Clark *et al.*, 1999; Dokken and Jansen, 1999; Keigwin and Jones, 1989; Sarnthein *et al.*, 1994). It could be speculated, therefore, that during the glacial/interglacial transition the flow of water across the Rainbow sill may have been reduced, or net current flow may even have been in the opposite direction. Assuming the hydrothermal output from Rainbow before 12 ^{14}C kyr was similar to today, a reversed net flow of water over the sill would mean that the Rainbow plume would be carried predominantly southwards, rather than to the north-east as at present, leading to a reduced influence in the "downstream" sediments at cores 316, 325 and 329. Whether or not this were the case, however, what is also important to remember is that core 343, itself, was taken within 2km of the vent, which is less than the Rossby radius (l=3km). This is an important observation, because what that implies is that any plume-material rising above the Rainbow vent-site should spread rapidly to overlie an area measuring >2km from its source, radially - including this particular core-site - regardless of the prevailing current direction. That is exactly what is seen, for example, in the TAG hydrothermal plume, where no strong deep-ocean currents prevail (e.g. Rudnicki and Elderfield, 1993). To summarize: so long as the Rainbow vent-site remained active, deposition at near-vent site 343 should remain relatively unaffected by changes in "background" deep-ocean current regimes.

(ii) Perhaps more important is the observation that Rainbow is located on a fault scarp, in an area that is tectonically but not volcanically active (German *et al.*, 1996a; Parson *et al.*, 2000). Local seismic activity could lead to an enhancement in venting, by opening of new pathways for fluid circulation through, and escape from, the underlying crust. Any sudden increase in vent output that was subsequently maintained at a steady level would lead to a sustained increase in the hydrothermal input to the sediments, even though the onset of any such signal would be smoothed out by bioturbation, over time, until an equilibrium was reached (Albarede, 1995 p. 408-409). The presence of cm-size pieces of serpentinite in the sediments bracketing the 8-12 ^{14}C ky interval, coincident with the presence of discrete Ni and Cr peaks in the sediments (Fig. 3.8) might well be considered as evidence, therefore, for a period of seismicity (though more adjacent cores would be needed to confirm this) resulting in both localized downslope movement of rock fragments and - potentially - a complementary increase in hydrothermal output.

What is certainly the case is that the profiles of hydrothermal elements reported here

- both those derived from hydrothermal fluid and those scavenged by the hydrothermal plume - are consistent with an initiation or intensification of hydrothermal activity at the Rainbow hydrothermal field dating from 8-12 ^{14}C ky. The causes for this can only be speculated on, but an episode of discrete tectonic activity either initiating or reinvigorating hydrothermal circulation in this fault-controlled environment, remains an intriguing and plausible possibility.

3.4 Conclusions

The geochemistry of four sediment cores taken at increasing distances downstream from the Rainbow hydrothermal field on the MAR has been investigated. The cores, which contain > 80% $CaCO_3$, show mean sediment accumulation rates of between 2.65 and 3.75 cm.kyr^{-1} throughout the Holocene, with a lower pre-Holocene sedimentation rate of 1.11cm.kyr^{-1} observed in the longest core only. The Fe and Mn contents in the sediments show a significant hydrothermal input at all levels, with a pronounced increase some time between 12 and 8 ^{14}C ky seen in the longest proximal core. Other elements associated with hydrothermal processes (Cu, V, P, As) also show considerable enrichment over background N. Atlantic values. The hydrothermal component in the sediments has been calculated by subtracting the N. Atlantic background detrital signal and a local ultramafic detrital component (where applicable) from the total analyses. Hydrothermal Cu in the sediments decreases rapidly with distance from the vent site, but Fe and associated scavenged elements and Mn show an increase with distance. Ratios of scavenged elements to Fe are comparable to those previously reported in hydrothermal plumes and sediments. Calculated fluxes from hydrothermal plume fall-out are significantly greater than typical "background" N. Atlantic authigenic fluxes. The increase in the calculated hydrothermal input to the sediments, between 12 and 8 ^{14}C ky, indicates that localized venting at Rainbow may have been initiated and/or re-invigorated at that time. The coincident occurrence of ultramafic fragments in the sediments at this particular level raises the possibility that tectonic activity may have instigated or enhanced venting at this time.

Chapter 4

Sediment Trap Particles from the Rainbow plume: a comparison with core tops

Abstract

The geochemistry of particles collected in 5 sediment traps from a three-mooring deployment around the Rainbow hydrothermal vent site has been compared with the geochemistry of surficial sediments from cores collected beneath the spreading hydrothermal plume. Average sedimentation fluxes of particles into the sediment traps (11-25mg.m^{-2}.d^{-1}) are comparable to sedimentation rates in the cores throughout the Holocene (40-60mg.m^{-2}.d^{-1}). Fluxes of $CaCO_3$ and Al in the trap samples also compare within a factor of 2 with core top material. Major elements Mg, Mn, and Fe, and trace elements V, Co, Ni, Cu, and Zn, are enriched above N.E. Atlantic detrital background in all the sediment trap and core top samples. The greatest enrichments are found in 'near-field' trap samples 0.5km from the vent site, with lesser enrichments at a distance of 1.3km and in the core tops 2km to 25km 'downstream' of the vent site. Rare-earth element (REE) patterns in near-field trap samples show a positive Eu anomaly, indicative of co-precipitation of REE from the vent fluid, while far-field traps and core tops show little or no Eu anomaly, but a negative Ce anomaly, indicating scavenging of REE from seawater. Nd/Fe ratios in these far-field traps and sediments are similar. REE are accumulating in the Rainbow sediments at more than twice the rate for N. Atlantic sediments of similar high carbonate content. Calculations of the fluxes of hydrothermally-derived V, Mn, Fe, Co, Cu and Zn to the sediment traps are consistent with the calculated fluxes to the surficial sediments.

4.1 Introduction

High-temperature hydrothermal vents emit an estimated 3-6 x 10^{13} kg yr^{-1} of fluids to the oceans that carry high concentrations of dissolved chemicals (Elderfield and Schultz, 1996). These emitted chemicals are dispersed in hydrothermal plumes, remaining either dissolved, e.g. He, or else being precipitated either as sulfides or oxides in plume particles. Once precipitated, Fe-oxyhydroxide particles scavenge additional elements from both the vent fluid and, in particular, from the large volume of entrained seawater incorporated into hydrothermal plumes. Although the settling of plume particles is considered an important source for metalliferous sediments on the seafloor (e.g. Mills and Elderfield, 1995), relatively little attention has been devoted to direct measurements of settling fluxes from hydrothermal plumes using sediment traps (Lilley *et al.*, 1995), and only a few of those sediment trap studies have examined the detailed geochemistry of the plume particles (Dymond and Roth, 1988; German *et al.*, in press). To date, vent fluid, plume particle and underlying sediment data from a common vent site have never been correlated.

This work examines the major and trace element geochemistry of particles being sedimented from the Rainbow hydrothermal plume at 36°N on the Mid-Atlantic Ridge, using material from sediment traps and surficial sediments. The geochemistry of the particles is examined both from a spatial perspective that assesses changes with distance from the vent site, and from a temporal perspective that compares 'fresh' plume particles with 'aged' surficial mixed layer sediments which underlie the plume. During the last 20 years, several major oceanographic programmes (OMEX, SEEP, DEEPSEAS, JGOFS) have deployed sediment traps over extended periods of up to a year at various sites in both the eastern and western N. Atlantic. Although most of these experiments primarily involved quantification of the biological and nutrient content of trap material, some studies have included the characterisation of the detrital continental material transferred from the oceanic water column to the sediments (Brewer *et al.*, 1980; Jickells *et al.*, 1984; Kremling and Streu, 1993; Tachikawa *et al.*, 1997; Kuss and Kremling, 1999a; Fagel *et al.*, 1999). These latter studies provide background information on the composition of detrital material reaching N. Atlantic deep waters, against which the addition of hydrothermal signals from hydrothermal venting can be identified and quantified.

4.2 Material and Methods

4.2.1 Geologic setting

The Rainbow vent field is situated at 36°14'N on the Mid-Atlantic Ridge (MAR), in the N.E. corner of the South AMAR segment, on a westward-facing fault scarp near the intersection with the non-transform discontinuity (NTD) which exposes ultramafic rock (Fouquet *et al.*, 1997) (Fig. 2.2). The vent field, which hosts at least 10 distinct active vents, lies at a depth of 2300m, and its plume reaches neutral buoyancy at ~2100m water depth. Prevailing currents dictate that net transport of the plume is to the north and east, around Rainbow Ridge, approximately following the 2100m contour, then south and east around the NTD before continuing north following the eastern wall of the AMAR segment (German *et al.*, 1998c; Thurnherr and Richards, 2001). Mean current speeds in the area are fast, at up to 20cm s^{-1} at plume height, which combined with vigorous venting, ensures that a strong plume signal is observed tens of km from the vent site.

4.2.2 Sediment Trap samples

The samples used in this study are from the long-term sediment trap deployments described by Khripounoff *et al.* (2001). Three sediment trap moorings were deployed in the Rainbow area for 11 months during 1997/98. Two moorings, with paired traps at 150m and 300m above bottom (a.b.), were positioned in the path of the plume, 500m to the north, and 1300m to the north-north-east of the vent site, respectively (Fig. 2.6, Table 2.2). In this way it was intended to locate one trap of each pair on the moorings within the non-buoyant plume, with the other below the plume, at increasing distance from the vent site. An additional single trap was deployed 2km to the east of the vent site at 1950m water depth. This trap was 200m a.b., on the crest of Rainbow Ridge, above plume height and well away from the observed plume pathway. These will be referred to subsequently as near-field (500m from the vent site), far-field (1.3km distant), and ridge-top sediment traps.

All sediment traps were deployed with accompanying current meters and thermistors. Settling particles were collected in 22 carousel bottles over a period of 304 days using cone-shaped Technicap PPS5 traps. The trap sampling aperture was $1m^2$ and was covered with a honeycomb baffle of cells, each 10cm deep and 1cm in diameter. Prior to deployment, all sample bottles were filled with filtered seawater treated with

sodium borate-buffered formalin to give a final concentration of 3%. The sample period for each bottle was 14 days except for the final bottle which represented a sampling interval of just 10 days at the time of mooring recovery. A total of 20 samples from six collecting periods were available for this study (Table 2.3), other samples having been exhausted during earlier investigations (Khripounoff *et al.*, 2001). Six of the samples were too small for individual analysis, so were combined in pairs, according to which trap they came from (one pair from upper near-field trap, two pairs from ridge-top trap). As there were not sufficient samples from each trap to look at temporal trends, single annual average fluxes have been calculated and are presented for each trap where comparisons are made with averaged data for the surficial sediments from each individual core. Data for individual samples can be found in the appendices.

4.2.3 Core samples

Coring operations have been described in detail elsewhere (see Chapter 2, and Cave *et al.*, 2002). For this study, samples were taken from the top 3cm of 4 box cores, collected at 2km (core 343), 5km (core 316), 10km (core 325) and 25km (core 329) downstream of the vent site (Table 2.1, Fig. 2.2). Surficial samples from 2 off-ridge north-eastern Atlantic cores were also analyzed at the same time and by the same methods to provide a 'background' sediment composition (i.e. one unaffected by hydrothermal inputs) for comparison. These cores (23#12M from 32°33.3'N, 20°21.0'W, and 22#6M from 32°53.9'N 19°16.7'W) have high (> 75%) carbonate contents, similar to the Rainbow cores, and comparable accumulation rates (1.5-1.9cm.kyr^{-1}, Cave *et al.*, 2002). Averaged data for the core samples are presented for individual cores, for comparison with average trap sample data. Data for individual samples can be found in the appendices.

4.2.4 Analytical methods

Samples of 100-200mg of sediment trap and core sample material were first treated with a few ml of 6M HCl to dissolve carbonate and allow Ca to be separated from the residue by centrifuging, thereby preventing formation of insoluble Ca-fluorides during subsequent HF dissolution. The residue was then treated with a combination of HF/HNO_3, followed by dissolution in 6M HCl. The residue and supernatant were then recombined and made up into x300 dilutions in 6M HCl.

Major elements (Mg, Al, Ca, Ti, Fe, Mn) and high-level trace elements (V, Cr,

Co, Cu, Zn, Ni) were measured on a Phillips PV8060 ICP-AES for sediment trap and core top samples alike using a method of standard additions. Rare-earth elements were measured on a VG Elemental PlasmaQuad PQ2+ ICP-MS, by comparison with matrix-matched SGR-1 (Green River Shale) and synthetic standards. Interferences of Ba and LREE on Eu and Gd were corrected for by running dilutions of single element standards of Ba, La, Ce, Pr and applying a correction factor to the counts for the affected elements. Repeat measurements of SGR-1 agreed within 5%.

Calculation of hydrothermal component

Excess concentrations of Fe, Cu, Zn, Co, V and the REE have been calculated in the manner described in section 2.2.9, equations (1) and (2) (Cave *et al.*, 2002). Ratios of Ni/Fe and Ni/Al in the trap samples are low, indicating that there is no significant contamination of trap material by ultramafic material resuspended or otherwise incorporated into the samples, as has been seen previously in certain horizons in the sediment cores (Cave *et al.*, 2002). The surficial sediments likewise do not appear to have any ultramafic contamination.

4.3 Results and Discussion

4.3.1 Sedimentation fluxes and bulk accumulation rates

Between 30°N and 40°N, the central N. Atlantic is oligotrophic, and experiences a low input of detrital material to the surface waters (Kuss and Kremling, 1999b). The Rainbow fluxes to the sediment traps and surficial sediments compare closely with open ocean fluxes to deep water measured throughout the N. Atlantic at these latitudes, which all fall in the range 15-85 $mg.m^{-2}.d^{-1}$ (Jickells *et al.*, 1984; Kuss and Kremling, 1999b; Tachikawa *et al.*, 1997). The total material fluxes recorded for the five sediment traps averaged 10-11$mg.m^{-2}.d^{-1}$ for the near-field and ridge-top traps, and 17-25$mg.m^{-2}.d^{-1}$ for the far-field traps (Table 4.1, with a maximum flux recorded of 61$mg.m^{-2}.d^{-1}$ in the ridge-top trap (Khripounoff *et al.*, 2001). For comparison, the long-term bulk sediment accumulation rates from the Rainbow cores estimated by radiocarbon dating (Table 2.4, Fig. 3.2) are 40-60$mg.m^{-2}.d^{-1}$ (Table 4.1). In general it is expected that the flux of material from the water column will be greater than its accumulation rate in sediments, due to the presence of organic carbon and opal in the freshly settled material that is remineralised in the sediments after deposition.

The lower fluxes observed in the trap samples compared to the cores at Rainbow could reflect low trap efficiency values (Heussner *et al.*, 1999; Rutten *et al.*, 2000; Yu *et al.*, 2001). Placing a large solid object such as a sediment trap in the water column can affect the local water flow, for example causing water moving horizontally to flow upward to go over the obstruction, or to be deflected around it, and if the flow is fast enough, causing turbulence on the downstream side. In areas of strong currents such as are found around the Rainbow Ridge, the tethered trap may lie at an angle to the current. The flux of material into the trap may therefore be reduced compared to the flux to the seafloor in its vicinity. Other possibilities are that the collection period may not have provided a good representation of the mean annual flux, or additional focusing of material to the coring sites on the ridge valley floor may occur. Other hydrothermal sediment trap studies include several from the East Pacific Rise e.g. Dymond and Roth (1988), who recorded fluxes of 34-67mg.m^{-2}.d^{-1} at 2km and 754mg.m^{-2}.d^{-1} within a few metres of the vent, and German *et al.* (in press), who recorded fluxes of 53-87mg.m^{-2}.d^{-1} a few hundred metres from a vent site at 13^{o}N on the EPR, and 192-795mg.m^{-2}.d^{-1} close to the vent itself.

Sediment Trap	mg.m^{2}.d^{-1}	Core top	mg.m^{2}.d^{-1}
Near-field(l)	11.3	St. 343	52.8
Near-field(u)	10.6	St. 316	50.7
Far-field(l)	17.5	St. 325	44.3
Far-field(u)	25.0	St. 329	64.6
Ridge-top	11.2		

Table 4.1: Average mass flux data for sediment traps and core tops. Data for sediment traps is from Khripounoff *et al.* (2001). Data for core tops is from this work.

4.3.2 Major and Trace Elements

Major and trace element data for individual samples can be found in Appendix 3. While the core samples all contain > 80wt.% $CaCO_3$, the sediment trap samples contain a wider range of 40-85% $CaCO_3$. Values less than 75% $CaCO_3$ are found only in the near-field trap samples, where high concentrations of S (up to 15%) (Khripounoff *et al.*, 2001) and Fe (up to 20%, this work) are present. The N. Atlantic background for S in sediment trap samples is <0.3% (A. Khripounoff pers. comm.). Iron content varies from 20% in

the near-field traps to <1% in the upper far-field traps, reflecting the greater input of hydrothermal material to the near-field sediment traps. Iron in the core top samples varies between 2-3%. Aluminium varies from 0.3-0.8% in the sediment trap samples, and between 0.6-0.8% in the core top samples. For the background N. Atlantic cores, $CaCO_3$ comprises 75-80%, Al is 1.5-2.7%, and Fe is 0.9-1.4%. Iron concentration in N. Atlantic open ocean sediments is generally about half the Al concentration.

The Mn content in all the sediment trap samples exceeds the N. Atlantic background Mn/Al value of 0.03 for sediment trap material (Kuss and Kremling, 1999a) by a factor of 3-4, and in the core tops the Mn/Al ratio increases from 4 times the N.E. Atlantic background value (0.026) in the proximal cores to 6 times the background value in the distal cores.

The metalliferous sediment index of Bostrom *et al.* (1969), 100*Al/(Al+Fe+Mn), is a measure used to discriminate between pelagic sediments from continental sources and sediments which have acquired extra Fe and Mn either from hydrothermal or hydrogenous sources. Non-metalliferous pelagic sediments have an index > 50, and this index tends towards lower values as sediments become more metalliferous. The N.E. Atlantic background core samples examined in this work have an index of 60-65, as do sediment trap and suspended particulate material in N. Atlantic deep waters remote from the ridge-crest (Brewer *et al.*, 1980; Jickells *et al.*, 1984; Kremling and Streu, 1993; Kuss and Kremling, 1999a; Sherrell and Boyle, 1992). The index for the surficial Rainbow sediments is 21-24, but varies between 1-18 for the near-field sediment traps, between 21-25 (cf. surficial sediments) in the lower far-field trap samples and between 34-37 in the upper far-field trap. The two samples from the ridge-top ("background") trap have index values of 18 and 34, which provide clear evidence that this trap must receive some hydrothermal input (Table 4.2). Although the ridge-top position was selected to avoid the influence of the Rainbow plume, subsequent work, post-deployment, has revealed that occasional eddies formed by the Rainbow plume do indeed rise high enough in the water column, above the vent site, to pass directly across the top of Rainbow Ridge (Thurnherr and Richards, 2001). Extensive water-column surveys over the top of the ridge found no evidence for any shallow hydrothermal source there (German *et al.*, 1996b; German *et al.*, 1998c), so the Rainbow plume is believed to be the only possible source of the hydrothermal input to this trap. Results from the ridge-top trap cannot therefore be taken to be representative of background sedimentation, as they have clearly received some input from the hydrothermal plume.

Magnesium is entirely absent or below detection levels in high-temperature hy-

Sediment Trap	index	Core top	index
Near-field(l)	1-3	St. 316	24
Near-field(u)	9-18	St. 343	24
Far-field(l)	21-25	St. 329	22
Far-field(u)	34-37	St. 325	21
Ridge-top	18-34	Av b.ground	62

Table 4.2: Metalliferous sediment index for sediment trap samples, core top samples, and background samples.
Index is from Bostrom *et al.* (1969). The closer the index to 1, the greater the metalliferous content. Background value is the average from the BOFS samples, representing NE Atlantic background sediments. World-wide, non-metalliferous sediments fall into the range 55-65.

drothermal vent fluids, because it is stripped out of seawater by water-rock reactions as it circulates through the hydrothermal system (e.g. Mottl and Wheat, 1994; Von Damm, 1995). Particles collected from vent plumes nevertheless often show high Mg/Al ratios, which Dymond and Roth (1988) suggested is due to the presence of Mg-rich smectites that form when a hydrothermal fluid reacts with seawater. Salt-free Mg/Al ratios in the sediment trap samples from Rainbow are as high as 1.8 in the near-field trap samples, reducing to 0.6 in the upper-trap far-field samples. In the samples from the two proximal cores from Rainbow, Mg/Al is ~0.8, falling to 0.5 in the more distal core samples. For comparison, the mean Mg/Al in the two cores selected to represent NE Atlantic background is 0.3, and this same value is determined in sediment trap material from the deep Sargasso Sea (Brewer *et al.*, 1980). Plotting excess Mg in the sediment trap and core samples against hydrothermal Fe yields a good correlation (Fig. 4.1), implying that Mg from seawater is being co-precipitated with vent-fluid Fe close to the Rainbow vents, as suggested by Trocine and Trefry (1988), rather than solely being incorporated into smectites. No X-Ray diffraction data are available to confirm this, however. In this study the flux of Mg stripped from seawater and deposited in the traps is ~4 μmol.m^{-2}.d^{-1} in the near-field, and 2-3 μmol.m^{-2}.d^{-1} in the far-field. The calculation for the surficial Rainbow sediments is potentially more complicated than for the plume particulates because the two proximal core sites are located on the ultramafic block that hosts the Rainbow vent site, and the sediments there could contain small amounts of ultramafic rock material that would enhance the Mg in the bulk sediment (Cave *et al.*, 2002). However, the low (and similar) Ni/Al ratios in the

near and far-field surficial sediments reveal no ultramafic contamination of these samples. Even in the far-field cores the excess Mg is on the order of 40-80μmol.g^{-1}, which translates to an accumulation rate of ~2μmol.m^{-2}.d^{-1}. It therefore appears that high temperature venting not only strips Mg from seawater during sub-surface circulation, but that a further removal of Mg occurs from the seawater that is entrained and mixed with hot vent fluids after their emission from the seafloor.

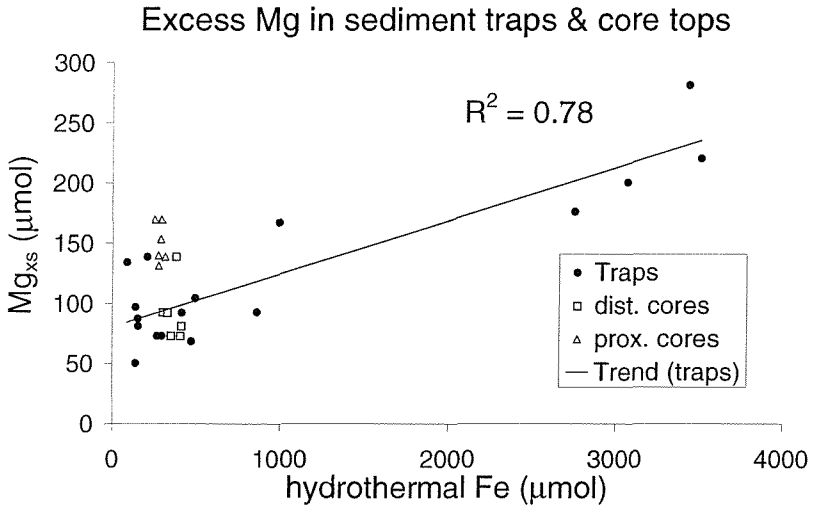

Figure 4.1: Excess Mg vs. Fe in the Rainbow sediment traps and core tops. Trendline is for the sediment trap samples. Even the distal core samples show a large excess Mg, implying that hydrothermal plumes may remove significant amounts of Mg from seawater, possibly by co-precipitation with hydrothermal Fe.

Due to the apparent presence of hydrothermal material in the ridge-top trap (see earlier), it could not be used a a reference background material. Instead, the average of the NE Atlantic background sediments analysed here has been used for normalising both the sediment trap and core-top data in the discussion which follows, as well as for calculating the background to be subtracted to provide the 'excess' of the hydrothermally-derived elements in the samples. This approach demonstrates that both sediment trap (Fig. 4.2a)and core-top samples (Fig. 4.2b) exhibit strong enrichments in all of V, Mn, Fe, Co, Cu and Zn, with variable enrichments of Ni. Both far-field traps and the ridge-top trap exhibit enrichments over N.E. Atlantic background which are very similar to that observed in core-top sediments at all distances from the vent site (Fig. 4.2; Cave *et al.*, 2002). By contrast, enrichments in the two near-field traps

are even higher, with the lower near-field trap exhibiting the greatest enrichments of all (Fig. 4.2a).

One of the characteristics of the Rainbow vent site is the very high Fe:H_2S ratios measured in the vent fluids. Fe in the vent fluid is ~24mM, the highest yet measured in a vent fluid, while H_2S is <2.5mM (Chiba *et al.*, 1999; Douville *et al.*, 2002), within the range measured at other high-temperature vents. This leads to a disproportionate amount of the Fe forming low-density Fe-oxyhydroxides (compared to other vent sites on the MAR), which can be carried long distances by the strong currents, leading to the strong optical plume signal observed several tens of kilometres downstream (German *et al.*, 1998c). Copper and Zn are also present in high concentrations, at 140μM and 160μM respectively. Several of the sediment trap samples contained high concentrations of S (A. Khripounoff, pers. comm.). If we assume that all the hydrothermal Cu and Zn in the near-field (S-bearing) sediment trap samples are present as monosulfides (CuS and ZnS), and that the remainder of the S present is in the form of FeS, then we can calculate what proportion of the 'excess' Fe is likely to be present as Fe-oxyhydroxides. Excess concentrations of Fe, Cu, Zn, Co, V and the REE have been calculated in the manner described in section 2.2.9, equations (1) and (2) (Cave *et al.*, 2002) and are presented in Appendix 3 (trace elements), Appendix 4 (sediment trap REE) and Appendix 5 (core-top REE).

In the sections of the discussion which follow these different elements are considered according to the three types of behaviour identified previously in plume particulate matter from MAR hydrothermal plumes (see e.g. German *et al.* (1991)):

a) chalcophile metals (e.g. Cu, Zn) which show evidence of preferential settling/removal relative to Fe from hydrothermal plumes;

b) oxyanion metals (e.g. V) which show tight linear correlations with Fe throughout the neutrally-buoyant portion of hydrothermal plumes and

c) particle-reactive metals (e.g. Be, Y, REE) which show evidence for continuous scavenging from seawater as Fe-oxyhydroxide material is dispersed through hydothermal plumes, away from the source vent site.

4.3.3 Chalcophile metals: Cu, Zn and Co

Ratios of Cu:Fe are in excess over vent-fluid ratios in all the sediment trap samples (Fig. 4.3a) and surficial samples (Fig. 4.3b). Cu:Fe ratios decrease significantly with

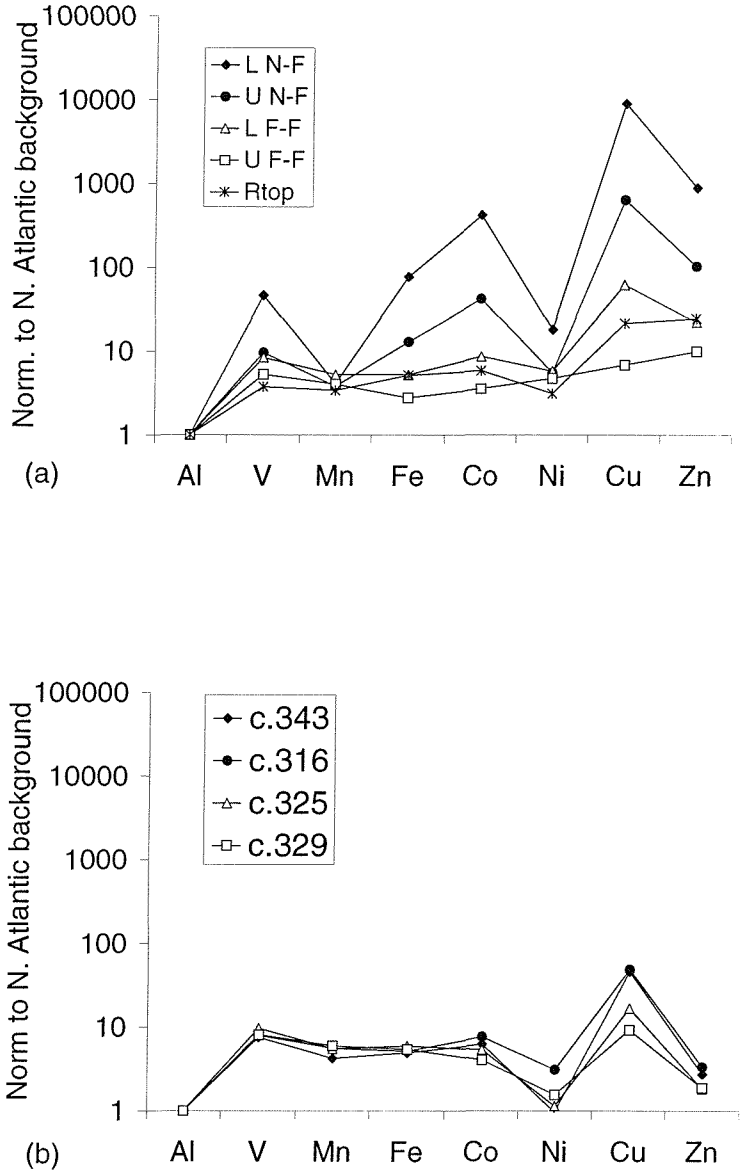

Figure 4.2: Sediment traps normalised to N. Atlantic background
Major and trace elements in bulk samples from (a) the sediment traps and (b) the core tops, from the Rainbow area, normalized to N. Atlantic background core material from this study (see Table 2.1 for location of background cores). Note log scale. Cu is much more strongly enriched than Zn, despite their similar concentrations in Rainbow vent fluid (Douville *et al.*, 2002).

increasing distance from the vent site, however, and only begin to approach end-member vent-fluid ratios (Douville *et al.*, 2002) in the upper far-field trap and surficial sediments from cores 325 and 329, 10-25km from the vent site (Fig. 4.3b). Ratios of Zn:Fe are an order of magnitude lower in the near-field traps than Cu:Fe (Fig. 4.3c, and decline sharply from far-field to surficial sediments (Fig. 4.3d). The excess Co/Fe data in the sediment traps shows a similar pattern to Cu, with a large excess in the near field traps, which is down by more than an order of magnitude by the time the plume gets to the lower far-field trap (Fig. 4.3e), and with excesses in the core tops dwindling with distance down plume (Fig. 4.3f).

The Rainbow vent fluids have high and similar concentrations of Zn (160 μM) and Cu (140 μM), giving a Zn/Cu vent fluid ratio of ~1.1 (Douville *et al.*, 2002). The sediment trap particles from Rainbow ($\geq$500m from the vent) show molar excess Zn/Cu ratios of 0.04-0.35 in the near-field and lower far-field samples (Table 4.3), similar to the range found in particles from the non-buoyant hydrothermal plume at TAG (German *et al.*, 1991; Trocine and Trefry, 1988), while surficial sediments from beneath the Rainbow plume also exhibit low Zn/Cu ratios, as a result of high excess Cu content in the sediments (400 ppm in the proximal cores to 100 ppm in the distal cores) compared to a maximum excess Zn of 30 ppm (Appendix 3). Upper far-field samples have Zn/Cu $\geq$1, as excess Cu declines with respect to excess Zn. Both ridge-top samples have higher excess Zn than either the upper far-field samples or the surficial sediments (Appendix 3). Black smoker fluids at TAG have Zn/Cu $<$ 0.3, i.e. proportionately less Zn-rich, but very near-field particles (from the buoyant plume) do exhibit fluid-like Zn/Cu values, although these decrease farther afield. Similarly, samples from the vent site at 13°N on the EPR (German *et al.*, in press), which are from traps close enough to intercept the buoyant plume ($<$ 50m), show extreme Zn:Cu ratios of 20-50:1, compared to vent fluid ratios for Zn:Cu of 4:1. Buoyant plume samples from Monolith vent on the Juan de Fuca Ridge (Feely *et al.*, 1994) also showed order-of-magnitude greater Zn than Cu, while samples from the non-buoyant plume were closer to 1:1. Consistent with this, the Zn/Cu of particles from the near-field trap at Rainbow (500m from vent site) is only 0.1, indicating that much of the Zn may already have been extremely rapidly and preferentially deposited, as anomalously dense (hence, rapidly-sinking) Zn-rich sulfidic material, much closer to the vent site than any of the trap and core-top samples analysed here. Massive Zn-sulfides have indeed been observed within the Rainbow vent field (Y. Fouquet pers. comm.). It therefore appears that Zn is preferentially precipitated from vent fluids close to the vent, compared with Cu, so that only a small proportion of Zn persists into the spreading plume. Data from buoyant plume particles from a

site in North Cleft segment on the Juan de Fuca Ridge led Feely *et al.* (1994) to the conclusion that Cu and Zn sulfides precipitate preferentially to Fe sulfides in the buoyant plume, during the early stages of sulfide formation. The low H_2S content of the Rainbow fluids (< 2.5 mM; Douville *et al.*, in press) may lead to competition between differing potential sulfide-forming metals within the Rainbow hydrothermal plume and, consequently, contribute to the preferential deposition of Zn as sulfides rather than Cu and Fe in the very near-field (0-500m) hydrothermal plume.

Cobalt has been measured at 13μmol l^{-1} in the Rainbow vent fluid, but has only been found at nanomolar levels in other vent fluids (Douville *et al.*, 2002). Excess Co/Fe in the Rainbow sediment trap samples is an order of magnitude greater than that reported for the TAG non-buoyant plume samples (German *et al.*, 1991). Cobalt is of high commercial interest (Mannheim, 1986) and has generally been studied in association with ferromanganese crusts, where it tends to be present in high concentrations (e.g. Halbach *et al.*, 1989, Hein *et al.*, 1990), but is rarely reported for marine hydrothermal sediments. Co/Fe in the sediment trap and core samples at Rainbow show a decrease away from the vent similar to Cu/Fe , but Co/Fe values are two orders of magnitude lower than Cu/Fe, reflecting the lower concentrations of Co in the vent fluid (Fig. 4.3e,f).

Sediment Trap	Zn/Cu	Core top	Zn/Cu
Near-field(l)	0.04-0.12	St. 343	0.04-0.05
Near-field(u)	0.09-0.23	St. 316	0.05-0.07
Far-field(l)	0.21-0.35	St. 325	0.05-0.10
Far-field(u)	0.81-1.30	St. 329	0.08-0.22
Ridge-top	0.64-2.96	Av b.ground	1.28

Table 4.3: Zn/Cu for sediment trap and core-top samples.

Although Zn and Cu are present in the vent-fluid at similar concentrations, it appears that little Zn escapes the immediate confines of the vent field, unlike Cu which is present in very high concentrations (up to 10% by weight) in sediment trap samples, and in moderately high concentrations in the core top samples (up to 460ppm), compared to N. Atlantic background values of a few tens of ppm.

4.3.4 V and Fe

Subtraction of the N. Atlantic shale component of V and Fe from the surficial core samples analysed by ICP-AES was made using V/Al = 0.0017 and Fe/Al =0.61 ratios

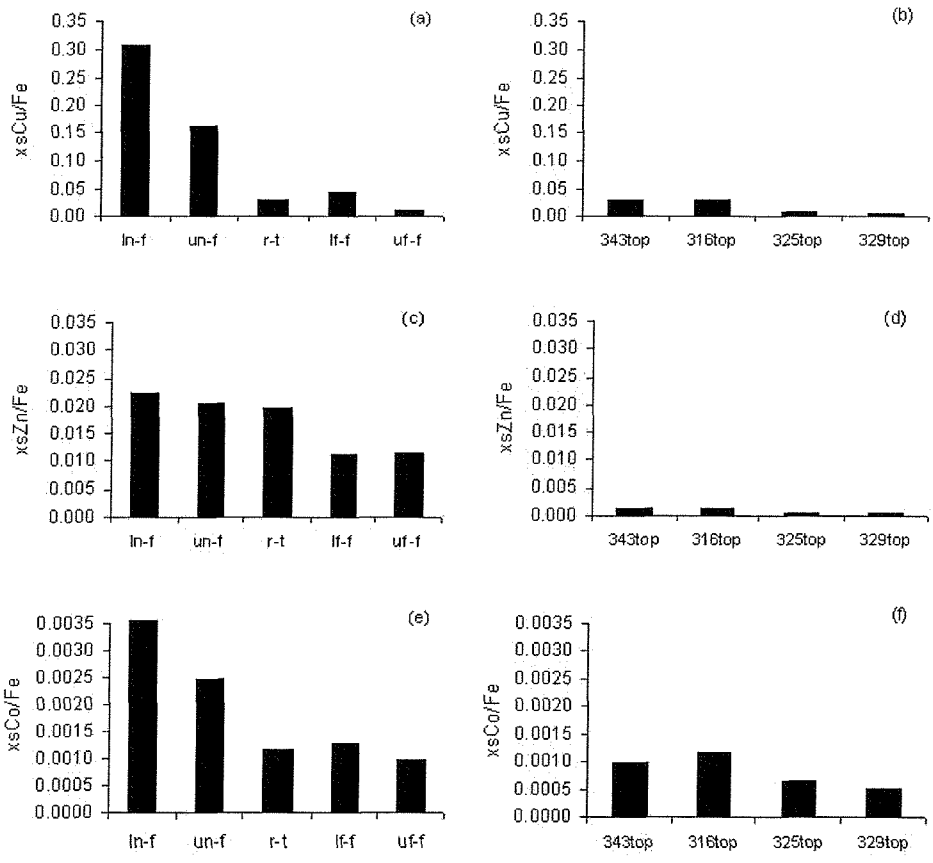

Figure 4.3: Cu/Fe, Zn/Fe and Co/Fe of trap and surficial sediment samples Cu/Fe declines rapidly with distance from the vent site. Zn is present in the fluid at similar concentrations to Cu, but appears to be removed from the plume much closer to the vent site, as even in the lower near-field trap, Zn/Fe is an order of magnitude lower than Cu/Fe. Co/Fe is an order of magnitude lower again in all samples, reflecting its lower concentration in the vent fluid, but declines with distance from the vent in a similar manner to Cu/Fe.

from N. Atlantic background sediments (Table 4.4). These are slightly lower than the values found by XRF (Chapter 3, Table 3.1) and give an average hydrothermal V:Fe ratio for the surficial sediments of 0.0050 (Fig. 4.4), which although higher than the average 0.0041 found by Trefry and Metz (1989) for hydrothermal particles, is well within their range. The average V/Fe ratios in the sediment trap samples are lower than the surficial sediment values, and increase from near to far-field (Fig. 4.5). The near-field samples are rich in sulfide (Khripounoff *et al.*, 2001), and if we assume that the sediment traps at Rainbow receive plume Fe-oxyhydroxide material with the same local V:Fe ratio of 0.0050 as the sediments, then this can be combined with measured V fluxes to calculate what proportion of the total Fe flux to any trap is present in the oxide form. Any excess flux of hydrothermal Fe (i.e. that part not associated with oxides in typical V:Fe proportions), can then be compared with complementary S data where available (Table 4.5). In 5 of the 7 near-field trap samples, the excess Fe is greater than the quantity of Fe required to scavenge the V present in the sample (Fig. 4.6) implying that in some samples a large proportion of the Fe is present as sulfides. In the remainder of the samples, including one near-field sample with a very high concentration of Fe, the excess Fe compares closely with the expected Fe calculated from the concentration of V present. Sulfide data are available for 6 of the near-field trap samples, and in each case S is in excess of the normal N. Atlantic background of ~ 0.3%. In two of these samples (S > 10%), there is more than sufficient S to make monosulfides of all the Cu, Zn and Fe remaining after the subtraction of that portion of Fe in the oxide form, implying that there may be some elemental S present. In 2 other samples, the S is insufficient, but by less than 10% of what is required, which is probably within error given our lack of knowledge of the sulfide forms present. In the remaining 2 samples, only about half the S needed for monosulfide formation is present, implying that there is more Fe present in the oxide form than is indicated by the V/Fe calculation. This is only likely to occur if particles enter the trap very soon after forming, and before they have encountered significant quantities of seawater.

4.3.5 Rare Earth Elements

In common with all other known high-temperature hydrothermal vent fluids, the rare-earth element (REE) patterns in Rainbow fluids exhibit a large positive Eu anomaly (Douville *et al.*, 2002) when normalised to shale (PAAS shale values from McLennan (1989) used for normalisation). The Rainbow vent fluids also show a distinct light REE (LREE) enrichment, with La > Ce > Pr (Fig. 4.7). By comparison with most MAR

El/Al	ratio
V/Al	0.0017
Mn/Al	0.025
Fe/Al	0.61
Co/Al	0.0004
Cu/Al	0.0014
Zn/Al	0.0018

Table 4.4: Element/Al ratios for N. Atlantic background.
These values are average ratios from the BOFS sediment samples, which are taken to be representative of N. Atlantic background sedimentation (see text for details).

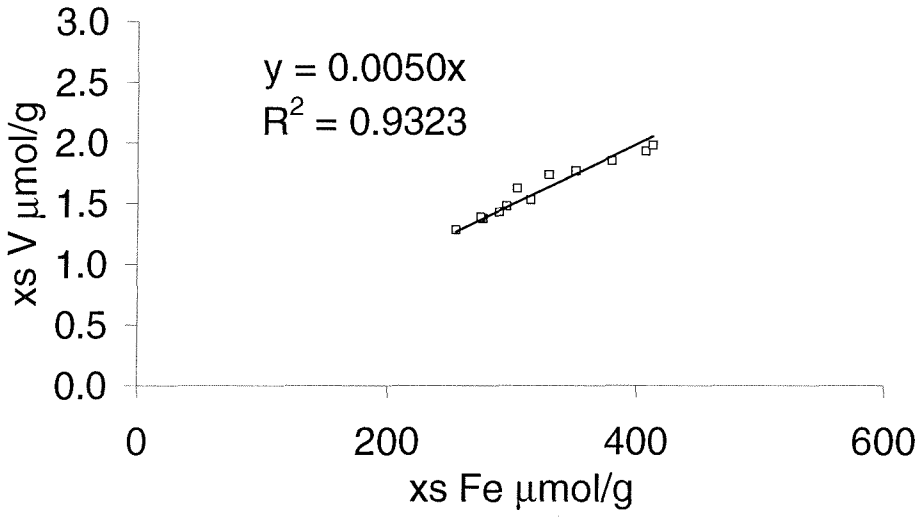

Figure 4.4: Excess V vs. Fe in Rainbow surficial sediments.
Samples are from each of the top 3cm of each of the four Rainbow cores. The 'excess' values are the concentrations in excess of what might be expected from background detrital material with the same Al content, and is here considered to be the hydrothermal input. The ratio of hydrothermal V to hydrothermal Fe for the core-top samples is in good agreement with values obtained from sediment trap studies at hydrothermal sites by other workers.

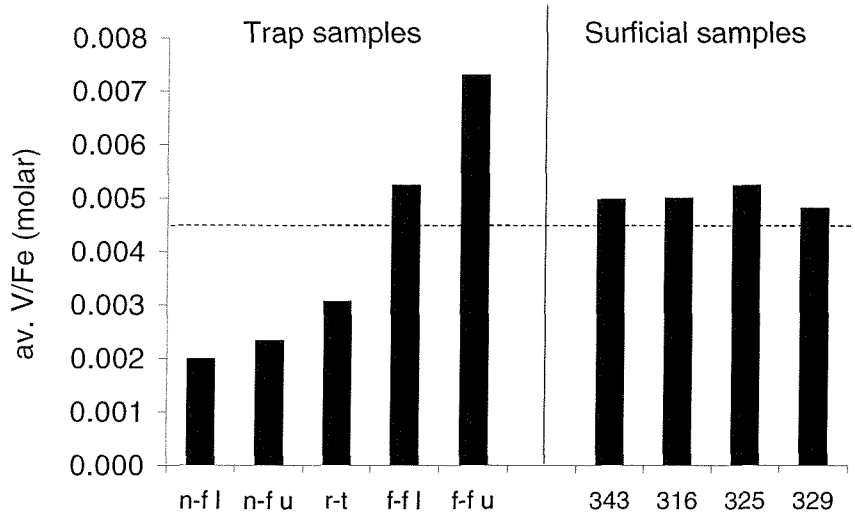

Figure 4.5: V/Fe in sediment traps and core tops
Note linear scale. Dashed lines indicate ratio of 0.0041 found by Trefry *et al.* (1989) for V:Fe in plume particles. V/Fe is low in near-field trap samples due to presence of Fe as sulfides, which do not scavenge V.

Trap Sample	hyd. Fe μmol	Fe req. for V μmol	remaining Fe μmol	S μmol
n-f l	2758	694	2064	3384
n-f l	3075	471	2604	4697
n-f l	3515	835	2680	2162
n-f u	494	313	181	212
n-f u	994	399	595	795
n-f u	861	315	546	162

Table 4.5: Potential for Fe as oxyhydroxide and sulfide in near-field sediment trap samples.

A simple mass balance calculation using hydrothermal V/Fe ratio of 0.0050 indicates the amount of Fe present as oxyhydroxides ('Fe required for V') and as sulfides ('remaining Fe', i.e. total hydrothermal Fe , less Fe present as oxides).

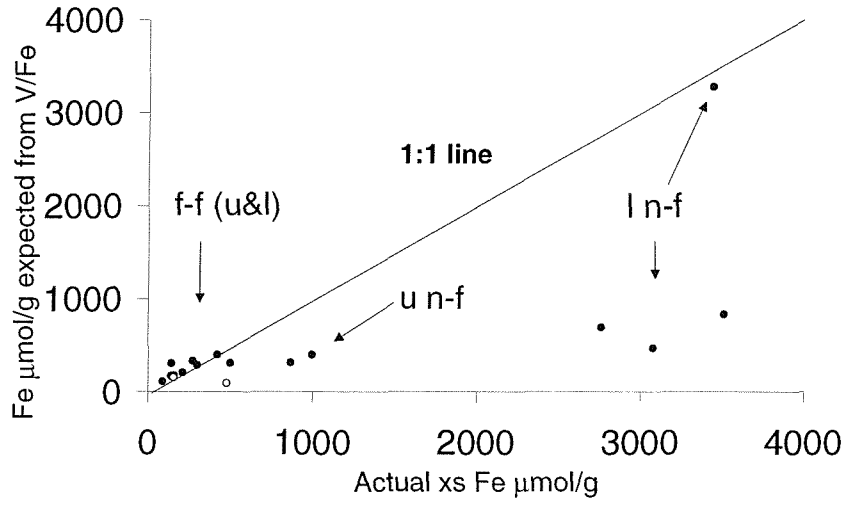

Figure 4.6: Fe as oxides and sulfides in Rainbow trap samples. Correlation between amount of hydrothermal Fe required to be present as oxide in order to scavenge the amount of V measured in the samples (at a constant hydrothermal V/Fe ratio of 0.005, see text), and the total excess of Fe over background. Difference should represent present as sulfides. Ridge-top samples are shown as open circles, other samples as filled circles.

fluids analysed to date, this is an unusual pattern, although a similar LREE-enriched pattern has been measured at the Snakepit site at 23°N on the MAR (Douville *et al.*, 2001). Compared to other MAR vent fluids and seawater, the total concentration of REE in the vent fluid is also very high (16.8nM) (Douville *et al.*, 2002).

Klinkhammer *et al.*,(1983) suggested that the REE might be removed from seawater by scavenging by Fe or Mn oxides from hydrothermal plumes. Research carried out by Ruhlin and Owen (1986), on Pacific metalliferous sediments spanning the last 16 million years from site 598 of DSDP Leg 92, concluded that Fe was the principal agent involved in removing REE from seawater in hydrothermal plumes and depositing them in sediments. This was confirmed by Owen and Olivarez (1988), on both site 598 sediments and younger sediments from west of the southern Juan de Fuca Ridge, who found a strong positive correlation between REE and Fe in these sediments, but a much weaker or no correlation with Mn. Ruhlin and Owen (1986) also indicated that the proportion of REE in the sediments compared to Fe increased with distance from the paleo-ridge axis, indicating that Fe-oxyhydroxides in hydrothermal plumes continue to

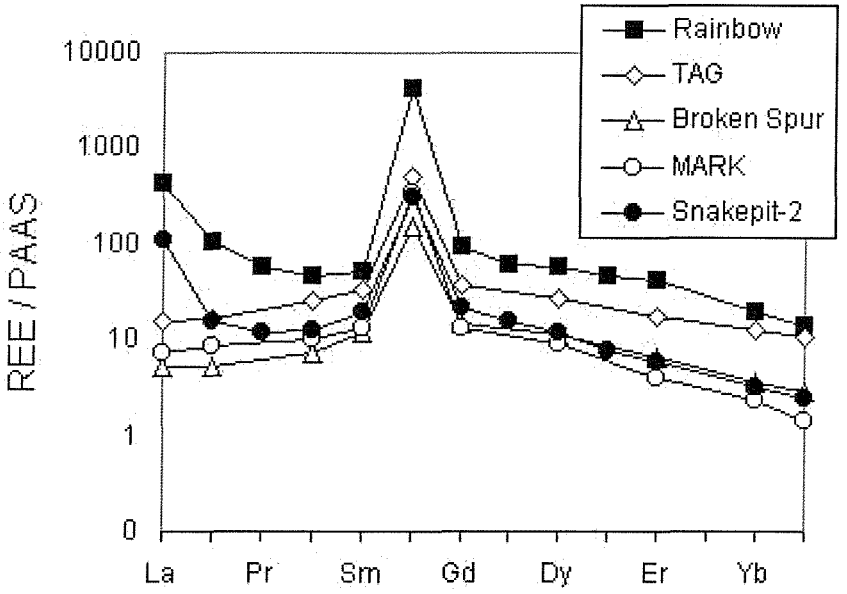

Figure 4.7: Rare-earth elements in MAR vent fluid.
MAR vent fluids normalized to PAAS. Note the LREE enrichment in the Snakepit fluids and the Rainbow fluid (Douville *et al.*, 2001). The peak in Eu is common to all known high-temperature vent fluids.

scavenge REE from seawater as they move away from the plume source, and this trend was confirmed by Barrett and Jarvis (1988) on sediments from four Leg 92 cores, and two Leg 85 cores, all from the Pacific Plate.

REE in sediment trap samples and surficial sediments

Excess 'hydrothermal' REE in the Rainbow sediment trap and core samples (i.e. derived from scavenging by hydrothermal Fe) is calculated as before by subtracting the shale component, using REE/Al ratios for the background N. Atlantic core top samples (Table 4.4). All but one of the near-field trap samples show a positive Eu anomaly and variable enrichments in LREE when the hydrothermally-derived REE are normalized to PAAS (Fig. 4.8a). Samples from the near-field traps that had the greatest excess Fe in sulfide show the largest Eu anomalies (Fig. 4.8a), indicating scavenging of REE from the vent fluids. One sample from the lower near-field trap which had high Fe (19%) but low sulfide compared to the others from this trap (<3% compared to <10% in high-S samples) has both a positive Eu anomaly and a large negative Ce anomaly, and is significantly more enriched in HREE than the other near-field samples, indicating that it has scavenged REE both from the plume and from seawater. By contrast with near-field

samples, the far-field samples show no significant Eu anomaly, but have small negative Ce anomalies, and are enriched in MREE (Fig. 4.9a). Surficial sediment samples show greater negative Ce anomalies than far-field and ridge-top samples (Fig. 4.10a). Bulk sediment REE are shown for comparison in each figure.

REE contents of the hydrothermal fluids are high, as are the Fe contents of the near-field samples (15-20% Fe). Despite this, the excess REE in the near-field trap samples is only 2-3 times the excess in the low-Fe samples (1-2% Fe). As indicated by the V/Fe data in the previous section, a large proportion of the Fe in the near-field samples is present as sulfides, which typically do not incorporate REE (German *et al.*, 1999). This can be seen clearly in the Nd/Fe ratios, which increase from near to far-fleld (Fig. 4.11). Ratios of Nd/Fe in the near-field trap samples range from 1-5 x 10^{-5}, similar to the range of 2-6 x10^{-5} found by German *et al.* (1990) for samples from the TAG plume, and by Mills and Elderfield (1993) for surficial samples from a highly metalliferous sediment at TAG (Fe = 11-28%, Nd/Fe(molar) = 1-4x10^{-5}). The surficial core sediments from Rainbow have higher excess REE/Fe concentrations than the near-field samples, with Nd/Fe ~1 x 10^{-4} (molar), similar to the ratio of 1-2 x 10^{-4} found in hydrothermally-enriched pelagic sediments (Fe = 3-5%) from the Juan de Fuca Ridge (German *et al.*, 1997).

4.3.6 Fluxes to sediment traps and surficial sediments

The measured material fluxes to the sediment traps are half to a third the long-term fluxes to the surficial sediments as calculated from ^{14}C dating (see section 4.3.1). Nonetheless, the fluxes of hydrothermally derived elements (Mn, Fe, Co, Cu, Zn) show good agreement between traps and cores, according to the behaviour expected from each (Table 4.7). Fluxes of Co and Cu to the two proximal cores fall between the values measured for the lower far-field and upper near-field traps, while the flux of Zn to the cores is lower than the average measured in any of the traps, consistent with earlier findings that Zn is lost most quickly from the plume. In the distal cores, Cu and Zn are lower than in the proximal cores, but still higher than the upper far-field and ridge-top traps, consistent with these traps receiving minimal plume input, while the cores, although distant, are under the plume path. Iron values for all surficial sediments fall between the upper and lower near-field sediment trap flux values, consistent with a large proportion of light Fe-oxyhydroxide material being transported by the plume for long distances downstream of the vent. Vanadium in the surficial sediments is similar to that found in the lower near-field trap, again pointing to the fact that a large

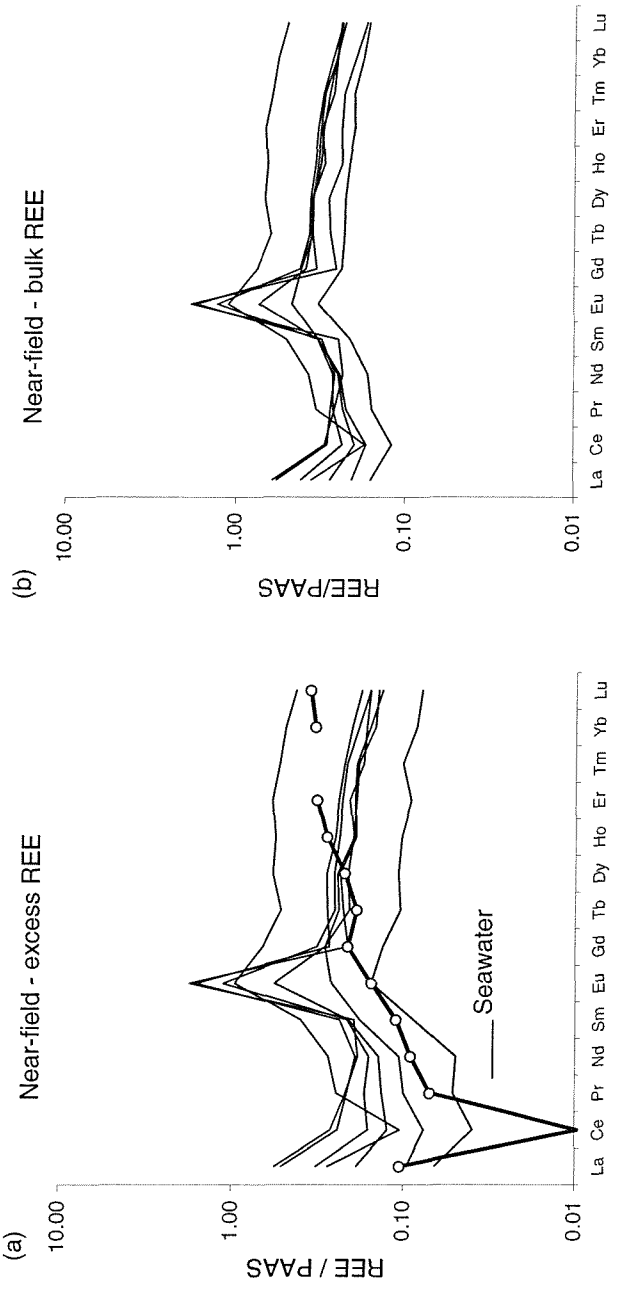

Figure 4.8: Rare-earth elements in near-field sediment trap samples (a) Calculated hydrothermal REE component in the near-field sediment trap samples, normalised to PAAS, showing positive Eu anomalies. Seawater data from Mitra *et al.* (1994). (b) Bulk sediment REE patterns for the near-field sediment trap samples, normalised to PAAS.

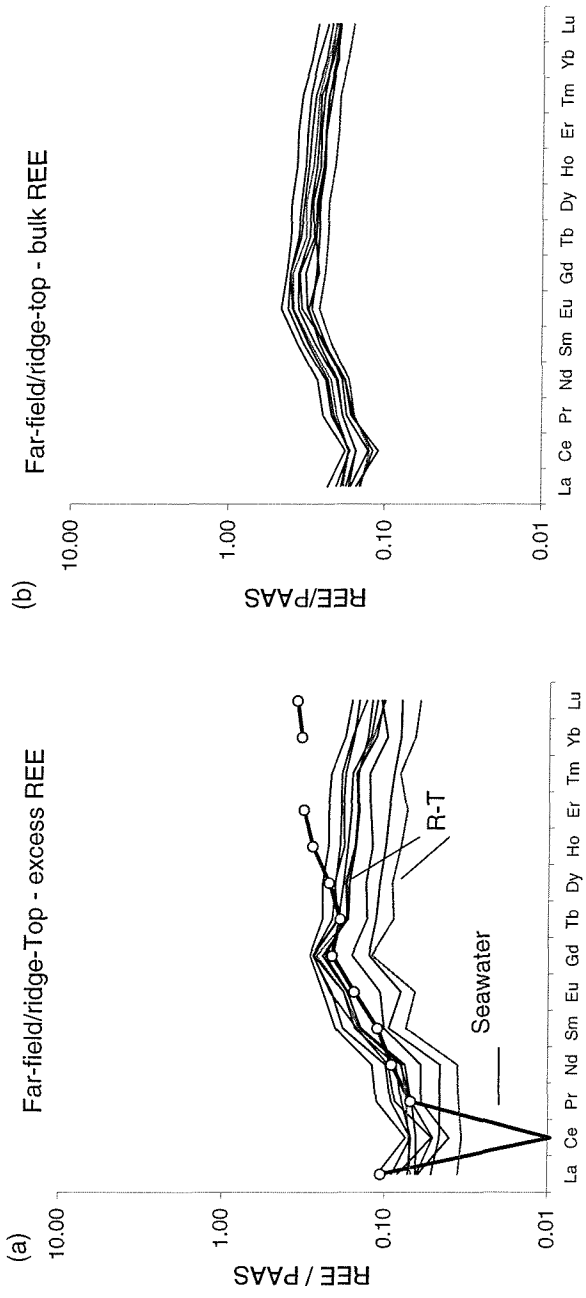

Figure 4.9: Rare-earth elements in far-field and ridge-top sediment trap samples (a) Calculated hydrothermal REE component in the far-field and ridge-top sediment trap samples, normalised to PAAS, showing negative Ce anomalies. Seawater data from Mitra *et al.* (1994). (b) Bulk REE patterns for the far-field and ridge-top sediment trap samples, normalised to PAAS.

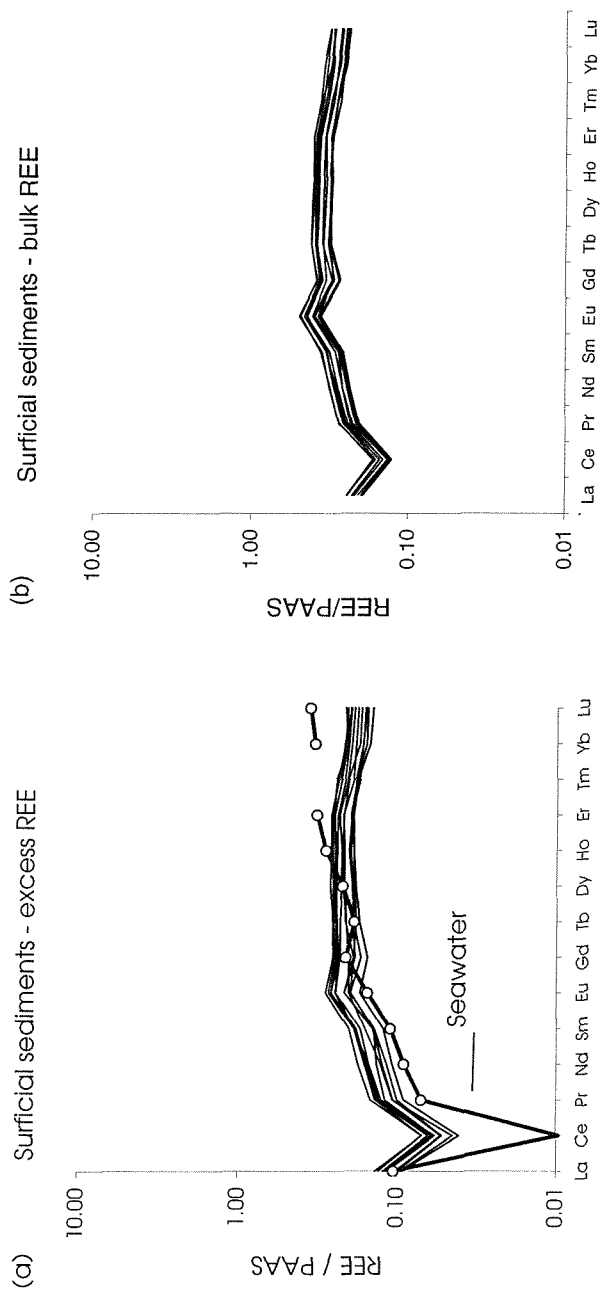

Figure 4.10: Rare-earth elements in core-top samples
(a) Calculated hydrothermal component in core-top samples, normalised to PAAS, showing distinct negative Ce anomalies with enriched MREE-HREE pattern. Seawater data from Mitra *et al.* (1994). (b) Bulk REE patterns for core-top samples, normalised to PAAS.

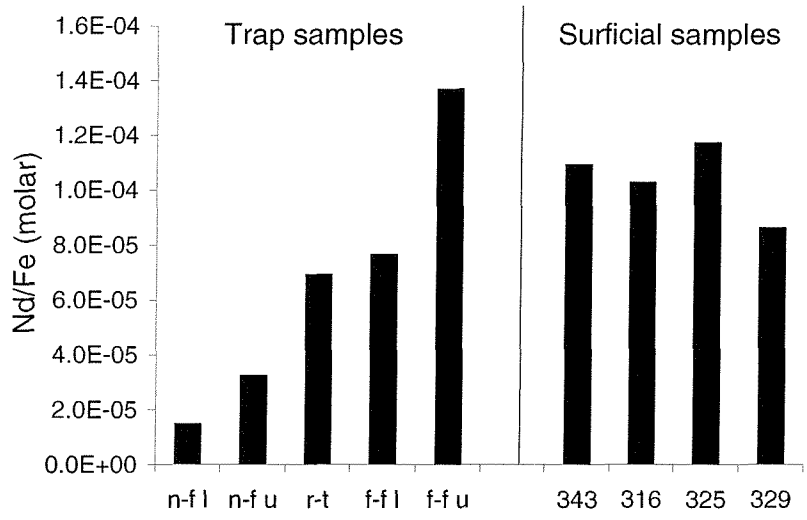

Figure 4.11: Nd/Fe in sediment traps and core tops.
Nd/Fe values are greater in the far-field sediment traps compared to the near-field traps, reflecting the greater proportion of Fe present as sulfides near-field, which do not incorporate significant quantities of REE. The cores show higher Nd/Fe than the lower far-field trap, indicating that REE continue to be scavenged for some distance downplume, unlike the situation for V/Fe (Fig. 4.5), where the lower far-field trap values are the same as the core tops.

proportion of the Fe-oxyhydroxides are carried far downstream. Manganese, low in the sediment traps due to its slower oxidation in seawater compared to Fe, is much higher in the surficial sediments, consistent with the passage of time allowing it to accumulate in the core sediment.

Although concentrations of hydrothermal Fe in the Rainbow sediments (1-2%) are much lower than those found in slowly accumulating metalliferous sediments from site 598 in the Pacific (10-30%), and the timescales are also very different (thousands of years at Rainbow versus millions of years at site 598),the mass accumulation rates for Fe are very similar (Rainbow 120-1377μmol cm^{-2} ky^{-1}, Site 598 40-1178μmol cm^{-2} ky^{-1} (Ruhlin and Owen, 1986).

Element	PAAS μg/g	Seawater ng/g	b.ground El/Al
La	38.2	4.03	5.97E-04
Ce	79.6	0.77	1.07E-03
Pr	8.83	0.62	1.57E-04
Nd	33.9	3.09	6.69E-04
Sm	5.55	0.62	1.18E-04
Eu	1.08	0.17	3.16E-05
Gd	4.66	0.99	8.44E-05
Tb	0.77	0.15	1.65E-05
Dy	4.68	1.04	9.52E-05
Ho	0.99	0.28	1.89E-05
Er	2.85	0.92	5.29E-05
Tm	0.41	-	6.86E-06
Yb	2.82	0.93	4.49E-05
Lu	0.43	0.15	6.30E-06

Table 4.6: REE concentrations for PAAS and background seawater, and average REE/Al ratios from background cores.
Background N. Atlantic samples are from cores 22#6 and 23#12. PAAS values from McLennan (1989) (used to normalize results), seawater values from Mitra *et al.* (1994).

μmol.cm^{-2}.ky^{-1}	V	Mn	Fe	Co	Cu	Zn
near-field(l)	2.72	2.39	1377	3.95	381.0	29.43
near-field(u)	0.66	3.12	303	0.62	40.26	4.97
far-field(l)	0.99	7.84	189	0.20	7.24	1.84
far-field(u)	0.88	8.37	120	0.11	1.03	1.12
ridge-top	0.26	3.19	128	0.09	1.72	1.45
c.343	2.76	19.26	555	0.45	12.7	0.61
c.316	2.59	24.12	519	0.50	11.89	0.73
c.325	2.77	20.26	530	0.28	3.33	0.22
c.329	4.53	44.71	942	0.39	3.50	0.45

Table 4.7: Comparison of fluxes of hydrothermally derived elements to sediment traps and surficial sediments

4.4 Conclusions

All the samples from the Rainbow area are significantly affected by hydrothermal activity. The results from the ridge-top trap indicate that plume material must occasionally reach well above nominal plume height observed by nephelometry in the water column, as no indication of a shallow source has been observed on the ridge-top, despite extensive water column surveys.

(1) Sediment trap Cu/Fe ratios decrease systematically away from the vents, as would be expected for an element such as Cu that forms sulfides as well as oxides. The Cu/Fe ratios in the traps converge with that of the surficial sediments, showing overlap between the far-field traps at ~1km from the vent site, and core 343, ~2km downstream. The core samples also show systematic variation in Cu/Fe downstream.

(2) Cobalt, more usually associated with hydrogenous sediments such as manganese nodules, is present in relatively high concentrations in the Rainbow sediments and in very high concentrations in near-field trap samples, due to its high concentration in the vent fluid. Its behaviour is very similar to that of Cu.

(3) Zn shows evidence of fractionation with respect to Cu, in that trap and surficial sediment Zn/Cu ratios are anomalously low compared to vent fluid ratios. The interpretation, consistent with previous buoyant-plume and proximal-to-vent-field studies, is that this results from preferential precipitation and settling of Zn sulfides closer to the active vent site than our nearest sample.

(4) The flux of V to the near-field sediment traps indicates that despite the presence of large amounts of sulfide in these traps, a high proportion of the Fe is present as oxyhydroxides rather than sulfides, consistent with the high Fe:H_2S ratio in the vent fluid.

(5) The flux of REE from seawater to sediments close to the Rainbow vent site, calculated from sediment trap data, is 2-3 times lower than that to the more distal core sediments, consistent with continuous scavenging of dissolved REE onto Fe-oxyhydroxides at increasing distance from the vent site, both within the dispersing plume, and following deposition to the seabed.

(6) Co-precipitation of Mg from seawater with vent-derived Fe may be a significant source of removal of Mg from seawater. Further studies of this process at other vent sites are needed to establish the magnitude of this sink.

Chapter 5

Scavenging of Osmium and other Platinum-Group elements by the Rainbow Hydrothermal Plume

Abstract

Osmium and other platinum-group elements (PGEs) have been measured in sediments accumulating directly under the Rainbow hydrothermal plume, at 36°N on the Mid-Atlantic Ridge. $^{187}Os/^{188}Os$ and PGE concentrations in the sediments of four cores taken 2-25 km from the active vent site reveal evidence of both radiogenic Os scavenged from seawater and of unradiogenic Os released by hydrothermal venting. The majority of analyses (n=16) yield $^{187}Os/^{188}Os$ ratios that fall in a narrow range (0.99- 1.06) close to that of modern seawater (1.07). In these samples, Os concentrations correlate linearly with hydrothermal Fe, V and P enrichments. A smaller subset of samples (n=6), characterized by unusually high concentrations of Ni and Cr derived from ultramafic rock fragments, exhibit distinctly lower $^{187}Os/^{188}Os$ ratios (0.53 - 0.96). Their Ir content is also higher, and their PGE patterns are more similar to mantle material than the PGE patterns of the larger set of samples dominated by seawater-scavenged Os. Compared with "background" (bg.) NE Atlantic sediments, Os is enriched in the seawater-dominated samples x4, Pd x2, Pt x10, but Ir enrichments are minor except in samples where an ultramafic input has been identified. Although the two proximal cores lack evidence for any ultramafic component in their surficial sediments, $^{187}Os/^{188}Os$ ratios in these samples are lower than that of ambient seawater, suggesting they may be influenced by unradiogenic Os from vent fluid incorporated into the plume. Burial fluxes of Os scavenged by hydrothermal Fe in these sediments are 200-400 $pg.cm^{-2}.ky^{-1}$, up to twice that found on the EPR, and several times the bg. of 50 $pg.cm^{-2}.ky^{-1}$. For Pt, burial fluxes are 1800-3000 $pg.cm^{-2}.ky^{-1}$ (bg. ~100$pg.cm^{-2}.ky^{-1}$), and for Pd 2700-4600 $pg.cm^{-2}.ky^{-1}$ (bg. ~800$pg.cm^{-2}.ky^{-1}$).

5.1 Introduction

Recent studies of platinum group elements (PGE) in marine sediments have tended to concentrate on Os and the evolution of the seawater $^{187}Os/^{188}Os$ ratio through time. Studies of metalliferous sediments have examined the long-term (10^7yr) (Peucker-Ehrenbrink and Blum, 1998; Peucker-Ehrenbrink *et al.*, 1995; Ravizza, 1993; Reusch *et al.*, 1998) and medium-term (10^5yr) records (Oxburgh, 1998; Ravizza *et al.*, 2001a), while anoxic sediments have been used to construct medium and short-term records (Oxburgh, 2001; Peucker-Ehrenbrink, 1996; Ravizza *et al.*, 1996). Studies have also been made on Fe-Mn crusts (Halbach *et al.*, 1989; Burton *et al.*, 1999), but only a few marine sediment studies have included the other PGEs: Pt, Pd, Ir, Ru (Bertine *et al.*, 1993; Colodner *et al.*, 1992; Koide *et al.*, 1991; Ravizza and Pyle, 1997; Ravizza *et al.*, 1999), although Pt and Pd are now receiving increasing attention as tracers of anthropogenic activity (e.g. Tuit *et al.*, (2000). Hydrothermal sediments have been shown to contain both mantle-derived Os from vent fluids, and continental-derived Os scavenged from seawater onto vent-plume particles (Ravizza *et al.*, 1996; Ravizza and McMurtry, 1993). So far however, measurements of hydrothermally derived or scavenged Pt and Pd have not been published, with the exception of a few data for the Cyprus Margi umbers (Ravizza *et al.*, 1999; Ravizza *et al.*, 2001b). Consequently little is known about how hydrothermal scavenging affects the concentrations of PGEs in sediments and seawater.

5.1.1 Platinum-group elements in seawater

Osmium isotopic composition and concentration

Osmium in seawater comes from three principal reservoirs - the continental crust which is radiogenic (average river water $^{187}Os/^{188}Os = 1.54$, Levasseur *et al.*, (1999)), the mantle which is unradiogenic ($^{187}Os/^{188}Os = 0.12$) (Roy-Barman and Allegre, 1994; Snow and Dick, 1995; Snow and Reisberg, 1995), and cosmic dust which exhibits unradiogenic $^{187}Os/^{188}Os$ similar to that of the mantle (Walker and Morgan, 1989). Cosmic dust input is believed to have been constant over time-scales of millions of years, with an estimated global flux of Os of 2-3ng.cm^{-2}.Ma^{-1} (Koide *et al.*, 1991), so that changes in the $^{187}Os/^{188}Os$ of seawater over shorter time scales should reflect changes in the relative inputs of continental and mantle-sourced Os. Both metalliferous and anoxic sediments can contain records of varying paleo-seawater $^{187}Os/^{188}Os$, that can be used

as proxies for continental weathering and/or changes in ocean circulation (Oxburgh, 1998). Studies of metalliferous sediments from the Pacific Ocean over the last 80 million years (Peucker-Ehrenbrink *et al.*, 1995) show a minimum $^{187}Os/^{188}Os$ value of 0.4 for seawater at the Cretaceous-Tertiary boundary, believed to result from the large inputs of cosmic dust at that time. Since then, a gradual increase in the inferred $^{187}Os/^{188}Os$ of seawater has been observed (Reusch *et al.*, 1998). The modern-day seawater Os concentration of 6-10pg.L^{-1} is similar to that of river water, while the seawater $^{187}Os/^{188}Os$ of 1.06 (Woodhouse *et al.*, 1999) is closer to (radiogenic) average river water/continental input than to (unradiogenic) mantle values. From a study of Fe-Mn crusts from the Atlantic, Pacific and Indian Oceans, Burton *et al.*, (1999) inferred that N. Atlantic seawater is slightly more radiogenic with respect to Os than that in the Pacific or Indian oceans, with $^{187}Os/^{188}Os$ of 1.07. Although most of the Fe-Mn crusts studied were high in Os (1000ppt), studies on sediments from the TAG hydrothermal site on the MAR (Ravizza *et al.*, 1996) included a 90-day old crust which had grown on an instrument placed close to the TAG vent site. This crust had less than 20ppt Os, with the concentration increasing slightly and becoming more radiogenic outwards, implying that the incorporation of seawater Os was an ongoing process. Sharma *et al.*, (2000) found Os concentrations in basalt hosted hydrothermal vent fluids from the Juan de Fuca Ridge to be similar in concentration to seawater, although very unradiogenic, and concluded that almost complete isotopic exchange between seawater and basalt takes place during seawater-rock reactions. They further concluded that subsurface hydrothermal fluids are highly enriched in Os but the precipitation processes at ridge crests cause a reduction in the concentration of Os in the emitted high temperature fluids (though without changing their Os isotopic composition). However, an off-axis low temperature fluid was found to have much higher concentrations of Os than seawater, with a very low $^{187}Os/^{188}Os$ (0.11), believed to be a result of the magma underneath the Juan de Fuca ridge having come into contact with very ancient depleted mantle material. The buffering effect of high-temperature systems led them to conclude that low temperature fluids may provide most of the supply of unradiogenic Os from venting to the oceans.

Palladium, Platinum and Iridium concentrations

Few studies so far have looked at PGEs in ocean waters. Platinum and palladium have been measured in the deep water (3000m) in the Pacific by Hodge *et al.*, (1985), who found Pt = 280pg.L^{-1} and Pd = 60pg.L^{-1}, while Hodge *et al.*, (1986) showed an increase in Pt from 90pg.L^{-1} in Pacific surface waters to 210-220pg.L^{-1} in deep

waters, exhibiting nutrient-like behaviour. However, Jacinto *et al.*, (1989) found that in the Indian Ocean, Pt was scavenged down the water column, and so was depleted at depth, with values ranging from 253pg.L^{-1} (1.3pmol.L^{-1}) at the surface to 55pg.L^{-1} (0.29pmol.L^{-1}) at depth. Lee, (1983) measured Pd in Pacific seawater, and found it to range from 19pg.L^{-1} (0.18pmol.kg^{-1}) at the surface to 70pg.L^{-1} (0.66pmol.kg^{-1}) in deep water. Pd exists only in the Pd (II) state in seawater, while Pt exists as Pt(II) and (IV)(Goldberg, 1987). Despite a Pt/Pd ratio in crustal materials of about 0.5(wt:wt) (Goldberg, 1987), Pt/Pd in seawater is ~4.5 (Hodge *et al.*, 1985). Both form strong chloro complexes, but the stability constant for Pt is higher than Pd (Hodge *et al.*, 1985; Goldberg and Koide, 1990). Kump and Byrne, (1989) showed strong complexing of Pd with chloride complexes in seawater, suppressing the hydrolysis of Pd^{2+}. Seawater Ir concentrations have been measured at 0.9pg.L^{-1} (Hodge *et al.*, 1986).

5.1.2 Platinum-group elements in marine sediments

The composition of the non-biogenic fraction of marine sediments can have a considerable effect on both the PGE concentrations and the Os isotopic composition of the bulk sediment. Mantle rocks such as peridotites have high concentrations of Os, av. 3ng.g^{-1}, with a $^{187}Os/^{188}Os = 0.12$ (Snow and Dick, 1995; Snow and Reisberg, 1995), and generally similar ng.g^{-1} levels of Ru, Pd, Pt and Ir, whereas continental and ocean floor basalts have lower PGE concentrations than mantle material with fractionated PGE patterns (e.g. Pd/Ir =100, Barnes et al., (1985)). Continental crust averages 50pg.g^{-1} Os, with a $^{187}Os/^{188}Os = 1.26$ ($^{187}Os/^{186}Os$ ratio = 10) (Esser and Turekian, 1993). Levasseur *et al.*, (1999) have shown that dissolved Os in average continental runoff has a mean concentration of 8pg.kg^{-1}, with $^{187}Os/^{188}Os = 1.54$ ($^{187}Os/^{186}Os$ of 12). Some of the detrital material in marine sediments far from land is composed of wind-borne material from the continents. Peucker-Ehrenbrink and Jahn (2001) recently proposed a revised upper crustal concentration of Os = 31pg.g^{-1}, following studies of loess from China, S. America and Europe, with $^{187}Os/^{188}Os = 1.05\pm0.23$. They further proposed a revised Pt/Pd ratio of ~1 (Pt=510 pg.g^{-1}, Pd=520pg.g^{-1}) rather than the ratio of 0.5 proposed by Goldberg (1987).

Sediments accumulating at ridge axes that are influenced by hydrothermal activity can have several components of crustal detritus as well as biogenic and hydrothermal inputs. To date, Os isotopic analyses are available from metalliferous sediments from the East Pacific Rise ridge-crest (Ravizza and McMurtry, 1993) and from the TAG hydrothermal area at 26^o N on the MAR (Ravizza *et al.*, 1996). The EPR samples

all comprised >80% $CaCO_3$, with concentrations of Os >100pg.g^{-1}, isotopically indistinguishable from seawater. By contrast, TAG samples showed unradiogenic Os isotope ratios in deposits from areas of low temperature venting, with Os concentrations of <30pg.g^{-1}, while metalliferous sediment samples recovered from a core close to the high temperature venting areas exhibited ratios between those of ocean crust and modern seawater, with a range of Os concentrations from 200-500pg.g^{-1}.

Many of the geochemical studies on Pt, Pd and Ir have been carried out on ore deposits e.g. (Barnes, 1990; Campbell and Barnes, 1984; Peck *et al.*, 2001; Reeves and Keays, 1995; Vogel and Keays, 1997). Platinum and palladium in particular are of economic importance, and are mined from both placer deposits and from Ni-Cu-PGE and Ni-Mo-PGE deposits (e.g. Horan *et al.*, (1994). A summary of PGE data for continental and mantle rocks can be found in Barnes *et al.*, (1985), while Pearson and Woodland, (2000) recently characterised a selection of volcanic rocks (picrites and andesites) for the full range of PGEs. Few analyses of these elements have been made on marine sediments, however, although Ir has been studied in several areas in relation to bolide impacts since they were first linked to mass extinction events (Alvarez *et al.*, 1980)). Goldberg and Koide, (1990) examined a range of marine sediments and found Pd and Pt at 1-20ng.g^{-1} concentrations, with Ir and Os concentrations an order of magnitude lower. Manganese nodules from the same study, by contrast, contained up to 900pg.g^{-1} Pt, 3 orders of magnitude higher than either Pd, Ir or Os. In an investigation of a selection of igneous rocks, metalliferous sediments and reducing sediments, Ravizza and Pyle, (1997) found that the relative PGE patterns in the metalliferous sediments were similar to basalts, but at concentrations up to two orders of magnitude higher. They concluded that PGEs were extracted from basalts as a result of hydrothermal alteration and then deposited with metalliferous sediments. A study of umbers from Margi (Cyprus) (Ravizza *et al.*, 1999), considered to be analagous to modern-day deposits of hydrothermal precipitates, found concentrations up to 20pg.g^{-1} of Pd and Pt, but less than 1pg.g^{-1} for Ir and Os.

While the importance of studying Os in the marine sedimentary environment is increasingly recognised - not least due to its potential as a paleoceanographic tracer, - the remainder of the PGEs continue to be relatively overlooked, and PGEs in marine sediments are rarely examined as a group. This study reports the Os isotope composition of, and PGE fluxes to, a suite of sediments accumulating under the hydrothermal plume at various distances from the high-temperature Rainbow vent site at 36^{o}N on the MAR.

5.2 Methods

Core collection methods have been described in detail in Chapter 2. The four principal cores studied were retrieved from directly beneath the hydrothermal plume which disperses away from the Rainbow vent field complex. Cores were taken at various distances downstream from the vent site (core 343 at 2 km, 316 at 5 km, 325 at 10 km and 329 at 25 km) and at water depths of 2300-2600m (Chapter 3; Cave *et al.*, 2002). PGE and Os isotopic analyses were carried out on dried and powdered bulk samples from these cores, and on similar samples from one "background" NE Atlantic carbonate sediment core from east of the MAR. Radiocarbon data were used to define the surface mixed layer depths and the accumulation rates for the five cores studied (Fig. 3.2, Cave *et al.*, 2002). For each of the Rainbow cores, 3 or 4 samples were analysed from the surface mixed layer, as well as samples from mid-core and the base. Mid-core samples from core 343 were deliberately chosen to include levels that were noted on sampling to be contaminated with ultramafic rock fragments that have subsequently been shown to affect trace metal compositions at those depths (Chapter 3; Cave *et al.*, 2002).

Samples of about 5g were spiked with a mixed PGE spike enriched in ^{99}Ru, ^{105}Pd, ^{190}Os, ^{191}Ir and ^{198}Pt for isotope dilution prior to pre-concentration of PGEs by NiS fire assay (Ravizza and Pyle, 1997). Analyses of $^{187}Os/^{188}Os$ were carried out by sparging volatile OsO_4 to a magnetic-sector ICP-MS, following which the residual solutions were diluted and analysed for Ru, Pd, Pt and Ir and Os by ICP-MS, using reference standards (Hassler *et al.*, 2000). This combination of methods allows for the determination of Os concentrations and isotopic compositions as well as concentrations of the other PGEs on the same sample split, thus avoiding difficulties in interpretation where samples are not fully homogenised. Blanks for Os were less than 1pg.g^{-1}, for Ru $<$ 20pg.g^{-1}, for Pd $<$ 120pg.g^{-1}, for Pt $<$ 6pg.g^{-1} and for Ir $<$ 3pg.g^{-1}. Standard deviations of better than 1% for Os were achieved for all samples except the low-concentration N. E. Atlantic background samples, where they were less than 4%. Both $^{187}Os/^{188}Os$ and $^{187}Os/^{186}Os$ are reported in Appendix 6 to allow full comparison with all other published data although only $^{187}Os/^{188}Os$ ratios are discussed in the text.

5.3 Results and Discussion

5.3.1 Osmium

The mixed layer (0-10 cm) samples of the Rainbow cores exhibit a range of Os concentrations from 132-165 pg.g^{-1}, with $^{187}Os/^{188}Os$ ratios between 0.95-1.06 (Fig. 5.1, Appendix 6). Samples from the mixed layer of the background N. E. Atlantic core, 23#12, have concentrations from 40-57pg.g^{-1} and $^{187}Os/^{188}Os$ of 1.02-1.07. Some samples from deeper parts of core 316 and 343 show much lower $^{187}Os/^{188}Os$, together with high Os concentrations (Fig. 5.1a,b) than the near-surface samples. The contributions of Os from various sources to the Rainbow sediments are discussed below.

The detrital Os contribution

Core 23#12 and the Rainbow cores have similar $CaCO_3$ contents of >80%, but the detrital component of the Rainbow sediments, as calculated from their Al content, is about half that of core 23#12 because of the presence of an additional hydrothermal component (Chapter 3, Cave *et al.*, 2002). Thus, NE Atlantic-type detrital material can only be expected to have contributed ca. 20-29pg.g^{-1} Os to the mixed-layer Rainbow samples, yielding an excess Os over NE Atlantic background of at least 100pg.g^{-1} in these samples, very similar to the values seen in the sediments from the crest of the EPR (Ravizza and McMurtry, 1993).

The cosmic Os contribution

Osmium concentrations of 93-112 pg.g^{-1} have been measured in a deep-sea clay from west of the Cape Verde abyssal plain (Peucker-Ehrenbrink and Ravizza, 2000), with bulk $^{187}Os/^{188}Os$ of 0.99-1.01. These samples are from core 10400, 25^{o}42.4'N, 30^{o}57.7'W, at 6044m water depth, one of the few brown clay areas in the N. E. Atlantic (Colley *et al.*, 1984). The upper samples from that core contain <1% $CaCO_3$. The sedimentation rate for the upper part of this core of ~ 0.27cm.ky^{-1} is similar to that of the clay fraction of core 23#12 of 0.31cm.ky^{-1}. Modelled estimates of the extra-terrestrial contribution of Os to core 10400 sediments are 4-6 pg.g^{-1} (Peucker-Ehrenbrink and Ravizza, 2000). Given that the bulk sedimentation rate of Core 23#12 is 1.51 cm.ky^{-1}, this gives a likely cosmic Os contribution of ~1pg.g^{-1}. The even higher sedimentation rate of the Rainbow cores of 2-3cm.ky^{-1}, suggests a likely cosmic Os contribution, as-

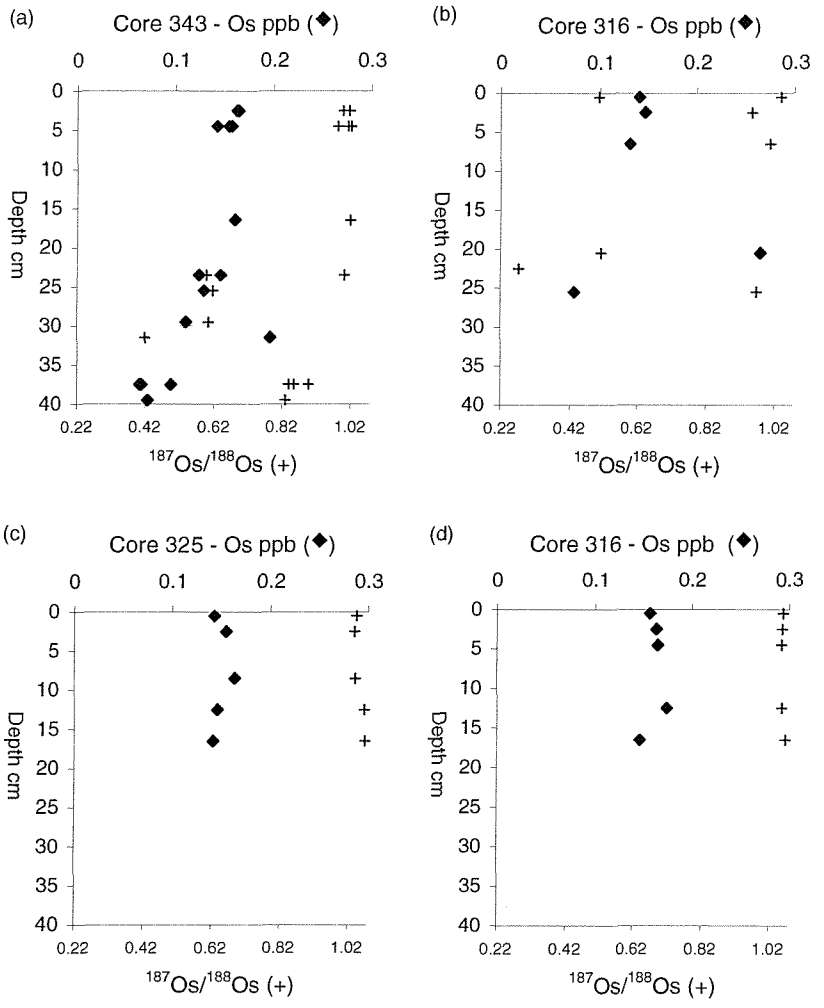

Figure 5.1: Osmium and $^{187}Os/^{186}Os$ in the Rainbow cores.
Most of the samples from the upper 20cm of all the cores have high Os concentrations, and high, seawater-like $^{187}Os/^{186}Os$, with the exception of one sample from the surface of core 316. Some deeper samples from the two proximal cores, 343 and 316, have much lower $^{187}Os/^{186}Os$, indicating an ultramafic contribution of Os.

suming a constant cosmic Os flux, which is even lower, ca. <1 $pg.g^{-1}$, i.e. than 1% of the total Os measured.

The hydrogenous contribution of Os

If all the Os in the samples from core 23#12 were associated with the clay component (about 20% of the bulk sample), then Os concentrations in these samples are 2-3 times the expected value for a North Atlantic clay (Peucker-Ehrenbrink and Ravizza, 2000). Given the observed seawater-like $^{187}Os/^{188}Os$ ratios (up to 1.06) in these samples, a simple explanation would be that a large part of the Os in these sediments is derived from seawater. This conclusion is supported by the fact that Os/Ir in marine clays is generally ~ 1 (Koide *et al.*, 1991), whereas Os/Ir in the 23#12 samples is ~ 2, implying that about half the Os is derived from seawater. The leachable fraction of core 10400 above, taken to represent the hydrogenous fraction, was 18-30$pg.g^{-1}$, up to one third of the 93-112 pg/g Os measured in those samples. The average Os/Al ratio of 2.09 x 10^{-9} from core 23#12 is therefore taken to be representative of the combined continental detrital and hydrogenous contribution of Os to the Rainbow cores. If this contribution is subtracted from the Rainbow core samples that have the most seawater-like $^{187}Os/^{188}Os$ ratios, a good relationship can be seen between the excess Os in these samples, and hydrothermal Fe and V (Fig. 5.2 (see chapter 3, and Cave *et al.*, 2002 for calculations of hydrothermal Fe and V) .

The ultramafic contribution of Os

The mantle Os concentration is several orders of magnitude greater than mid-ocean ridge basalt (MORB) or continental crust, being measured in ppb rather than ppt. The piece of serpentinite recovered from core 343 has a relatively low concentration of Os (1 ppb), similar to other peridotites measured on the MAR in the N. Atlantic (Roy-Barman and Allegre, 1994), but low compared to the 3-4 ppb measured in peridotites from the SW Indian and American-Antarctic ridges (Snow and Dick, 1995; Snow and Reisberg, 1995). However, the measured $^{187}Os/^{188}Os$ ratio of 0.12 in the Rainbow serpentinite is consistent for almost all peridotites so far measured, indicating that while hydrothermal processes may have extracted Os from the parent material, no appreciable exchange with seawater Os has taken place. Pieces of rock-like material recovered from core 316 were amalgamations of serpentinite and sulfide, and showed variable Os concentrations, with slightly more radiogenic $^{187}Os/^{188}Os$ ratios than the

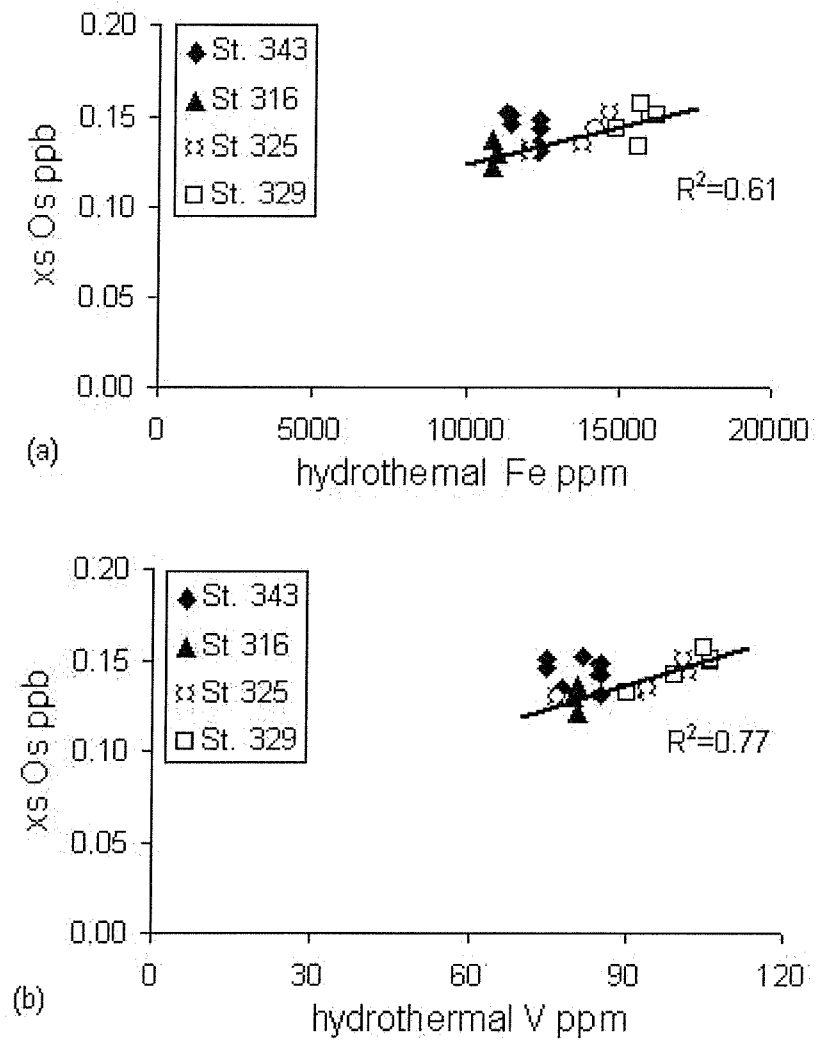

Figure 5.2: Excess Os in Rainbow sediments *versus* hydrothermal Fe and V
Osmium is believed to be scavenged from seawater by hydrothermal Fe-oxyhydroxides in the same way as oxyanions such as V. Trendlines do not include core 343 samples, as the excess Os calculation for these samples is complicated by the possible presence of vent-fluid Os, or Os derived from ultramafic debris in the sediments. See text for details.

serpentinite from core 343 (see Appendix 6a). Samples from core 343 from levels where an ultramafic contribution to the sediments had previously been noted from excess Ni and Cr (Chapter 3, Fig. 3.8, Cave *et al.*, 2002), showed similar concentrations of Os to the mixed layer samples, but with significantly lower $^{187}Os/^{188}Os$ ratios of 0.42-0.61. These samples were also enriched in Ir compared to samples from the mixed layer.

Fig 5.3 shows total Os plotted against Ni for the Rainbow sediment samples. Also shown are samples from the background N. Atlantic core, 23#12. It can be seen that most of the Rainbow samples are strongly enriched in Os over background values of < 0.05ppb. Looking first at samples from core 343 (black diamonds), it can be seen that they fall into two groups. One group, which comprises samples from the deeper part of the core, are rich in Ni, and this has previously been attributed to the presence of ultramafic material in these samples (Chapter 3, Cave *et al.*, 2002). Osmium is correlated with Ni in these samples. The remainder of the samples from core 343 are low in Ni, with values similar to N. Atlantic background, but are enriched in Os by up to three times background, as are all the samples from cores 325 and 329, 10km and 25km downplume of the vent site respectively, and not located on ultramafic basement.

The situation is a little different for samples from core 316, located 5km downplume from the vent site, but like core 343, on the same ultramafic block. One of the samples from core 316, falls on the mixing line for core 343 samples indicating the presence of ultramafic material. 3 of the samples fall in the high-Os low-Ni group, indicating the presence of plume-derived Os, while the remaining three have very high Os, but only small enrichments of Ni. In this case, the possibilities are either these samples contain very high amounts of scavenged Os, or they are contaminated by ultramafic or other debris which is low in Ni, and high in Os, or a combination of these.

Iridium is a much more sensitive indicator of the presence of ultramafic material than Ni, as it is present in very low concentrations in most pelagic sediments, but in very high concentrations in ultramafic rock. Its concentration in ultramafics is less variable than Ni concentrations, which in ultramafic rocks along the MAR vary by at least a factor of two (Cave *et al.*, 2002). Fig. 5.4a and b shows a plots of $^{187}Os/^{188}Os$ against 1/Ir and 1/Os for the samples from the four Rainbow cores. The data clearly fall into two sets, each of which shows mixing between two end members, and with one of those end members common to both trends. One of the trends, which incorporates all the samples from the distal cores 325 and 329, as well as samples from the upper 17cm of core 343 and several of the samples from core 316, has approximately seawater ratios for all samples over a range of Ir values. The second trend reflects mixing between samples

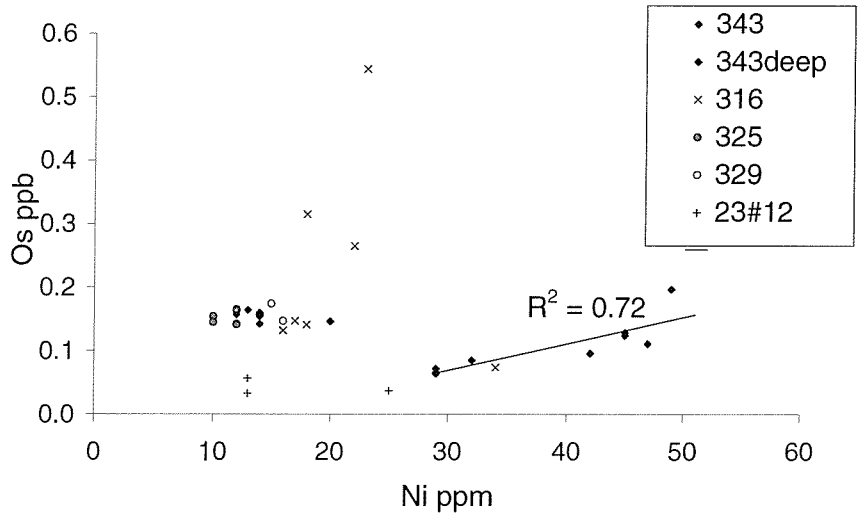

Figure 5.3: Os vs. Ni in Rainbow sediments
Ultramafic debris in the near-field core (343) from Rainbow has a high nickel content, and contains large concentrations of unradiogenic Os. Trendline through the samples from the deeper part of core 343 indicates that samples from the lower part of this core contain Os from this ultramafic source.

which have low contents of seawater-derived Os, (and, by analogy, Ir), and samples from deep within core 343 and 316, which have anomalously high concentrations of both Ir and Os, and with low (unradiogenic) Os isotopic ratios. These are samples which have been previously found to have high Ni and Cr content, indicating ultramafic contamination (Cave *et al.*, 2002).

The piece of serpentinite recovered from core 343, and the two serpentinite/sulfide amalagamations recovered from core 316, have both higher Os and Ir contents, and lower Os isotopic ratios, than any of the sediment samples (see Appendix 6a). The background samples from core 23#12 have both lower Ir and lower Os contents than the Rainbow samples, but with exclusively seawater-like Os isotopic ratios. However, the fact that the samples from the near-field Rainbow cores with seawater-like Os isotopic ratios, are clearly enriched in Ir over samples from the background core 23#12, despite their detrital component being smaller, implies that some scavenging of Ir from seawater (or, conceivably, vent fluid) has taken place. These near-field core-top samples also show evidence of a reduction in the overall $^{187}Os/^{188}Os$ ratio, compared to seawater and the far-field cores 325 and 329 (Fig. 5.5). This suggests that the enhanced hydrothermal

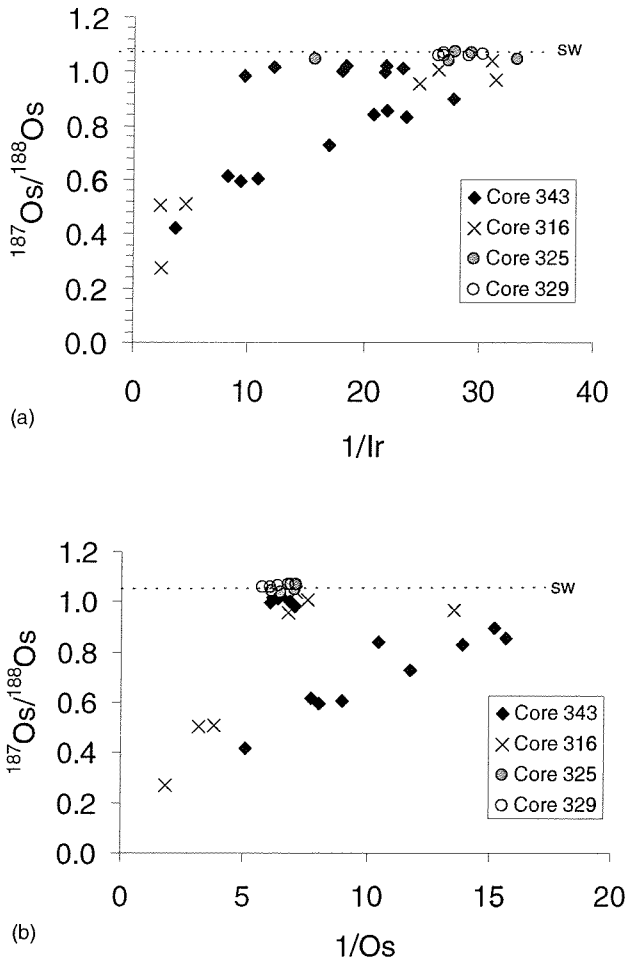

Figure 5.4: Os and Ir end members
(a) End members for Ir are (i) high Ir, low 187/188Os (ii) low Ir, high(seawater-like) 187/188Os, (iii) seawater derived Ir and Os (= scavenged). (b) End members for Os are (i) high Os, low 187/188Os (= mantle) (ii) low Os, high 187/188Os (= seawater). Rainbow samples which contain only scavenged Os (from seawater and vent fluid) sit on or about the seawater line.

plume fallout to these samples, already demonstrated by e.g. Cu/Fe ratios in the same samples (Cave *et al.*, 2002, Chapter 3) has also led to increased Ir. It further suggests that the Os input to this core retains some primary mantle-type Os signature, which has been transported to the core-top faster than the carrying agent (presumably Fe-oxyhydroxides) has been able to undergo full isotopic equilibration with the host seawater, as is to be expected from previous work carried out at the TAG vent site (Ravizza *et al.*, 1996), and has also occurred here, judging by the clearly seawater-like ratios in cores 325 and 329.

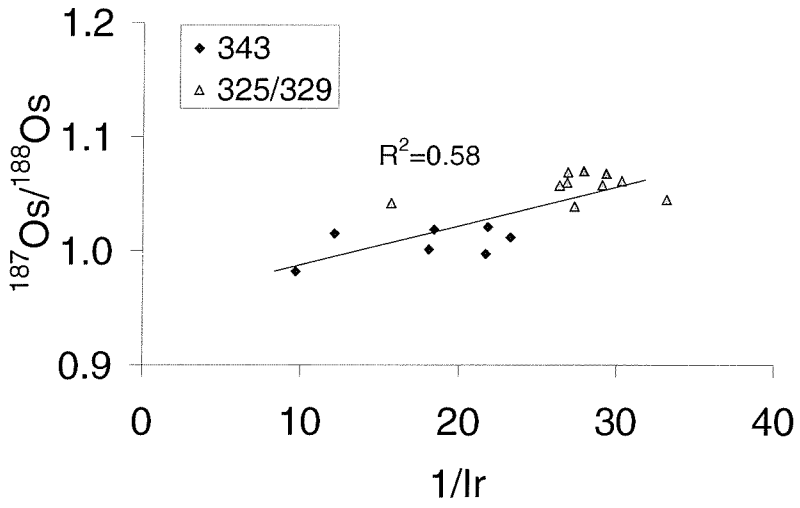

Figure 5.5: Scavenged Ir in Rainbow sediments.
The near-field core (343) shows enhanced Ir compared to the distal cores (325 and 329), as well as slightly more radiogenic $^{187}Os/^{188}Os$, indicating that as well as the presence of a small amount of vent-derived Os lowering the isotopic signature in the near-field samples, some scavenging of Ir has taken place either from seawater, or possibly from vent fluid.

The hydrothermal contribution of Os

Little is yet known about the behaviour of Os in hydrothermal plumes. At the TAG hydrothermal area, 26°N on the MAR, Ravizza *et al.*, (1996) studied Os in a range of metalliferous sediments, including samples from the bottom of Alvin pushcore 2182-4, which the German *et al.*, (1993) study showed were samples of mixed biogenic carbonate and near-field plume fall-out. Ravizza *et al.*, (1996) concluded that the Os in the core

samples was derived predominantly from seawater, not only for the samples containing plume derived Fe-oxyhydroxides, but also for samples containing oxidised sulfides. In the case of the sulfides, however, the interpretation was that Os had been taken up from seawater during the oxidation process, and had overprinted any mantle-derived Os that might have been scavenged from the vent fluid, whether by addition or by isotopic exchange.

The data from Rainbow show a range of samples greatly enriched in Os over N. Atlantic background, and with seawater-like ratios, as well as samples clearly contaminated by ultramafic debris, rich in unradiogenic Os. Of the uncontaminated samples, the samples closest to the vent (cores 343 and 316) have slightly lower $^{187}Os/^{188}Os$ ratios than samples from the more distal cores (325 and 329), indicating the presence of some unradiogenic Os scavenged from the vent fluid in the near-field cores. This implies that plume fallout in these cores has been deposited before enough time has elapsed for the Os to fully equilibrate with seawater.

World-wide, the only vent fluid Os data available are from 3 volcanic-hosted sites on the Juan de Fuca Ridge (Sharma *et al.*, 2000), who found $^{187}Os/^{188}Os$ between 0.13 and 0.38 for high temperature fluids, with concentrations similar to seawater. The vent fluid produced at these basalt-hosted sites is unlikely to be directly analagous to the fluid from the ultramafic-hosted site at Rainbow, which has the potential to be more strongly enriched in Os due to the high concentrations in ultramafic rock compared to basalt. However, the buffering processes that appear to operate sub-surface on the Juan de Fuca Ridge, maintaining low concentrations in the emitted high-temperature fluids, may also operate at Rainbow.

Ratios of plume-derived Os/Fe in the Rainbow cores are ~ $1x\ 10^{-8}$, the highest found for any metalliferous sediment so far, with the exception of the fresh ridge-crest sediment from the EPR (Ravizza and McMurtry, 1993). They are an order of magnitude greater than has been found in metalliferous sediments from the flanks of the EPR (Oxburgh, 1998), and in older metalliferous sediments from DSDP Leg 92 (Ravizza, 1993; Ravizza and Pyle, 1997; Reusch *et al.*, 1998), in the TAG sediments (Ravizza *et al.*, 1996) and in the Margi umbers (Ravizza *et al.*, 1999) (Fig. 5.6). This indicates that fresh Fe-oxyhydroxides in hydrothermal plumes are much more efficient at scavenging Os from seawater than either oxidising sulfides, or hydrogenous Fe precipitation processes. Burial fluxes of seawater-derived Os to the Rainbow sediments are given in Table 5.1. These data are from samples that contain seawater-like Os isotope ratios, implying no addition of ultramafic debris, and from which the average N. Atlantic back-

ground concentrations have been subtracted, using element/Al ratios from the BOFS samples studied here. However, burial fluxes of Os in the Rainbow hydrothermal sediments are still much less than has been found in anoxic sediments (Oxburgh, 1997). A comparison between Os fluxes to Rainbow and other metalliferous sediments, and to anoxic sediments from the Cariaco basin, are given in Table 5.2.

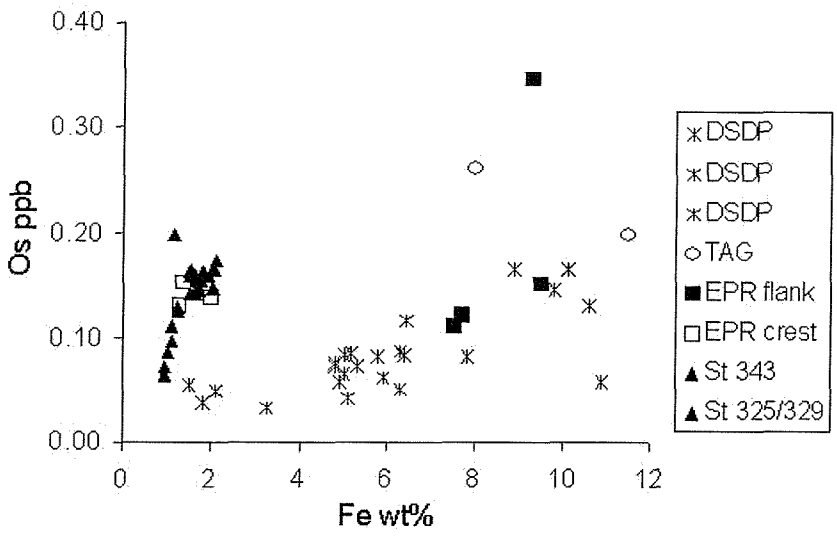

Figure 5.6: Scavenged Os in metalliferous sediments.
Os/Fe in Rainbow sediments is similar to ridge-crest samples from the East Pacific Rise (EPR), but is much higher than is found in EPR flank sediments, and in older sediments from DSDP Leg 92 drill sites. EPR ridge-crest data from Ravizza and McMurtry (1993), EPR flank data from Oxburgh (1998), DSDP data from Ravizza (1993), Ravizza and Pyle (1997), Reusch *et al.*, (1998), TAG data from Ravizza *et al.*, (1996).

Hydrothermal sediments as records of past seawater Os isotopic composition

One of the sediment cores collected at Rainbow, core 343, goes back to the last glacial maximum (Chapter 3, Cave *et al.*, 2002), and all samples contain Os scavenged from seawater by the hydrothermal plume. Such records provide the potential to test whether or not $^{187}Os/^{188}Os$ ratios lower than present-day values characterised the entire N. Atlantic during the LGM, as has been proposed by Oxburgh (1997) from studies of anoxic sediments from the Cariaco basin in the southern N. Atlantic. While the present study shows that seawater Os is efficiently scavenged by the hydrothermal plume and buried in sediments, several possible complications are indicated for studying small temporal Os isotopic variations:

Table 5.1: Platinum-group element burial fluxes in the Rainbow cores.

Core	Os	Pt	Pd	Ir
343	$ng.cm^{-2}.ky^{-1}$	$ng.cm^{-2}.ky^{-1}$	$ng.cm^{-2}.ky^{-1}$	$ng.cm^{-2}.ky^{-1}$
1-2cm	0.29	1.85	2.38	0.08
2-3cm	0.29	2.19	2.65	0.11
4-5cm	0.28	1.79	2.58	0.12
16-17cm	0.28	2.68	3.07	0.11
316	$ng.cm^{-2}.ky^{-1}$	$ng.cm^{-2}.ky^{-1}$	$ng.cm^{-2}.ky^{-1}$	$ng.cm^{-2}.ky^{-1}$
0-1cm	0.24	1.61	2.89	0.06
6-7cm	0.24	1.95	3.08	0.07
325	$ng.cm^{-2}.ky^{-1}$	$ng.cm^{-2}.ky^{-1}$	$ng.cm^{-2}.ky^{-1}$	$ng.cm^{-2}.ky^{-1}$
1-2cm	0.20	1.26	2.13	0.04
2-3cm	0.24	1.82	3.02	0.06
8-9cm	0.26	1.92	3.23	0.11
12-13cm	0.26	2.09	3.43	0.07
16-17cm	0.32	2.54	4.35	0.09
329	$ng.cm^{-2}.ky^{-1}$	$ng.cm^{-2}.ky^{-1}$	$ng.cm^{-2}.ky^{-1}$	$ng.cm^{-2}.ky^{-1}$
1-2cm	0.33	2.23	3.67	0.08
2-3cm	0.36	2.74	4.38	0.09
4-5cm	0.44	3.60	5.46	0.11
12-13cm	0.41	3.12	5.40	0.09
16-17cm	0.41	3.48	5.69	0.11

Table 5.2: Seawater-derived Os concentrations and burial fluxes in metalliferous and anoxic sediments

Sample Site	Os conc. $pg.g^{-1}$	$CaCO_3$ %	Os flux $pmol.cm^{-2}.ky^{-1}$	ref
Rainbow	120-160	80	1.58	this work
TAG	200-500	0-70	n.a.	Ravizza 1996
EPR flank	100-400	60-90	0.79-1.21	Oxburgh 1998
EPR crest	130-150	80	0.50-0.86	Ravizza 1993
Cariaco B.	100-150	n.a.	4.73	Oxburgh 1987

(i) hydrothermal sediments would need to be an unknown minimum distance from the source venting area in order to avoid the presence of variable amounts of unradiogenic Os scavenged from vent fluid,

(ii) inputs of even very small amounts of ultramafic material to the sediments have a significant effect on the bulk Os isotopic composition of the sediment (cf. Fig. 5.4. Along the MAR, such material can come from weathering of local outcrops, or during glacial periods, from greater inputs of land-derived ultramafic material present in dust. While in the Rainbow area, sedimentation decreased during glacial times, 100km or so further north in the Lucky Strike segment, which also hosts significant hydrothermal activity, sedimentation rates and inputs of continental detritus were much greater during the last glacial maximum, up to $30cm.kyr^{-1}$, compared to a Holocene sedimentation rate of ~$7cm.kyr^{-1}$ in this segment (Richter, 1998),

(iii) a long-term vigorous source of venting is required to be operational over the time-scale to be studied. Because of these constraints, the core at Rainbow is unsuitable for this kind of study.

5.3.2 Palladium, Platinum and Iridium

The N. Atlantic background samples from core 23#12 show a significant enrichment of Pd over Pt (av. Pt/Pd = 0.1) in keeping with the apparent greater removal of Pd from the water column than Pt (seawater Pt/Pd = 4.5) despite their similar crustal abundances (Goldberg, 1987; Peucker-Ehrenbrink and Jahn, 2001). For the Rainbow samples unaffected by ultramafic contamination, Pd/Al is ~3×10^{-4} , compared to

~3 x 10^{-8} for the background sediments, and Pt/Pd is 0.5-0.7, indicating considerable scavenging of of both Pd and Pt by the hydrothermal plume.

The C1 chondrite-normalised patterns for Pd, Pt, Ir and Os are plotted in Fig. 5.7. Fig. 5.7a and b show samples from cores 329 (25km downplume) and core 343 (2km downplume, on the side of the ultramafic block that hosts the vent site). Core 325 patterns are identical to 329, and so are not shown here. The chondrite normalised pattern for the background NE Atlantic core 23#12, is also shown on each figure. It can be clearly seen that the Rainbow cores are greatly enriched in Pd, Pt and Os with respect to 23#12, and that some samples from core 343 show significant enrichments of Ir. The pattern for the serpentinite recovered from core 343 is shown on Fig. 5.7b for comparison. Core 316 (Fig. 5.7c) shows 4 samples which have similar patterns to the more distal cores 325 and 329, but shows other samples with a much flatter more chondritic pattern, and one sample which has Pt > Pd. Shown in grey on this figure are the patterns for the pieces of amorphous serpentinite/sulfide material from this core The incorporation of such material into the sediments, derived from up-slope, appears to have led to these patterns. The sample with Pt > Pd in core 316 is from the top cm of this core, and as well as its unusual PGE pattern, showed a very low $^{187}Os/^{188}Os$ ratio, of 0.50 (see Appendix 6a). Two splits of this sample were analysed, and the other split had high $^{187}Os/^{188}Os$ = 1.04, and a PGE pattern similar to the other samples with seawater-like Os isotope ratios. This implies that this sample may not have been well homogenised during the grinding process, and contained some material high in Pt and Pd, with a low Os isotope ratio. The patterns for the two splits of this sample are shown in Fig. 5.8, together with a chondrite-normalised pattern from a representative sample from the Margi umbers (Ravizza *et al.*, 1999). The pattern for the replicate sample from core 316 core top can be seen to be very similar to the pattern for the umber, indicating the presence of some oxidised sulfide material in this sample.

The metalliferous samples from DSDP Leg 92, shown in Fig. 5.7d, by contrast are more enriched in Pd, and less enriched in Os, than the samples from Rainbow, although still strongly enriched in Pt, and with small Ir enrichments.

Platinum, Pd and Ir fluxes from seawater to the Rainbow sediments are shown in Table 5.2. These data are from samples that contain seawater-like Os isotope ratios, implying no addition of ultramafic debris, and from which the average N. Atlantic background concentrations have been subtracted, using element/Al ratios from the BOFS samples studied here.

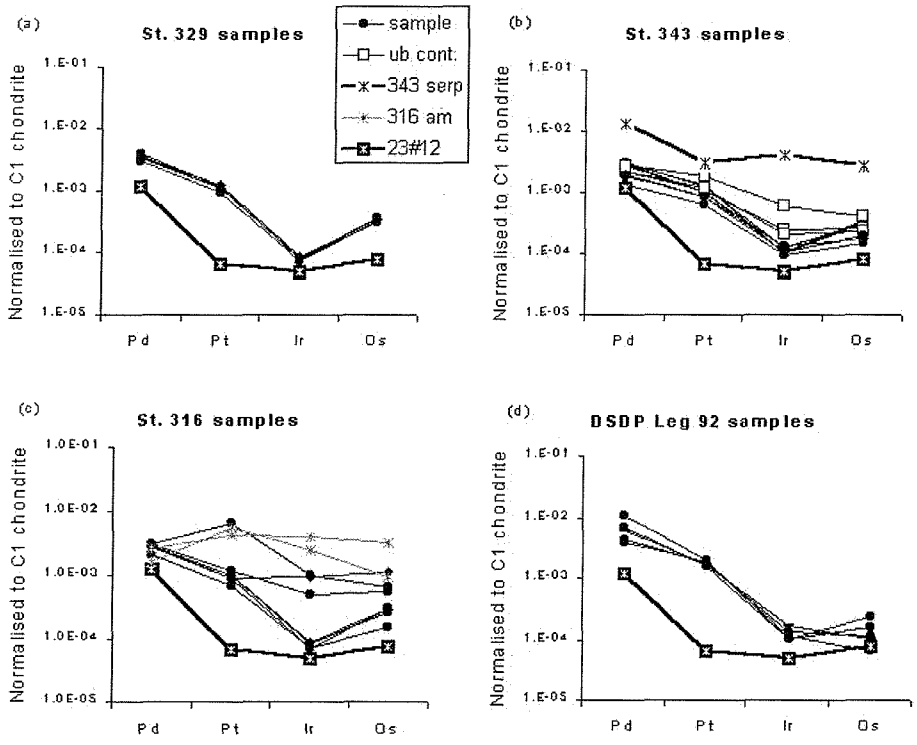

Figure 5.7: PGE patterns in Rainbow sediments.
(a) Samples from distal cores 329 and 325 show significant enhancement in Pd, Pt and Os over background N. Atlantic sediments. (b)Samples from proximal core 343 are generally similar to the distal samples, but with enhanced Ir over background. Samples from layers enriched in ultramafic content (open boxes) show a flatter pattern, with strong Ir and Os enrichments over background. Pattern for serpentinite recovered from core 343 is shown for comparison. (c) Samples from core 316, more distant than core 343, again show similar patterns to the distal cores for some samples, but very strong enrichments in Ir and Os in other samples, pointing to ultramafic input. Patterns from amorphous rock samples recovered from core 343 shown for comparison. See Fig. 5.8 for more detail. (d)Samples from DSDP Leg 92 (Ravizza and Pyle, 1997) appear less enriched in Os, and more variably enriched in Pd compared to distal Rainbow samples.

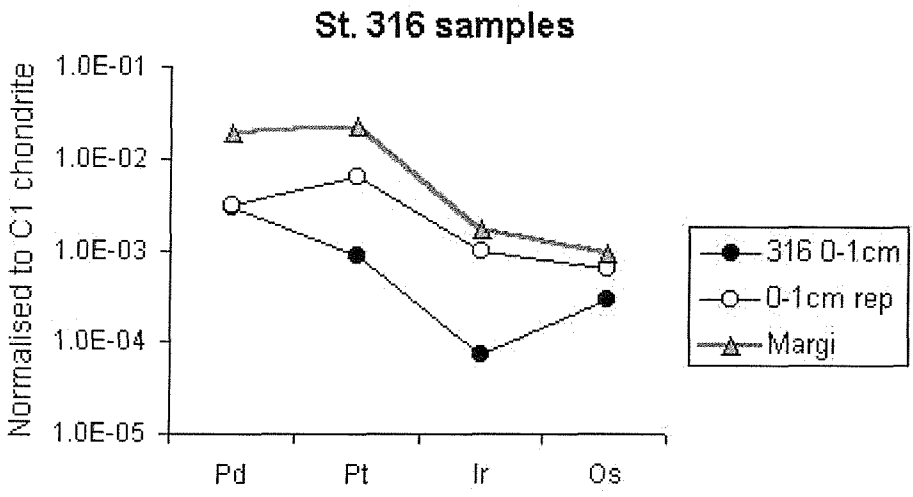

Figure 5.8: Core 316 surface sample PGE patterns.
Different splits of the surface 1cm sample from core 316 indicated a 'nugget' effect,whereby one split was enriched in Pt, Ir and Os compared to the other. The pattern for the enriched surface sample compares well with samples from the Margi umbers (Ravizza *et al.*, 1999), which are believed to be oxidised hydrothermally -derived sulphide material, indicating the presence of sulphide material in this split.

Table 5.3.2 shows the ratios of seawater derived Pt and Pd to Fe for the Rainbow sediments (hydrothermal Fe-oxyhydroxides), the Margi umbers (oxidised ancient hydrothermal sulfides) and sediments from DSDP Leg 92, metalliferous sediments from the flanks of the EPR. It can be seen that hydrothermal Fe-oxyhydroxides, as exemplified by the Rainbow sediments, have comparable Pt/Fe to the other two metalliferous sediment types, but appear to be at least an order of magnitude more efficient at scavenging Os, and an order of magnitude less efficient at scavenging Pd, than other metalliferous sediment types.

5.4 Conclusions

The Rainbow area is unlike most other hydrothermal areas that have been investigated so far (Ravizza *et al.*, 1996; Ravizza, 1993; Sharma *et al.*, 2000) because the vent field is intimately associated with outcrops of ultramafic rock. This aspect of the Rainbow hydrothermal system is significant for two reasons. First, the local influence of very PGE-rich ultramafic rocks confounds our efforts to reconstruct changes in seawater $^{187}Os/^{188}Os$ during the last 20kyrs , by adding mantle-derived unradiogenic Os to

Table 5.3: PGE/Fe ratios (wt:wt) for some metalliferous sediments. Rainbow data (this work), Margi umbers data from Ravizza *et al.* (1999), DSDP Leg 92 data from Ravizza and Pyle (1997). While Pt/Fe ratios of all three metalliferous sediment types are similar, Pd/Fe and Os/Fe in the Rainbow samples is higher than the other two sediments, more than an order of magnitude in the case of Os/Fe.

Ratio	Rainbow	Margi	DSDP L92
Pt/Fe	8×10^{-8}	3×10^{-8}	3×10^{-8}
Pd/Fe	1×10^{-7}	3×10^{-8}	6×10^{-8}
Os/Fe	$1x\ 10^{-8}$	5×10^{-10}	1×10^{-9}

the sediment. Second, as an ultramafic hosted hydrothermal system, the Rainbow area provides the only data to date that allows us to seek evidence of hydrothermal fluids stripping unradiogenic Os from ultramafic rocks, and releasing dissolved Os to seawater. Although existing major and trace element data demonstrate the influence of ultramafic detritus in some portions of these cores (Cave *et al.*, 2002), it is also possible that alteration of ultramafic rocks has influenced the chemistry of the hydrothermal fluids themselves, and that this influence is recorded in the hydrothermal component of the Rainbow cores.

Lastly, the cores investigated here have well established accumulation rates and are well characterised with respect to major and trace element geochemistry (Cave *et al.*, 2002). Therefore it is possible to use these data in conjunction with the new PGE data reported here to make the first quantitative estimates of PGE burial fluxes associated with scavenging in hydrothermal plumes Os = 0.20-0.4ng.cm^{-2}.kyr^{-1}, Pt =1.6-3.6ng.cm^{-2}.kyr^{-1}, Pd = 2.1-5.7ng.cm^{-2}.kyr^{-1}, Ir = 0.04-0.12ng.cm^{-2}.kyr^{-1}.

Chapter 6

Conclusions and Future Work

6.1 Summary and Conclusions

A geochemical investigation has been conducted of a suite of 4 sediment cores collected from directly beneath the hydrothermal plume at distances of 2-25km from the Rainbow hydrothermal field. As well as a large biogenic component (>80% $CaCO_3$) these sediments record clear enrichments of the elements Fe, Cu, Mn, V, P and As from hydrothermal plume fallout but only minor detrital background material. Systematic variations in the abundances of "hydrothermal" elements are observed at increasing distance from the vent site, consistent with chemical evolution of the dispersing plume. Further, pronounced Ni and Cr enrichments at specific levels within each of the two cores collected from closest to the vent site are indicative of discrete episodes of additional input of ultramafic material at these two near-field locations. Radiocarbon dating reveals mean Holocene accumulation rates for all four cores of 2.7-3.7 $cm.kyr^{-1}$, with surface mixed layers 7-10+ cm thick, from which a history of deposition from the Rainbow hydrothermal plume can be deduced. Deposition from the plume supplies elements to the underlying sediments that are either directly hydrothermally sourced (e.g. Fe, Mn, Cu) or scavenged from seawater via the hydrothermal plume (e.g. V, P, As). The hydrothermal component in the sediments has been calculated by subtracting the N. Atlantic background detrital signal and a local ultramafic detrital component (where applicable) from the total analyses. Hydrothermal Cu in the sediments decreases rapidly with distance from the vent site, but Fe and associated scavenged elements, as well as Mn, show an increase with distance. Ratios of scavenged elements to Fe are comparable to those previously reported in hydrothermal plumes and sediments. Holocene fluxes into to the cores' surface mixed layers are presented which, typically, are an order of magnitude greater than "background" authigenic fluxes from the open N. Atlantic. One core, collected closest to the vent-site, indicates that both the concentration and flux of hydrothermally-derived material increased significantly at some point between

8 and 12 ^{14}C kyr ago; the preferred explanation is that this variation reflects the initiation/intensification of hydrothermal venting at the Rainbow hydrothermal field at this time - perhaps linked to some specific tectonic event in this fault-controlled hydrothermal setting. The coincident occurrence of ultramafic fragments in the sediments at this particular level raises the possibility that tectonic activity may have instigated or enhanced venting at this time.

The inorganic chemistry of particles collected in 5 sediment traps from a three mooring deployment around the Rainbow hydrothermal vent site has been compared with the geochemistry of surficial sediments from cores collected beneath the spreading hydrothermal plume. Average sedimentation fluxes of particles into the sediment traps (11-25mg.m^{-2}.d^{-1}) are comparable to sedimentation rates in the cores throughout the Holocene (40-60mg.m^{-2}.d^{-1}). Fluxes of $CaCO_3$ and Al in the trap samples also compare within a factor of 2 with core top material. Major elements Mg, Mn, Fe, and trace elements V, Co, Ni, Cu, Zn, are enriched above N.E. Atlantic detrital background in all the sediment trap and core top samples. The greatest enrichments are found in 'near-field' trap samples 0.5km from the vent site, with lesser enrichments at a distance of 1.3km and in the core tops 2km to 25km 'downstream' of the vent site. Rare-earth element (REE) patterns in near-field trap samples show a positive Eu anomaly, indicative of co-precipitation of REE from the vent fluid, while far-field traps and core tops show little or no Eu anomaly, but a negative Ce anomaly, indicating scavenging of REE from seawater. Nd/Fe ratios in these far-field traps and sediments are similar. REE are accumulating in the Rainbow sediments at more than twice the rate for N. Atlantic sediments of similar high carbonate content. Calculations of the fluxes of hydrothermally-derived V, Mn, Fe, Co, Cu and Zn to the sediment traps are consistent with the calculated fluxes to the surficial sediments. All the samples from the Rainbow area are significantly affected by hydrothermal activity. The results from the ridge-top trap indicate that plume material must occasionally reach well above nominal plume height observed by nephelometry in the water column.

Sediment trap Cu/Fe ratios decrease systematically away from the vents, as would be expected for an element such as Cu that forms sulfides as well as oxides. The Cu/Fe ratios in the traps converge with that of the surficial sediments, showing overlap between the far-field traps at ~1km from the vent site, and core 343, ~2km downstream. The core samples also show systematic variation in Cu/Fe downstream. Although Zn data show similar trends Cu, Zn shows evidence of fractionation with respect to Cu, in that trap and surficial sediment Zn/Cu ratios are anomalously low compared to vent

fluid ratios. The interpretation, consistent with previous buoyant-plume and proximal-to-vent-field studies, is that this results from preferential precipitation and settling of Zn sulfides closer to the active vent-site than our nearest sample.

The fiux of V to the near-field sediment traps indicates that a significant proportion of the Fe is escaping from the immediate confines of the vent site as oxyhydroxides rather than sulfides, consistent with the high Fe:H_2S ratio in the vent fluid. The flux of REE from seawater to sediments close to the Rainbow vent site, calculated from sediment trap data, is 3-4 times lower than that to the more distal core sediments, consistent with continuous scavenging of dissolved REE onto Fe-oxyhydroxides at increasing distance from the vent-site, both within the dispersing plume, and following deposition to the seabed.

Osmium and other platinum-group elements (PGEs) have also been measured in sediments accumulating directly under the Rainbow hydrothermal plume. $^{187}Os/^{188}Os$ and PGE concentrations in the sediments of four cores taken 2-25 km from the active vent site reveal evidence of both radiogenic Os scavenged from seawater and of unradiogenic Os released by hydrothermal venting. The majority of analyses (n=16) yield $^{187}Os/^{188}Os$ ratios that fall in a narrow range (0.99 - 1.06) close to that of modern seawater (1.07). In these samples, Os concentrations correlate linearly with hydrothermal Fe, V and P enrichments. A smaller subset of samples (n=6), characterized by unusually high concentrations of Ni and Cr derived from ultramafic rock fragments, exhibit distinctly lower $^{187}Os/^{188}Os$ ratios (0.53 - 0.96). Their Ir content is also higher, and their PGE patterns are more similar to mantle material than the PGE patterns of the larger set of samples dominated by seawater-scavenged Os. Compared with "background" NE Atlantic sediments, Os is enriched in the seawater-dominated samples x4, Pd x2, Pt x10, but Ir enrichments are minor except in samples where an ultramafic input has been identified. Although the two proximal cores lack evidence for any ultramafic component in the surficial sediments, $^{187}Os/^{188}Os$ ratios in these samples are lower than that of ambient seawater, suggesting they may also be influenced by unradiogenic Os from vent fluid incorporated into the plume. PGE/Fe ratios are significantly higher for these hydrothermally-enriched sediments are up to orders of magnitude higher than for non-hydrothermal metalliferous sediments. Hydrothermal plumes are therefore efficient scavengers of PGEs from seawater, and may have a significant effect on their oceanic residence times.

The Rainbow area is unlike most other hydrothermal areas that have been investigated so far (Ravizza *et al.*, 1996; Ravizza, 1993; Sharma *et al.*, 2000) because the

vent field is intimately associated with outcrops of ultramafic rock. This aspect of the Rainbow hydrothermal system is significant for two reasons. First, the local influence of very PGE-rich ultramafic rocks confounds our efforts to reconstruct changes in seawater $^{187}Os/^{188}Os$ during the last 20kyrs , by adding mantle-derived unradiogenic Os to the sediment. Second, as an ultramafic hosted hydrothermal system, the Rainbow area provides the only data to date that allows us to seek evidence of hydrothermal fluids stripping unradiogenic Os from ultramafic rocks, and releasing dissolved Os to seawater. Although existing major and trace element data demonstrate the influence of ultramafic detritus in some portions of these cores, it is also possible that alteration of ultramafic rocks has influenced the chemistry of the hydrothermal fluids themselves, and that this influence is recorded in the hydrothermal component of the Rainbow cores.

Lastly, the cores investigated here have well established accumulation rates and are well characterised with respect to major and trace element geochemistry (Cave *et al.*, 2002). Therefore it is possible to use these data in conjunction with the new PGE data reported here to make the first quantitative estimates of PGE burial fluxes associated with scavenging in hydrothermal plumes Os = 0.20-0.4ng.cm^{-2}.kyr^{-1}, Pt = 1.6-3.6ng.cm^{-2}.kyr^{-1}, Pd = 2.1-5.7ng.cm^{-2}.kyr^{-1}, Ir = 0.04-0.12ng.cm^{-2}.kyr^{-1}.

6.2 Future Work

The data suggest that venting at Rainbow was initiated or intensified some time between 8-12 thousand radiocarbon years ago. However, there is some potential for the enhancement of vent-derived metals in the sediment beginning at this time to have been caused instead by a change in the current regime flowing around the Rainbow Ridge, possibly associated with changes in the circulation in the N. Atlantic at the start of the Holocene. To further test this hypothesis, therefore, a suite of cores needs to be collected to the south and west of the Rainbow vent site, and a geochemical study similar to that described in chapter 3 needs to be carried out to examine them for the presence of hydrothermal enrichments. Two of the possible outcomes from such a study would be:

(i) weak hydrothermal signals in the Holocene sediments, corresponding to the small amount of plume flow to the south-west which results from diurnal tidal current reversal, with still weaker or non-existent hydrothermal signals in the pre-Holocene. This would imply that the hypothesis of switch-on or enhancement of venting at 8-12kyr is correct,

and would lead to further studies at other vent sites along the MAR to see if other vents also switched on at this time, perhaps due to enhanced tectonic activity caused by the change in ocean volume from melting ice-sheets.

(ii) weak hydrothermal signals are found in the Holocene sediments as described in (i), with stronger hydrothermal signals being found in pre-Holocene sediments. This would imply that the Rainbow vent site had been just as active in the pre-Holocene as it is today, but that the main flow of current around the Rainbow Ridge had been in a south-westerly direction prior to the Holocene, and had changed over to a predominantly north-easterly direction in Holocene times. Such a result would be of immense interest to the paleoceanographic community, as there is a strong focus on the N. Atlantic circulation in relation to its effects on climate, and the study of hydrothermal sediments laid down under a changing current regime could help to date both the onset and duration of such changes, enabling them to be linked to causative factors.

The results from the study of hydrothermally-derived Co, Cu and Zn in the Rainbow sediments and sediment trap particles indicate that during sulfide precipitation, Zn is preferentially precipitated over Cu close to the vent site. A small scale study on cores taken within the confines of the site would help to quantify the efficiency of this process. Further, there is some potential for a strong enrichment of Co in hydrothermal fluids from ultramafic-hosted vent sites such as Rainbow, compared to fluids from basalt hosted sites. Such very near-field cores would yield information on Co enrichments in the precipitates from the vent, which have potential to be of economic importance.

Results from the platinum-group element studies on the Rainbow sediments confirm that hydrothermal Fe-oxyhydroxides are efficient scavengers of seawater Os, Pt and Pd. Such sediments, therefore, where not affected by inputs of mantle-derived Os, have the potential to be used to trace the changing Os isotope composition of seawater over relatively short timescales, such as glacial-interglacial periods. Further, the apparent efficiency of such hydrothermal precipitates at scavenging Pt from seawater, compared to hydrogenous scavenging of Pt by non-hydrothermal metalliferous sediments, means that the Pt/Fe ratio may be a good way of discriminating between metalliferous sediments derived from hydrothermal fallout, and metalliferous sediment derived from hydrogenous sources, in the geological record. One application of this, if further studies found it to be the case, would be to help quantify the amount of hydrothermal activity in a given area at different times in the past. There is also the possibility that scavenging of Pt in vent plumes may have had a significant effect on the residence time of Pt in the oceans during periods of intense hydrothermal activity

in the geological past.

One final potential direction for future research is for the marine science community to develop closer links with the economic geologists, in order to discover more about what is happening subsurface in hydrothermal systems. Marine scientists know almost nothing about the plumbing of hydrothermal vents, and still less about the mechanisms leading to low-temperature venting, which is currently believed to be an end-product after sub-surface mixing of high-temperature vent fluid and cold seawater has caused most of the metals from the vent fluid to precipitate out. Many economic geologists, however, spend their lives digging through the plumbing systems of hydrothermal vents, but the concepts and theories in the literature produced from each discipline rarely shows signs of having been contributed to by the other. Great benefits could be derived from some more collaboration in this area.

References

Aballea, M., Radford-Knoery, J., Appriou, P., Bougault, H., Charlou, JL, Donval, JP, Etoubleau, J, Fouquet, Y., German, C. R., and Miranda, M. 1998. Manganese distribution in the water column near the Azores Triple Junction along the Mid-Atlantic Ridge and in the Azores domain. *Deep-Sea Res. Part I*, **45**(8), 1319–1338.

Albarede, F. 1995. *Introduction to Geochemical Modeling.* Cambridge University Press.

Alvarez, L. W., Alvarez, W., Asaro, F., and Michel, H. V. 1980. Extraterrestrial cause for the Cretaceous-Tertiary extinction. *Science*, **208**, 1095–1108.

Arimoto, R., Duce, R. A., Ray, B. J., Ellis, W. G., Cullen, J. D., and Merrill, J. T. 1995. Trace elements in the atmosphere over the North Atlantic. *J. Geophys. Res.*, **100(D1)**, 1199–1213.

Arrhenius, G., and Bonatti, E. 1965. Neptunism and vulcanism in the ocean. *Pages 7–22 of:* Sears, M. (ed), *Progress in Oceanography.* Pergamon, London.

Baker, E. T., Massoth, G. J., Feely, R. A., Embley, R. W., Thompson, R. E., and Burd, B. J. 1995. Hydrothermal event plumes from the CoAxial sea-floor eruption site, Juan de Fuca Ridge. *Geophys. Res. Lett.*, **22**(2), 147–150.

Balsam, W. L. 1988. Sediment accumulation rates west of the Mid-Atlantic Ridge (35°N). *Mar. Geology*, **81**, 1–13.

Balsam, W. L., and McCoy, F. W. 1987. Atlantic sediments: glacial/interglacial comparisons. *Paleoceanography*, **2**(5), 531–542.

Balsam, W. L., Otto-Bliesner, B., and Deaton, B. C. 1995. Modern and last glacial maximum eolian sedimentation patterns in the Atlantic Ocean interpreted from sediment iron oxide content. *Paleoceanography*, **10**(3), 493–507.

Barnes, S. J. 1990. The Use of Metal Ratios in Prospecting for Platinum-Group Element Deposits in Mafic and Ultramafic Intrusions. *J. Geochem. Explor.*, **37**, 91–199.

Barnes, S-J., Naldrett, A. J., and Gorton, M. P. 1985. The origin of the fractionation of platinum-group elements in terrestrial magmas. *Chem. Geology*, **53**, 303–XX.

Barrett, T. J., and Jarvis, I. 1988. Rare earth element geochemistry of metalliferous sediments from DSDP Leg 92: the East Pacific Rise transect. *Chem. Geol.*, **67**, 243–259.

Bau, M., and Dulski, P. 1999. Comparing yttrium and rare earth elements in hydrothermal fluids from the Mid-Atlantic Ridge: implications for Y and REE behaviour during near-vent mixing and for the Y/Ho ratio of proterozoic seawater. *Chem. Geol.*, **155**, 77–90.

Bertine, K. K., Koide, M., and Goldberg, E. D. 1993. Aspects of rhodium marine chemistry. *Mar. Chemistry*, **42**, 199–210.

Blondel, Ph. 1997. Segmentation of the Mid-Atlantic Ridge south of the Azores, based on acoustic classification of TOBI data. *Pages 17–28 of:* MacLeod, C. J., Tyler, P. A., and Walker, C. L. (eds), *Tectonic, magmatic, hydrothermal and biological segmentation of mid-ocean ridges.*, vol. 118. Geological Society of London.

Bohrmann, G., Chin, C., Petersen, S., Sahling, H., Schwarz-Schampera, U., Greinert, J., Lammers, S., Rehder, G., Daehlmann, A., Wallmann, K., Dijkstra, S., and Schenke, H. W. 1999. Hydrothermal activity at Hook Ridge in the Central Bransfield Basin, Antarctica. *Geo-Marine Letters*, **18**, 277–284.

Bonatti, E., Honnorez, J., Kirst, P., and Radicati, F. 1975. Metagabbros from the Mid-Atlantic Ridge at 06°N: contact hydrothermal dynamic metamorphism beneath the axial valley. *J. Geology*, **83**, 61–78.

Booty, B. 1985. *Status report on research at the Institute of Oceanographic Sciences related to the possible disposal of radioactive waste on or below the seafloor: April 1974-March 1984. (IOSDL Report No. 204).* Institute of Oceanographic Sciences.

Bostrom, K., and Fisher, D. E. 1969. Distribution of mercury in East Pacific sediments. *Geochim. Cosmochim. Acta*, **33**, 743–745.

Bostrom, K., and Peterson, M. N. 1966. Precipitates from the hydrothermal exhalations on the East Pacific Rise. *Econ. Geol.*, **61**, 1258–1265.

Bostrom, K., and Peterson, M. N. 1969. The origin of aluminium-poor ferromanganoan sediments in areas of high heat flow on the East Pacific Rise. *Mar. Geology*, **7**, 427–447.

Bostrom, K., Joensuu, O., Valdes, S., and Reira, M. 1972. Geochemical history of South Atlantic ocean sediments since Late Cretaceous. *Mar. Geology*, **12**, 85–112.

Brewer, P. G., Nazaki, Y., Spencer, D. W., and Fleer, A. P. 1980. Sediment trap experiments in the deep North Atlantic: isotopic and elemental fluxes. *J. Marine Res.*, **38**(4), 703–728.

Burton, K. W., Bourdon, B., Birck, J-L., Allegre, C. J., and Hein, J. R. 1999. Osmium isotope variations in the oceans recorded by Fe-Mn crusts. *Earth Planet. Sci. Lett.*, **171**, 185–197.

Campbell, A. C., Palmer, M. R., Klinkhammer, G. P., Bowers, T. S., Edmond, J. M., Lawrence, J. R., Casey, J. F., Thompson, G., Humphris, S., Rona, P., and Karson, J. A. 1988. The chemistry of hot springs on the Mid-Atlantic Ridge. *Nature*, **335**, 514–519.

Campbell, A. C., German, C. R., Palmer, M. R., Gamo, T., and Edmond, J. M. 1994. Chemistry of Hydrothermal Fluids from Escanaba Trough, Gorda Ridge. *Pages 201–221 of:* Morton, J. L., Zierenberg, R. A., and Reiss, C. A. (eds), *Geologic, Hydrothermal and Biologic Studies at Escanaba Trough, Gorda Ridge, Offshore Northern California.* U.S. Geological Survey, Denver, CO.

Campbell, I. H., and Barnes, S. J. 1984. A Model for the Geochemistry of the Platinum-Group Elements in Magmatic Sulfide Deposits. *Can. Mineralogist*, **22**, 151–160.

Carpenter, M. S. N., Colley, S., Elderfield, H., Kennedy, H. A., Thomson, J., and Wilson, T. R. S. 1983. Geochemistry of the near surface sediments of the Nares Abyssal Plain. *IOSDL Internal Report*, **174**, 66.

Cave, R. R., and German, C. R. 1998a. Box-coring around Rainbow? Have you lost your MARbles? *BRIDGE Newsletter*, **15**, 12–15.

Cave, R. R., and German, C. R. 1998b. Hydrothermal plume detection in the deep ocean - a combination of technologies. *Underwater Technology*, **23**(2), 71–75.

Cave, R. R., German, C. R., Thomson, J., and Nesbitt, R. W. 2002. Fluxes to sediments from the Rainbow hydrothermal plume, 36°14'N on the MAR. *Geochim. Cosmochim. Acta*, **66**, 1905–1923.

Charlou, J.L., Bougault, H., Donval, J.P., Pelle, H., Langmuir, C., and Party, FAZAR Scientific. 1993. Seawater CH4 concentration over the Mid-Atlantic Ridge from the Hayes F.Z. to the Azores Triple Junction. *EOS, Trans. Am. Geophys. U*, **74 supl.**, 380.

Chester, R. 1982. Regional trends in the distribution and sources of aluminosilicates and trace metals in recent North Atlantic deep-sea sediments. *Bull. Inst. Geol. Bassin d'Aquitaine*, **31**, 325–335.

Chiba, H., Masuda, H., Lee, S., and Fujioka, K. 1999. Fluid chemistry of TAG and Rainbow seafloor hydrothermal systems at the Mid-Atlantic Ridge : Results from MODE'98 Leg 2 Cruise. *JAMSTEC J. Deep Sea Res.*, **15**(II), 29–38.

Clark, P. U., Alley, R. B., and Pollard, D. 1999. Northern hemisphere ice-sheet influences on global climate change. *Science*, **286**, 1104–1111.

Cocherie, A., Calvez, J. Y., and Oudin-Dunlop, E. 1994. Hydrothermal activity as recorded by Red Sea sediments: Sr-Nd isotopes and REE signatures. *Mar. Geology*, **118**, 291–302.

Cochran, J. K. 1992. The oceanic chemistry of the uranium and thorium series nuclides. *In:* Ivanovich, M., and Harmon, R. S. (eds), *Uranium-series disequilibrium: applications in earth, marine and environmental sciences.* Clarendon Press, Oxford.

Colley, S., Thomson, J., Wilson, T. R. S., and Higgs, N. C. 1984. Post-depositional migration of elements during diagenesis in brown clay and turbidite sequences in the North East atlantic. *Geochim. Cosmochim. Acta*, **48**, 1223–1235.

Colodner, D., Boyle, E. A., Edmond, J. M., and Thomson, J. 1992. Post-depositional mobility of platinum, iridium and rhenium in marine sediments. *Nature*, **358**, 402–404.

Conway, E.J. 1943. The chemical evolution of the oceans. *Proc. of the Royal Irish Academy*, **48**(B), 161–212.

Corliss, J. B., Dymond, J., Gordon, L. I., Edmond, J. M., Herzen, R. P. V., Ballard, R. D., Green, K., Williams, D., Bainbridge, A., Crane, K., and Andel, T. H. V. 1979. Submarine thermal springs on the Galapogos Rift. *Science*, **203**, 1073–1083.

Cowen, J. P., Massoth, G. J., and Feely, R. A. 1990. Scavenging rates of dissolved manganese in a hydrothermal vent plume. *Deep-Sea Res.*, **37**, 1619–1637.

Cremer, M., Grousset, F., Faugeres, J. C., Duprat, J., and Gonthier, E. 1992. Sediment flux patterns in the northeastern Atlantic: variability since the Last Interglacial. *Mar. Geology*, **104**, 31–53.

Cronan, D. S. 1972. The Mid-Atlantic Ridge near 45°N, XVII: Al, As, Hg and Mn in Ferruginous Sediments from the Median Valley. *Canadian J. Earth Sci.*, **9**, 319–322.

Cronan, D. S. 1976. Basal metalliferous sediments from the eastern Pacific. *Bull. Geol. Soc. Am.*, **87**, 928–934.

Curry, W. B. 1996. Late Quaternary deep circulation in the Western Equatorial Atlantic. *Pages 577–598 of:* Wefer, G., Berger, W. H., Siedler, G., and Webb, D. J. (eds), *The South Atlantic: present and past circulation.* Springer-Verlag.

Curry, W. B., Duplessy, J. G., Labeyrie, L. D., and Shackleton, N. J. 1988. Changes in the distribution of $\delta^{13}C$ of deep water σCO_2 between the last glaciation and the Holocene. *Paleoceanography*, **3**(3), 317–341.

Dando, P. R., Stuben, D., and Varnavas, S. 1999. Hydrothermalism in the Mediterranean Sea. *Progress in Oceanography*, **44**, 333–367.

de Jongh, W. K. 1979. The Atomic Number Z=0: Loss and Gain on Ignition in XRF Analysis Treated by the JN-Equations. *X-Ray Spectrometry*, **8**(2), 52–56.

Delaney, M. L. 1998. Phosphorus accumulation in marine sediments and the oceanic phosphorus cycle. *Global Biogeochem. Cycles*, **12**(4), 563–572.

Delany, A. C., Delany, Au. C., Parkin, D. W., Griffin, G. G., Goldberg, E. D., and Reimann, B. E. F. 1967. Airborne dust collected at Barbados. *Geochim. Cosmochim. Acta*, **3**, 885–809.

Dennielou, B., Auffret, G. A., Boelaert, A., Richter, T., Garlan, T., and Kerbrat, R. 1999. Controle exercise par la dorsale medio-Atlantique et le Gulf Stream sur la sedimentation quaternaire sur le plateau des Acores. *Comptes Rendus de l'Academie des Sciences*, **328**, 831–837.

Detrick, R. S., Honnorez, J., and Party, Leg 106 Scientific. 1986. Drilling the Snake Pit hydrothermal field on the Mid Atlantic Ridge, Lat. 23^{o}22'N. *Geology*, **14**, 1004–1007.

Dokken, T. M., and Jansen, E. 1999. Rapid changes in the mechanism of ocean convestion during the last glacial period. *Nature*, **401**, 458–461.

Donval, J. P., Charlou, J. L., Douville, E., Knoery, J., and Fouquet, Y. 1997. High H2 and CH4 content in the hydrothermal fluids from Rainbow site newly sampled

at 36°14'N on the AMAR segment, Mid-Atlantic Ridge: Comparison with other MAR sites. *EOS Trans., AGU*, **78**, 832.

Douville, E., Charlou, J. L., Donval, J. P., Knoery, J., and Fouquet, Y. 1997. Trace elements in fluids from the new Rainbow hydrothermal field (36°14'N): a comparison with other Mid-Atlantic Ridge fluids. *EOS Trans., AGU*, **78**, 832.

Douville, E., Charlou, J-L., Donval, J-P., Hureau, D., and Appriou, P. 1999. Le comportement de l'arsenic (As) et de l'antimone (Sb) dans les fluides provenant de differents systemes hydrothermaux oceaniques. *Comptes rendus de l'Academie des Sciences*, **328**(2), 97–104.

Douville, E., Bienvenu, P., Charlou, J.-L., Donval, J.-P., Fouquet, Y., Appriou, P., and Gamo, T. 2001. Yttrium and Rare Earth Elements in fluids from various deep-sea hydrothermal systems. *Geochim. Cosmochim. Acta*, **63**, 627–643.

Douville, E., Charlou, J.-L., Oelkers, E. H., Bienvenu, P., Colon, C. F. Jove, Donval, J.-P., Fouquet, Y., Prieur, D., and Appriou, P. 2002. The Rainbow vent fluids (36 degrees 14 N, MAR): the influence of ultramafic rocks and phase separation on trace metal content in Mid-Atlantic Ridge hydrothermal fluids. *Chem. Geol.*, **184**, 37–48.

Dymond, J. 1981. Geochemistry of the Nazca Plate surface sediments: an evaluation of hydrothermal, biogenic, detrital and hydrogenous sources. *Geol. Soc. Am. Memoir*, **154**, 133–173.

Dymond, J., and Roth, S. 1988. Plume dispersed hydrothermal particles: A time series record of settling flux from the Endeavour Ridge using moored sensors. *Geochim. Cosmochim. Acta*, **52**, 2525–2536.

Edmond, J. M., Damn, K. L. Von, McDuff, R. E., and Measures, C. I. 1982. Chemistry of hot springs on the East Pacific Rise and their effluent dispersal. *Nature*, **297**, 187–191.

Edmonds, H., Michael, P. J., Baker, E. T., Graham, D. W., Vock, M., Snow, J. E., Muhe, R., Connolly, D. P., and German, C. R. 2001. Hot springs in a cold ocean: evidence for abundant hydrothermal venting on the ultra-slow spreading Gakkel Ridge. *Eos, Trans. AGU*, **82**, F647.

Edmonds, H. N., Green, D. R. H., Moran, S. B., and German, C. R. 1998. Geochemistry of particulate material in the Rainbow hydrothermal plume, Mid-Atlantic Ridge. *Eos, Trans. AGU, AGU Supplement*, **79**(45), T12C–07.

Elderfield, H., and Schultz, A. 1996. Mid-ocean ridge hydrothermal fluxes and the chemical composition of the ocean. *Ann. Rev. Earth Planet. Sci.*, **24**, 191–224.

Esser, B. K., and Turekian, K. K. 1993. The osmium isotopic composition of the continental crust. *Geochim. Cosmochim. Acta*, **57**, 3093–3104.

Fagel, N., Andre, L., and Dehairs, F. 1999. Advective excess Ba transport as shown from sediment and trap geochemical signatures. *Geochim. Cosmochim. Acta*, **63**(16), 2353–2367.

Feely, R. A., Trefry, J. H., Massoth, G. J., and Metz, S. 1991. A comparison of the scavenging of phosphorous and arsenic from seawater by hydrothermal iron oxyhydroxides in the Atlantic and Pacific Oceans. *Deep-Sea Res.*, **38**, 617–623.

Feely, R. A., Massoth, G. J., Baker, E. T., Lebon, G. T., and Geiselman, T. L. 1992. Tracking the dispersal of hydrothermal plumes from the Juan de Fuca Ridge using suspended matter compositions. *J. Geophys. Res.*, **97**(B3), 3457–3468.

Feely, R. A., Massoth, G. J., Trefry, J. H., Baker, E. T., Paulson, A. J., and Lebon, G. T. 1994. Composition and sedimentation of hydrothermal plume particles from North Cleft segment, Juan de Fuca Ridge. *J. Geophys. Res.*, **99**(B3), 4985–5006.

Feely, R. A., Trefry, J. H., Lebon, G. T. A., and German, C. R. 1998. The Relationship between P/Fe and V/Fe Ratios in Hydrothermal precipitates and dissolved Phosphate in Seawater. *Geophys. Res. Lett.*, **25**(13), 2253–2256.

Field, M. P., and Sherrell, R. M. 2000. Dissolved and particulate Fe in a hydrothermal plume at 9°45'N, East Pacific Rise : slow Fe (II) oxidation kinetics in Pacific plumes. *Geochim. Cosmochim. Acta*, **64**(4), 619–628.

Fouquet, Y., Charlou, J. L., Donval, J. P., Knoery, J., Pelle, H., Ondreas, H., Segonzac, M., Costa, I., Lourenco, N., and Tivey, M. K. 1994. Geological setting and comparison of the Menez Gwen and Lucky Strike vent fields at 37°17'N and 37°50'N on the Mid Atlantic Ridge. Preliminary results of the DIVA1 diving cruise with Nautile. *EOS Trans., AGU*, **75 supl.**, 313.

Fouquet, Y., Charlou, J. L., Ondreas, H., Knoery, J., Donval, J. P., Douville, E., Apprioual, R., Cambon, P., Pelle, H., Landure, J. Y., Normand, A., Ponsevera, E., German, C., Parson, L., Barriga, F., Costa, I., Relvas, J., and Ribeiro, A. 1997. Discovery and first submersible investigations on the Rainbow hydrothermal field on the MAR (36°14'N). *EOS Trans., AGU*, **78**, 832.

Froelich, P. N., Bender, M. L., Luedtke, N. A., Heath, G. R., and DeVries, T. 1982. The marine phosphorus cycle. *American Journ. Sci.*, **282**, 474–511.

Gamo, T., Sakai, H., Ichibashi, J., Nakayama, E., Isshiki, K., Matsuura, H., Shitashima, K., Takeuchi, K., and Ohta, S. 1993. Hydrothermal plumes in the eastern Mauns Basin, Bismarck Sea: CH4, Mn, Al and pH anomalies. *Deep-Sea Res. I*, **40**(11/12), 2335–2349.

Ganopolski, A., Rahmstorf, S., Petoukhov, V., and Claussen, M. 1998. Simulation of modern and glacial climates with a coupled global model of intermediate complexity. *Nature*, **391**, 351–356.

German, C. R., and Sparks, R. S. J. 1993. Particle recycling in the TAG hydrothermal plume. *Earth Planet. Sci. Lett.*, **116**, 129–134.

German, C. R., Klinkhammer, G. P., Edmond, J. M., Mitra, A., and Elderfield, H. 1990. Hydrothermal scavenging of rare-earth elements in the ocean. *Nature*, **345**, 516–518.

German, C. R., Campbell, A. C., and Edmond, J. M. 1991. Hydrothermal scavenging at the Mid-Atlantic Ridge: Modification of trace element dissolved fluxes. *Earth Planet. Sci. Lett.*, **107**, 101–114.

German, C. R., Higgs, N. C., Thomson, J., Mills, R., Elderfield, H., Blusztajn, J., Fleer, A. P., and Bacon, M. P. 1993. A geochemical study of metalliferous sediment from the TAG hydrothermal mound, 26^{o}N, Mid-Atlantic Ridge. *J. Geophys. Res.*, **98**(B6), 9683–9692.

German, C. R., Parson, L. M., and HEAT Scientific Team. 1996a. Hydrothermal exploration near the Azores Triple Junction: tectonic control of venting at slow spreading ridges? *Earth Planet. Sci. Lett.*, **138**, 93–104.

German, C. R., Klinkhammer, G. P., and Rudnicki, M. D. 1996b. The Rainbow hydrothermal plume, 36^{o}15'N, MAR. *Geophys. Res. Lett.*, **23**(21), 2979–2982.

German, C. R., Bourles, D. L., Brown, E. T., Hergt, J., Colley, S., Higgs, N. C., Ludford, E. M., Nelsen, T. A., Feely, R. A., Raisbeck, G., and Yiou, F. 1997. Hydrothermal scavenging on the Juan de Fuca Ridge: $^{230}Th_{xs}$, ^{10}Be and REEs in ridge-flank sediments. *Geochim. Cosmochim. Acta*, **61**(19), 4067–4078.

German, C. R., Richards, K., Thurnherr, A., Cave, R., J.Eley, Knoery, J., Khripounoff, A., Crassous, P., Dapoigny, A., Magalhaes, V., Taylor, P., and Howarth,

P. 1998a. *The Fluxes at AMAR Experiment: FLAME 2 (SOC Cruise Report No. 20).* Southampton Oceanography Centre.

German, C. R., Baker, E. T., mevel, C., and Tamaki, K. 1998b. Hydrothermal activity along the South-West Indian Ridge. *Nature*, **395**, 490–493.

German, C. R., Richards, K. J., Rudnicki, M. D., Lam, M. M., Charlou, J. L., and FLAME Scientific Party. 1998c. Topographic control of a dispersing hydrothermal plume. *Earth Planet. Sci. Lett.*, **156**, 267–273.

German, C. R., Hergt, J., Palmer, M. R., and Edmond, J. M. 1999. Geochemistry of hydrothermal sediments from the OBS vent-field: 21°N, East Pacific Rise. *Chem. Geol.*, **155**, 65–75.

German, C.R., Livermore, R. A., Baker, E. T., Bruguier, N. I., Connolly, D. P., Cunningham, A. P., Morris, P., Rouse, I. P., Statham, P. J., and Tyler, P. A. 2000. Hydrothermal plumes above the East Scotia Ridge: an isolated high-latitude back-arc spreading centre. *Earth Planet. Sci. Lett.*, **184**, 241–250.

German, C.R., Colley, S., Palmer, M. R., Khripounoff, A., Klinkhammer, G. P, and Palmer, M. R. in press. Hydrothermal sediment trap fluxes at 13°N on the East Pacific Rise. *Deep-Sea Res.*

Goldberg, E. D. 1987. Comparative chemistry of the platinum and other heavy metals in the marine environment. *Pure and Appl. Chem.*, **59**(4), 565–571.

Goldberg, E. D., and Koide, M. 1990. Understanding the marine chemistries of the platinum group metals. *Mar. Chemistry*, **30**, 249–257.

Gracia, E., Charlou, J-L., Radford-Knoery, J., and Parson, L. M. 2000. Non-transform offsets along the Mid-Atlantic Ridge south of the Azores (38 degrees N - 34 degrees N): Ultramafic exposures and hosting of hydrothermal vents. *Earth Planet. Sci. Lett.*, **177**(1–2), 89–103.

Grousset, F., and Donard, O. 1984. Enrichments in Hg, Cd, As and Sb in Recent Sediments of Azores-Iceland Ridge. *Geo-marine letters*, **4**, 117–124.

Halbach, P. E., Sattler, C. D., Teichmann, F., and Wahsner, M. 1989. Cobalt-Rich and Platinum-Bearing Manganese Crust Deposits on Seamounts - Nature, Formation, and Metal Potential. *Mar. Mining*, **8**, 23–39.

Hannington, M. D., and Jonasson, I. R. 1992. Fe and Mn oxides at Seafloor Hydrothermal Vents. *Catena Supplement*, **21**, 351–370.

Hassler, D. R., Peucker-Ehrenbrink, B., and Ravizza, G. E. 2000. Rapid determination of Os isotopic composition by sparging OsO_4 into a magnetic-sector ICPMS. *Chem. Geology*, **166**, 1–14.

Hekinian, R., Fevrier, M., Avedik, F., Cambon, P., Charlou, J.L., Needham, H. D., Raillard, J., Boulegne, J., Merlivat, L., Moinet, A., Manganini, S., and Lange, J. 1983. East Pacific Rise near 13°N: geology of new hydrothermal fields. *Science*, **219**, 1321–1324.

Heussner, S., de Madron, X. D., Radakovitch, O., Beaufort, L, Biscaye, P. E., Carbonne, J., Delsaut, N., Etcheber, H., and Monaco, A. 1999. Spatial and temporal patterns of downward particle fluxes on the continental slope of the Bay of Biscay (northeastern Atlantic). *Deep-Sea Res. Part II-Topical Studies in Oceanography*, **46**, 2101–2146.

Hodge, V. F., Stallard, M., Koide, M., and Goldberg, E. D. 1985. Platinum and the platinum anomaly in the marine environment. *Earth Planet. Sci. Lett.*, **72**, 158–162.

Hodge, V. F., Stallard, M., Koide, M., and Goldberg, E. D. 1986. Determination of platinum and iridium in marine waters, sediments and organisms. *Anal. Chemistry*, **58**, 616–620.

Hoffert, M., Perseil, A., Hekinian, R., Choukroune, P., Needham, H. D., Francheteau, J., and le Pichon, X. 1978. Hydrothermal deposits sampled by diving saucer in Transform Fault A near 37°N on the Mid-Atlantic Ridge, Famous Area. *Oceanologia Acta*, **1**(1), 73–86.

Horan, M. F., Morgan, J. W., Grauch, R. I., Coveney, R. M., Murowchick, J. B., and Hulbert, L. J. 1994. Rhenium and osmium isotopes in black shales and Ni-Mo-PGE-rich sulfide layers, Yukon territory, Canada, and Hunan and Guizhou provinces, China. *Geochim. Cosmochim. Acta*, **58**, 257–265.

Hudson, G. P. Klinkhammer A. 1986. Dispersal patterns for hydrothermal plumes in the south Pacific using manganese as a tracer. *Earth Planet. Sci. Lett.*, **79**, 241–249.

Humphris, S. E., and Cann, J. R. 2000. Constraints on the energy and chemical balances of the modern TAG and ancient Cyprus seafloor sulfide deposits. *J. Geophys. Res. - Solid Earth*, **105**(B12), 28477–28488.

Jacinto, G. S., and van den Berg, C. M. G. 1989. Different behaviour of platinum in the Indian and Pacific Oceans. *Nature*, **338**, 332–334.

James, R. H., Elderfield, H., and Palmer, M. R. 1995. The chemistry of hydrothermal fluids from the Broken Spur site, 29°N, Mid-Atlantic Ridge. *Geochim. Cosmochim. Acta*, **59**(4), 651–659.

Jickells, T. D., Deuser, W. G., and Knap, A. H. 1984. The sedimentation rates of trace elements in the Sargasso Sea measured by sediment trap. *Deep-Sea Res.*, **31**, 1169–1178.

Jickells, T. D., Dorling, S., Deuser, W. G., Church, T. M., Arimoto, R., and Prospero, J. M. 1998. Air-borne dust fluxes to a deep water sediment trap in the Sargasso Sea. *Global biogeochemical cycles*, **12**(2), 311–320.

Juniper, S. K., and Tebo, B. M. 1995. Microbe-Metal Interactions and Mineral Deposition at Hydrothermal Vents. *In:* S.E.Humphris, R.A.Zierenberg, M., L. S., and R.E.Thomson (eds), *Seafloor hydrothermal systems: physical, chemical, biological and geological interactions. Geophys. Monograph 91.* AGU.

Kadko, D. 1993. An assessment of the effect of chemical scavenging within submarine hydrothermal plumes upon ocean geochemistry. *Earth Planet. Sci. Lett.*, **120**, 361–374.

Kadko, D., Baross, J., and Alt, J. 1995. The magnitude and implications of hydrothermal flux. *Pages 446–466 of:* Humphris, S. E., Zierenberg, R. A., Mullineaux, L. S., and Thomson, R. E. (eds), *Seafloor Hydrothermal Systems: Physical, Chemical, Biological and Geological Interactions. Geophys. Monograph 91.* AGU.

Keigwin, L. D., and Jones, G. A. 1989. Glacial-Holocene stratigraphy, chronology and paleoceanographic observations on some North Atlantic sediment drifts. *Deep-Sea Res.*, **36**(6), 845–867.

Khripounoff, A., Comtet, T., Vangriesheim, A., and Crassous, P. 2000. Near-bottom biological and mineral particle flux in the Lucky Strike hydrothermal area (Mid-Atlantic Ridge). *J. Marine Systems*, **25**(2), 101–118.

Khripounoff, A., Vangriesheim, A., Crassous, P., Segonzac, M., Colaco, A., Desbruyeres, D., and Barthelemy, R. 2001. Particle flux in the Rainbow hydrothermal vent field (Mid-Atlantic Ridge): dynamics, mineral and biological composition. *J. Marine Systems, in press.*

Klinkhammer, G., Elderfield, H., and Hudson, A. 1983. Rare earth elements in seawater near hydrothermal vents. *Nature*, **305**, 185–188.

Klinkhammer, G. P., Rona, P., Greaves, M. J., and Elderfield, H. 1985. Hydrothermal manganese plumes over the Mid-Atlantic Ridge rift-valley. *Nature*, **314**, 727–731.

Klinkhammer, G. P., Chin, C. S., Keller, R. A., Dahlmann, A., Sahling, H., Sarthou, G., Petersen, S., and Smith, F. 2001. Discovery of new hydrothermal vent sites in Bransfield Strait, Antarctica. *Earth Planet. Sci. Lett.*, **193**, 395–407.

Koide, M., Goldberg, E. D., Niemeyer, S., Gerlach, D., Hodge, V., Bertine, K. K., and Padova, A. 1991. Osmium in Marine-Sediments. *Geochim. et Cosmochim. Acta*, **55**, 1641–1648.

Koski, R. A., Benninger, L. M., Zierenberg, R. A., and Jonasson, I. R. 1994. Composition and Growth History of Hydrothermal Deposits in Escanaba Trough, Southern Gorda Ridge. *Pages 293–324 of:* Morton, J. L., Zierenberg, R. A., and Reiss, C. A. (eds), *Geologic, Hydrothermal and Biologic Studies at Escanaba Trough, Gorda Ridge, Offshore Northern California.* U.S. Geological Survey, Denver, CO.

Kremling, K., and Streu, P. 1993. Saharan dust influenced trace element fluxes in deep North Atlantic subtropical waters. *Deep-Sea Res. I*, **40**(6), 1155–1168.

Kuhn, T., Burger, H., Castradori, D., and Halbach, P. 2000. Volcanic and hydrothermal history of ridge segments near the Rodrigues Triple Junction (Central Indian Ocean) deduced from sediment geochemistry. *Mar. Geology*, **169**, 391–409.

Kump, L. R., and Byrne, R. H. 1989. Palladium chemistry in seawater. *Environ. Sci. Technol.*, **23**(6), 663–665.

Kuss, J., and Kremling, K. 1999a. Particulate trace element fluxes in the deep northeast Atlantic Ocean. *Deep-Sea Res. I*, **46**, 149–169.

Kuss, J., and Kremling, K. 1999b. Spatial variability of particle associated trace elements in near-surface waters of the North Atlantic (30°N/60°W to 60°N/2°W), derived by large volume sampling. *Mar. Chemistry*, **68**, 71–86.

Lalou, C., Thompson, G., Rona, P. A., Brichet, E., and Jehanno, C. 1986. Chronology of selected hydrothermal Mn oxide deposits from the transatlantic geotraverse "TAG" area, Mid-Atlantic Ridge 26°N. *Geochim. Cosmochim. Acta*, **50**, 1737–1743.

Lalou, C., Thompson, G., Arnold, M., Brichet, E., Druffel, E., and Rona, P. A. 1990. Geochronology of TAG and Snakepit hydrothermal fields, Mid-Atlantic Ridge: witness to a long and complex hydrothermal history. *Earth Planet. Sci. Lett.*, **97**, 113–128.

Lalou, C., Reyss, J. L., Brichet, E., Arnold, M., Thompson, G., Fouquet, Y., and Rona, P. A. 1993. New age data for Mid-Atlantic Ridge hydrothermal sites: TAG and Snakepit revisited. *J. Geophys. Res.*, **98**(B6), 9705–9713.

Lambert, C. E., Bishop, J. K. B., Biscaye, P. E., and Chesselet, R. 1984. Particulate aluminium, iron and manganese chemistry at the deep Atlantic boundary layer. *Earth Planet. Sci. Lett.*, **70**, 237–248.

Langmuir, C. H., Fornari, D., Colodner, D., Charlou, J. L., Costa, I., Desbruyeres, D., Desonie, D., Emerson, T., Fiala-Medioni, A., Fouquet, Y., Humphris, S., Saldanha, L., Sours-Page, R., Thatcher, M., Tivey, M., Dover, C. Van, Damm, K. Von, Wiese, K., and Wilson, C. 1993. Geological setting and characteristics of the Lucky Strike vent-field at 37°17'N on the Mid-Atlantic Ridge. *EOS, Trans. Am. Geophys. U.*, **74**, 99.

Lee, D. S. 1983. Palladium and nickel in north-east Pacific waters. *Nature*, **305**, 47–48.

Levasseur, S., Birck, J-L., and Allegre, C. J. 1999. The osmium riverine flux and the oceanic mass balance of osmium. *Earth Planet. Sci. Lett.*, **174**, 7–23.

Li, X., Maring, H., Savoie, D., Voss, K., and Prospero, J. M. 1996. Dominance of mineral dust in aerosol light-scattering in the North Atlantic trade winds. *Nature*, **380**, 416–419.

Libes, S. 1992. *An introduction to Marine Biogeochemistry.* New York: John Miley & Sons.

Lilley, M. D., Feely, R. A., and Trefry, J. H. 1995. Chemical and biochemical transformations in hydrothermal plumes. *Pages 369–391 of:* Humphris, S. E., Zierenberg, R. A., Mullineaux, L. S., and Thomson, R. E. (eds), *Seafloor Hydrothermal Systems: Physical, Chemical, Biological and Geological Interactions. Geophys. Monograph 91.* AGU.

Lisitzin, A. P. 1996. *Oceanic Sedimentation, lithology and geochemistry.* AGU.

Lonsdale, P. F., Bischoff, J. L., andM. Kastner, V. M. Burns, and Sweeney, R. E. 1980. A high-temperature hydrothermal deposit on the seabed at a Gulf of California spreading center. *Earth Planet. Sci. Lett.*, **48**, 1–7.

Lupton, J. E., and Craig, H. 1981. A major helium-3 source at 15°S on the East Pacific Rise. *Science*, **214**(4516), 13–18.

Mannheim, F. T. 1986. Marine cobalt resources. *Science*, **232**, 600–608.

McLennan, S. M. 1989. Rare earth elements in sedimentary rocks: Influence of provenance and sedimentary processes. *Pages 169–200 of:* Lipin, B. R., and McKay, G. A. (eds), *Sedimentary Rocks: influence of provenance and sedimentary processes.* Mineralogical Society of America, Washington DC.

Melkert, M. J., Ganssen, G., Helder, W., and Troelstra, S. 1992. Episodic preservation of pteropod oozes in the deep Northeast Atlantic Ocean: Climatic change and hydrothermal activity. *Mar. Geology*, **103**, 407–422.

Metz, S., and Trefry, J. H. 1993. Field and laboratory studies of metal uptake and release by hydrothermal precipitates. *J. Geophys. Res. - Solid Earth*, **98**(B6), 9661–9666.

Metz, S., Trefry, J. H., and Nelsen, T. 1988. History and geochemistry of a metalliferous sediment core from the Mid-Atlantic Ridge. *Geochim. Cosmochim. Acta*, **48**, 47–62.

Mills, R., Elderfield, H., and Thomson, J. 1993. A dual origin for the hydrothermal component in a metalliferous sediment core from the Mid-Atlantic Ridge. *J. Geophys. Res.*, **98**(B6), 9671–9681.

Mills, R. A., and Elderfield, H. 1995a. Hydrothermal activity and the geochemistry of metalliferous sediments. *Pages 392–407 of:* Humphris, S. E., Zierenberg, R. A., Mullineaux, L. S., and Thomson, R. E. (eds), *Seafloor Hydrothermal Systems: Physical, Chemical, Biological and Geological Interactions. Geophys. Monograph 91.* AGU.

Mills, R. A., and Elderfield, H. 1995b. Rare earth element geochemistry of hydrothermal deposits from the active TAG Mound, Mid-Atlantic Ridge. *Geochim. Cosmochim. Acta*, **59**, 3511–3524.

Mitra, A., Elderfield, H., and Greaves, M. J. 1994. Rare earth elements in submarine hydrotherml fluids and plumes from the Mid-Atlantic Ridge. *Mar. Chemistry*, **46**, 217–235.

Mottl, M. J., and Wheat, C. G. 1994. Hydrothermal Circulation through Midocean Ridge Flanks - Fluxes of Heat and Magnesium. *Geochim. Cosmochim. Acta*, **10**, 2225–2237.

Murton, B. J., Klinkhammer, G., Becker, K., Briais, A., Edge, D., Hayward, N., Millard, N., Mitchell, I., Rouse, I., Rudnicki, M., Sayanagi, K., Sloan, H., and Parson, L. 1994. Direct evidence for the distribution and occurrence of hydrothermal activity between 27°N-30°N on the Mid-Atlantic Ridge. *Earth Planet. Sci. Lett.*, **125**, 119–128.

Nelsen, T. A., Klinkhammer, G.P., Trefry, J. H., and Trocine, R. P. 1986. Real-time observation of dispersed hydrothermal plumes using nephelometry: examples from the Mid-Atlantic Ridge. *Earth Planet. Sci. Lett.*, **81**, 245–252.

Nozaki, Y., Cochran, J. K., Turekian, K. K., and Keller, G. 1977. Radiocarbon and ^{210}Pb distribution in submersible-taken deep-sea cores from project Famous. *Earth Planet. Sci. Lett.*, **34**, 167–173.

Nunes, O. C., Donato, M. M., and Dacosta, M. S. 1992. Isolation and Characterization of Rhodothermus Strains from S. Miguel, Azores. *Systematic and Applied Microbiology*, **15**, 92–97.

Olafsson, J., Thors, K., and Cann, J. 1991. A sudden cruise off Iceland. *Ridge Events*, **2**, 35–38.

Olivarez, A. M., and Owen, R. M. 1989. REE/Fe variations in hydrothermal sediments: Implications for the REE content of seawater. *Geochim. Cosmochim. Acta*, **53**, 757–762.

Olsson, I. U., El-Daoushy, M.F. A. F., Abd-El-Mageed, A. I., and Klasson, M. 1974. A comparison of different methods of pretreament of bones. *Geologiska Foreningens i Stockholm Forhandlingar*, **96**, 171–181.

Onishi, H. 1970. Arsenic. *Pages 3301–3305 of:* Wedepohl, K. H. (ed), *Handbook of Geochemistry*, vol. II. Springer-Verlag.

Owen, R. M., and Olivarez, A. M. 1988. Geochemistry of rare Earth Elements in Pacific Hydrothermal Sediments. *Marine Chemistry*, **25**, 183–196.

Oxburgh, R. 1997. Osmium isotope variations in sea water since the last glacial maximum: evidence from the Cariaco Basin. *Eos Trans. AGU, Fall Meeting Suppl.*, **78**, 46.

Oxburgh, R. 1998. Variations in the osmium isotope composition of sea water over the past 200,000 years. *Earth. Planet. Sci. Lett.*, **159**, 183–191.

Oxburgh, R. 2001. Residence time of Osmium in the oceans. *G-cubed*, **2**, 17pp.

Parson, L. M., Gracia, E., Coller, D., German, C. R., and Needham, H. D. 2000. Second-order segmentation - the relationship between volcanism and tectonism at the MAR, 38°N-35°40'N. *Earth Planet. Sci. Lett.*, **78**, 231–251.

Pearce, T. J., and Jarvis, I. 1992. Applications of geochemical data to modelling sediment dispersal patterns in distal turbidites: late Quaternary of the Madeira Abyssal Plain. *J. Sedimentary Petrology*, **62**(6), 1112–1129.

Pearce, T. J., and Jarvis, I. 1995. High-resolution chemostratigraphy of Quaternary distal turbidites: a case study of new methods for the analysis and correlation of barren sequences. *Pages 107–143 of:* Dunay, R. E., and Hailwood, E. A. (eds), *Non-biostratigraphical methods of dating and correlation*, vol. 89. Geological Society.

Pearson, D. G., and Woodland, S. J. 2000. Solvent extraction/anion exchange separation and determination of PGEs (Os, ir, Pt, Pd, Ru) and Re-Os isotopes in geological samples by isotope dilution ICP-MS. *Chem. Geology*, **165**, 87–107.

Peck, D.C., Keays, R. R., James, R. S., Chubb, P. T., and Reeves, S. J. 2001. Controls on the formation of contact-type platinum-group element mineralization in the East Bull Lake intrusion. *Econ. Geol. Bull. Soc. Econ. Geol.*, **96**, 559–581.

Perry, K. D., Cahill, T. A., Eldred, R. A., and Dutcher, D. D. 1997. Long-range transport of N. African dust to the eastern United States. *J. Geophys. Res.*, **102**(D10), 11225–11238.

Peucker-Ehrenbrink, B. 1996. Accretion of extraterrestrial matter during the last 80 million years and its effect on the marine osmium isotope record. *Geochim. et Cosmochim. Acta*, **60**, 3187–3196.

Peucker-Ehrenbrink, B., and Blum, J. D. 1998. Re-Os isotope systematics and weathering of Precambrian crustal rocks: Implications for the marine osmium isotope record. *Geochim. et Cosmochim. Acta*, **62**, 3193–3203.

Peucker-Ehrenbrink, B., and Jahn, B. 2001. Rhenium-osmium isotope systematics and platinum group element concentrations: Loess and the upper continental crust. *G-cubed*, **2**, 22pp.

Peucker-Ehrenbrink, B., and Ravizza, G. 2000. The effects of sampling artefacts on cosmic dust flux estimates: a reevaluation of nonvolatile tracers (Os,Ir). *Geochim. et Cosmochim. Acta*, **64**(11), 1965–1970.

Peucker-Ehrenbrink, B., Ravizza, G., and Hofmann, A. W. 1995. The marine $^{187}Os/^{186}Os$ record of the past 80 million years. *Earth Planet. Sci. Lett.*, **130**, 155–167.

Pluger, W. L., Herzig, P. M., Becker, K. L., Deissmann, G., Lange, J., Jenisch, A., Ladage, S., Richnow, H. H., Schulze, T., and Michaelis, W. 1990. Discovery of hydrothermal fields at the central Indian Ridge. *Mar. Mining*, **9**, 73–86.

Prospero, I. Chiapelloand J. M., Herman, J. R., and Hsu, N. C. 1999. Detection of mineral dust over the North Atlantic Ocean and Africa with the Nimbus 7 TOMS. *J. Geophys. Res. -Atmospheres*, **104**, 9277–9291.

Prospero, J. M. 1999. Long-term measurements of the transport of African mineral dust to the southeastern United States: Implications for regional air quality. *J. Geophys. Res. -Atmospheres*, **104**, 15917–15927.

Radford-Knoery, J., Thurnherr, A. M., German, C. R., Richards, K. J., Charlou, JL., Donval, JP., and Fouquet, Y. 1998. Dissolved manganese in AMAR and South AMAR axial valleys (MAR at 35°40-36°40N). *EOS Trans., AGU, AGU Supplement*, **79**(45), T12C–06.

Radford-Knoery, J., Charlou, JL., Donval, JP., and Fouquet, Y. 2001. Distribution and behaviour of dissolved hydrogen sulfide in hydrothermal plumes. *Limnology and Oceanography*, **46**(2), 461–464.

Ravizza, G. 1993. Variations of the $^{187}Os/^{186}Os$ ratio of seawater over the past 28 million years as inferred from metalliferous carbonates. *Earth Planet. Sci. Lett.*, **118**, 335–348.

Ravizza, G., and McMurtry, G. M. 1993. Osmium isotopic variations in metalliferous sediments from the East Pacific Rise and Bauer Basin. *Geochim. Cosmochim. Acta*, **57**, 4301–4310.

Ravizza, G., and Pyle, D. 1997. PGE and Os isotopic analyses of single sample aliquots with NiS fire assay preconcentration. *Chem. Geology*, **141**, 251–268.

Ravizza, G., Martin, C. E., German, C. R., and Thompson, G. 1996. Os isotopes as tracers in seafloor hydrothermal systems - metalliferous deposits from the TAG hydrothermal area, 26°N Mid-Atlantic Ridge. *Earth Planet. Sci. Lett.*, **138**, 105–19.

Ravizza, G., Sherrell, R. M., Field, M. P., and Pickett, E. A. 1999. Geochemistry of the Margi umbers, Cyprus, and the Os isotope composition of Cretaceous seawater. *Geology*, **27**(11), 971–974.

Ravizza, G., Norris, R. N., Blusztajn, J., and Aubry, M. P. 2001a. An osmium isotope excursion associated with the late Paleocene thermal maximum: Evidence of intensified chemical weathering. *Paleoceanography*, **16**, 155–163.

Ravizza, G., Blusztajn, J., and Prichard, H. M. 2001b. Re-Os systematics and platinum-group element distribution in metalliferous sediments from the Troodos ophiolite. *Earth Planet. Sci. Lett.*, **188**, 369–381.

Reeves, S. J., and Keays, R. R. 1995. The Platinum-Group Element Geochemistry of the Bucknalla Layered Complex, Central Queensland. *Australian J. Earth Sci.*, **42**, 187–201.

Reusch, D. N., Ravizza, G., Maasch, K., and Wright, J. D. 1998. Miocene seawater $^{187}Os/^{186}Os$ ratios inferred from metalliferous carbonates. *Earth Planet. Sci. Lett.*, **160**, 163–178.

Richter, T. 1998. Sedimentary fluxes at the Mid-Atlantic Ridge, Ph.D. Thesis. *Geomar Report*, **73**, 173.

Rona, P. A., Thompson, G., Mottl, M. J., Karson, J. A., Jenkins, W. J., Graham, D., Malette, M., von Damm, K., and Edmond, J. M. 1984. Hydrothermal activity at the Trans-Atlantic Geotraverse hydrothermal field, Mid-Atlantic ridge crest at 26°N. *J. Geophys. Res.*, **89**, 11365–11377.

Rona, P. A., Klinkhammer, G., Nelsen, T. A., Trefry, J. H., and Elderfield, H. 1986. Black smokers, massive sulphides and vent biota at the Mid-Atlantic Ridge. *Nature*, **321**, 33–37.

Roy-Barman, M., and Allegre, C. J. 1994. $^{187}Os/^{186}Os$ ratios of mid-ocean ridge basalts and abyssal peridotites. *Geochim. Cosmochim. Acta*, **58**(22), 5043–5054.

Rudnicki, M. D., and Elderfield, H. 1993. A chemical model of the buoyant and neutrally buoyant plume above the TAG vent field, 26 degrees-N Mid-Atlantic Ridge. *Geochim. Cosmochim. Acta*, **57**(13), 2939–2957.

Ruhlin, D. E., and Owen, R. M. 1986. The rare earth element geochemistry of hydrothermal sediments from the East Pacific Rise: examination of a seawater scavenging mechanism. *Geochim. Cosmochim. Acta*, **50**, 393–400.

Rutten, A., de Lange, G. J., Ziveri, P., Thomson, J., van Santvoort, P. J. M., Colley, S., and Corselli, C. 2000. Recent terrestrial and carbonate fluxes in the pelagic eastern Mediterranean; a comparison between sediment trap and surface sediment. *Palaeogeography Palaeoclimatology Palaeoecology*, **158**, 197–213.

Sarnthein, M., Winn, K., Jung, S. J. A., Duplessy, J-C., Labeyrie, L., Erlenkeuser, H., and Ganssen, G. 1994. Changes in the east Atlantic deepwater circulation over the last 30,000 years: Eight time slice reconstruction. *Paleoceanography*, **9**(2), 209–267.

Scott, M. R., Scott, R. B., Rona, P. A., Butler, I. W., and Nalwark, A. J. 1974. Rapidly accumulating manganese deposit from the median valley of the Mid-Atlantic Ridge. *Geophys. Res. Lett.*, **1**, 355–358.

Seyfried, W. E., and Mottl, M. J. 1995. Geologic setting and chemistry of deep-sea vents. *In:* Karl, D. M. (ed), *The microbiology of deep-sea hydrothermal vents.* CRC Press.

Sharma, M., Wasserburg, G. J., Hofmann, A. W., and Butterfield, D. A. 2000. Osmium isotopes in hydrothermal fluids from the Juan de Fuca Ridge. *Earth Planet. Sci. Lett.*, **179**, 139–152.

Sherrell, R. M., and Boyle, E. A. 1992. The trace metal composition of suspended particles in the oceanic water near Bermuda. *Earth Planet. Sci. Lett.*, **111**, 155–174.

Sherwood, B. A., Sager, S. L., and Holland, H.D. 1987. Phosphorus in foraminiferal sediments from North Atlantic Ridge cores and in pure limestones. *Geochim. Cosmochim. Acta*, **51**, 1861–1866.

Shimmield, G. 1990. *Leg C - Benthic studies, water column particulates and sediment trap deployments: components of the Biogeochemical Ocean Flux Study between 47°N and 18°N along the 20°W meridian in the northeast Atlantic Ocean.* Charles Darwin Cruise Report no. 53, University of Edinburgh,.

Snow, J. E., and Dick, H. J. B. 1995. Pervasive magnesium loss by marine weathering of peridotite. *Geochim. Cosmochim. Acta*, **59**(20), 4219–4235.

Snow, J. E., and Reisberg, L. 1995. Erratum of Os isotopic systematics of the MORB mantle - results from altered abyssal peridotites. *Earth Planet. Sci. Lett.*, **136**, 723–733.

Spiess, F.N., MacDonald, K. C., Atwater, T., Ballard, R., Caranza, A., Cordoba, D., Cox, C., Diaz-Garcia, V. M., Francheteau, J., Guerrero, J., Hawkins, J., Haymon, R., Hessler, R., Juteau, T., Kastner, M., Larson, R., Luyendyke, B., Macdougall, J. D., Miller, S., Normark, W., Orcutt, J., and Rangin, C. 1980. East Pacific Rise: hot springs and geophysical experiments. *Science*, **207**, 1421–1433.

Tachikawa, K., Jeandel, C., and Dupre, B. 1997. Distribution of rare earth elements and neodynium isotopes in settling particulate material of the tropical Atlantic Ocean (EUMELI site). *Deep-Sea Res.*, **44**(11), 1769–1792.

Taylor, S. R., and McLennan, S. M. 1985. The geochemical evolution of the continental crust. *Rev. Geophys.*, **33**(2), 241–265.

Thompson, G., Humphris, S. E., Schroeder, B., Sulanowska, M., and Rona, P. A. 1988. Active vents and massive sulphides at 26°N (TAG) and 23°N (Snakepit) on the Mid-Atlantic Ridge. *Canadian Mineralogist*, **26**, 697–711.

Thomson, J., Carpenter, M. S. N., Colley, S., Wilson, T. R. S., Elderfield, H., and Kennedy, H. 1984. Metal accumulation rates in northwest Atlantic pelagic sediments. *Geochim. Cosmochim. Acta*, **48**, 1935–1948.

Thomson, J., Mackenzie, A. B., Cook, G. T., and Harkness, D. D. 1993. Application of radionuclide studies to the BOFS programme. *In: NERC Biogeochemical Ocean Flux Study Communtiy Res. Project 1987-1993*, vol. 2. UK JGOFS.

Thomson, J., Higgs, N. C., and Colley, S. 1996. Diagenetic redistributions of redox-sensitive elements in northeast Atlantic glacial/interglagial transition sediments. *Earth Planet. Sci. Lett.*, **139**, 365–377.

Thomson, J., Brown, L., Nixon, S., Cook, G. T., and MacKenzie, A. B. 2000. Bioturbation and Holocene sediment accumulation fluxes in the north-east Atlantic Ocean (Benthic Boundary Layer experiment sites). *Mar. Geology*, **169**, 21–39.

Thurnherr, A. M., and Richards, K. J. 2001. Hydrography and high-temperature heat flux of the Rainbow hydrothermal site (36^{o}14'N, Mid-Atlantic Ridge). *J. Geophys. Res. (Oceans)*, **106**(C5), 9411–9426.

Thurnherr, A. M., Richards, K. J., german, C. R., Lane-Serff, G. F., and Speer, K. G. in press. Flow and mixing in the rift valley of the Mid-Atlantic Ridge. *Phys. Oceanog.*

Trefry, J. H., and Metz, S. 1989. Role of hydrothermal precipitates in the geochemical cycling of Vanadium. *Nature*, **342**, 531–533.

Trocine, R. P., and Trefry, J. H. 1988. Distribution and chemistry of suspended particles from an active hydrothemal vent site on the Mid-Atlantic Ridge at 26^{o}N. *Earth Planet. Sci. Lett.*, **88**, 1–15.

Tuit, C. B., Ravizza, G. E., and Bothner, M. H. 2000. Anthropogenic platinum and palladium in the sediments of Boston Harbor. *Env. Sci. and Tech.*, **34**, 927–932.

Turekian, K. K., and Wedepohl, K. H. 1961. Distribution of the elements in some major units of the earth's crust. *Geol. Soc. Am. Bulletin*, **73**, 175–192.

USGS. 1986. Juan de Fuca Ridge Study Group. Submarine fissure eruptions and hydrothermal vents on the southern Juan de Fuca Ridge: preliminary observations from the submersible *Alvin*. *Geology*, **14**, 823–827.

van Aken, H. M. 2000. The hydrography of the mid-latitude northeast Atlantic Ocean I: The deep water masses. *Deep-Sea Res. Part I-Oceanographic Research Papers*, **47**(5), 757–788.

van Dover, C. L., German, C. R., Speer, K. G., Parson, L. M., and Vrijenhoek, R. C. 2002. Marine biology - Evolution and biogeography of deep-sea vent and seep invertebrates. *Science*, **295**, 1253–1257.

Vogel, D. C., and Keays, R. R. 1997. The petrogenesis and platinum-group element geochemistry of the Newer Volcanic Province, Victoria, Australia. *Chem. Geology*, **136**, 181–204.

von Damm, K. L. 1995. Controls on the Chemistry and Temporal Variability of Seafloor Hydrothermal Fluids. *Pages 222–247 of:* Humphris, S. E., Zierenberg, R. A., Mullineaux, L. S., and Thomson, R. E. (eds), *Seafloor Hydrothermal Systems: Physical, Chemical, Biological and Geological Interactions. Geophys. Monograph 91.* AGU.

von Damm, K. L., Edmonds, J. M., Measures, C. I., and Grant, B. 1985. Chemistry of submarine hydrothermal solutions at Guaymas Basin, Gulf of California. *Geochim. Cosmochim. Acta*, **49**, 2221–2237.

von Stackelberg, U., and Party, . Shipboard. 1988. Active hydrothermalism in the Lau Back-arc basin (SW Pacific): first results from the SONNE 48 cruise (1987). *Mar. Mining*, **7**, 431–442.

Walker, R. J., and Morgan, J. W. 1989. Rhenium-Osmium Isotope Systematics of Carbonaceous Chondrites. *Science*, **243**, 519–522.

Wallace, H. E., Thomson, J., Wilson, T. R. S., Weaver, P. P. E., Higgs, N. C., and Hydes, D. J. 1988. Active diagenetic formation of metal-rich layers in N.E. Atlantic sediments. *Geochim. Cosmochim. Acta*, **52**, 1557–1569.

Weiss, R. F., Lonsdale, P., Lupton, J. E., Bainbridge, A. E., and Craig, H. 1977. Hydrothermal plumes in the Galapagos Rift. *Nature*, **267**, 600–603.

Wheat, C. G., and Mottl, M. J. 2000. Composition of pore and spring waters from Baby Bare: global implications of geochemical fluxes from a ridge flank hydrothermal site. *Geochim. Cosmochim. Acta*, **64**(4), 629–642.

Wilson, T. R. S., Thomson, J., Colley, S., Hydes, D. J., Higgs, N. C., and Sorensen, J. 1985. Early organic diagenesis: the significance of progressive subsurface oxidation fronts in pelagic sediments. *Geochim. Cosmochim. Acta*, **49**, 811–822.

Wilson, T. R. S., Thomson, J., Hydes, D. J., Colley, S., Culkin, F., and Sorensen, J. 1986. Oxidation fronts in pelagic sediments: diagenetic formation of metal-rich layers. *Science*, **232**, 972–974.

Woodhouse, O. B., Ravizza, G., Faulkner, K. Kenison, Statham, P. J., and Peucker-Ehrenbrink, B. 1999. Osmium in seawater: vertical profiles of concentration and isotopic composition in the eastern Pacific Ocean. *Earth Planet. Sci. Lett.*, **173**, 223–233.

Yu, E. F., Francois, R., Bacon, M. P., Honjo, S., Fleer, A. P., Manganini, S. J., van der Loeff, M. M. R., and Ittekot, V. 2001. Trapping efficiency of bottom-tethered sediment traps estimated from the intercepted fluxes of Th-230 and Pa-231. *Deep-Sea Res. Part I-Oceanographic Research Papers*, **48**, 865–889.

Zierenberg, R. A., and Shanks, W. C. 1994. Sediment Alteration Associated with Massive Sulfide Formation in Escanaba Trough, Gorda Ridge: The Importance of

Seawater Mixing and Magnesium Metasomatism. *Pages 257–277 of:* Morton, J. L., Zierenberg, R. A., and Reiss, C. A. (eds), *Geologic, Hydrothermal and Biologic Studies at Escanaba Trough, Gorda Ridge, Offshore Northern California.* U.S. Geological Survey, Denver, CO.

Zimmermann, H. B. 1981. Fine grained sediment distribution in the late Pleistocene Holocene North Atlantic. *Bull. Inst. Geol. Basin d'Aquitaine*, **31**, 337–357.

Appendices

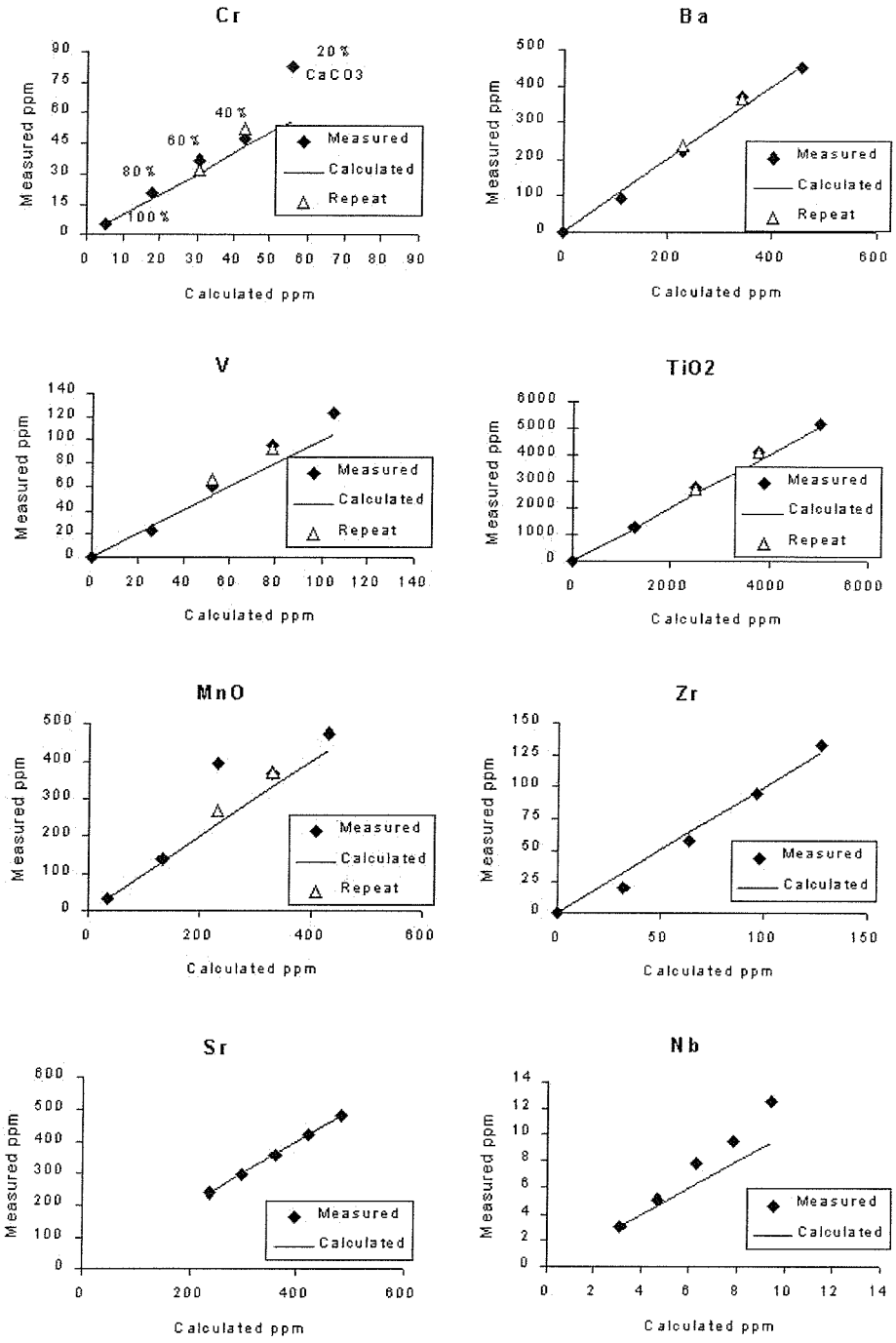
Cr
Measured ppm
Calculated ppm
20 % CaCO3
40 %
60 %
80 %
100 %
Measured
Calculated
Repeat
Ba
Measured ppm
Calculated ppm
Measured
Calculated
Repeat
V
Measured ppm
Calculated ppm
Measured
Calculated
Repeat
TiO2
Measured ppm
Calculated ppm
Measured
Calculated
Repeat
MnO
Measured ppm
Calculated ppm
Measured
Calculated
Repeat
Zr
Measured ppm
Calculated ppm
Measured
Calculated
Sr
Measured ppm
Calculated ppm
Measured
Calculated
Nb
Measured ppm
Calculated ppm
Measured
Calculated

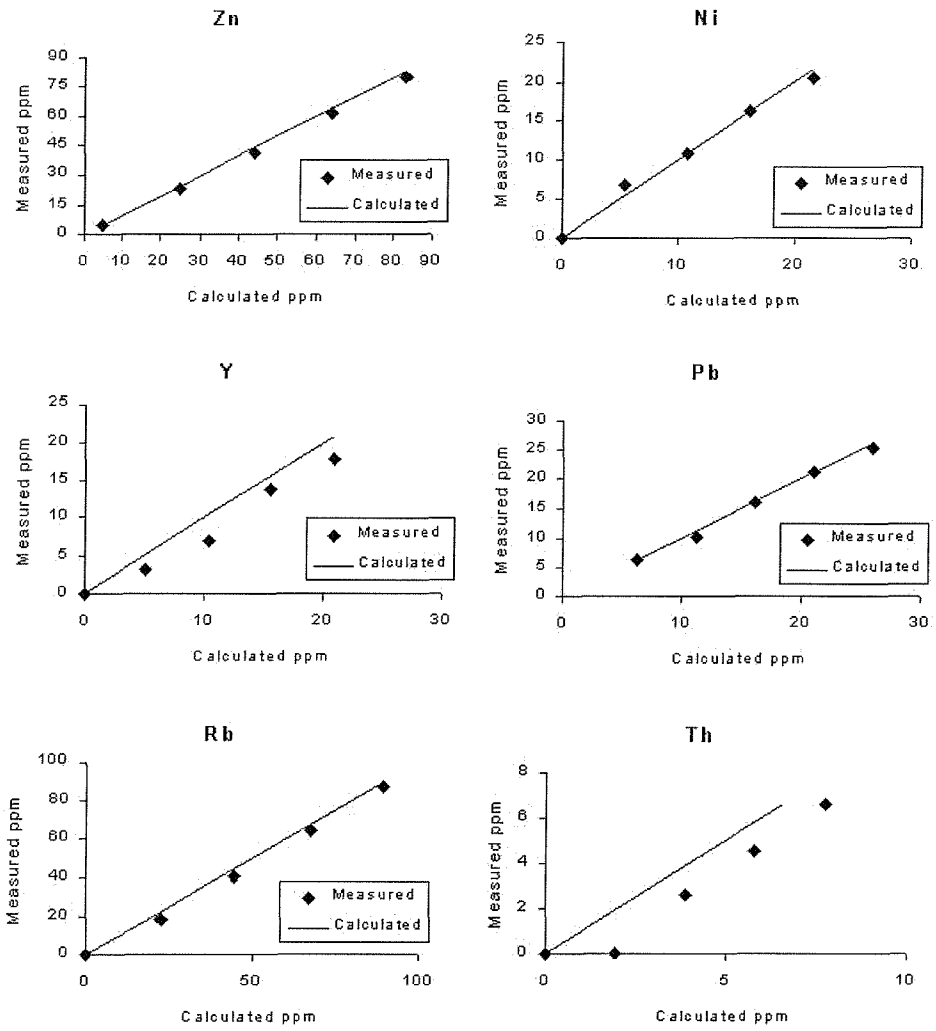
Zn
Measured ppm
Calculated ppm
Measured
Calculated
Ni
Measured ppm
Calculated ppm
Measured
Calculated
Y
Measured ppm
Calculated ppm
Measured
Calculated
Pb
Measured ppm
Calculated ppm
Measured
Calculated
Rb
Measured ppm
Calculated ppm
Measured
Calculated
Th
Measured ppm
Calculated ppm

Rainbow core 343

cm	%	%	%	ppm	ppm	ppm	ppm	ppm	ppm	ppm	ppm	%	%
Depth	**Al**	**Ti**	**Fe**	**P**	**V**	**Cr**	**Mn**	**Ni**	**Cu**	**Zn**	**As**	**CaCO3**	**Corg**
0.5	0.566	0.048	1.47	731	88	21	503	12	394	31	25	82.9	0.39
1.5	0.561	0.050	1.55	783	95	19	568	13	411	31	27	84.3	0.38
2.5	0.529	0.048	1.54	768	87	18	557	12	395	25	27	84.5	0.43
4.5	0.531	0.048	1.65	798	97	20	747	14	423	28	28	84.4	0.41
6.5	0.519	0.051	1.61	787	91	18	559	12	433	28	29	84.1	0.09
8.5	0.533	0.051	1.59	791	88	23	562	15	445	27	29	86.2	0.46
10.5	0.534	0.054	1.58	724	90	22	588	16	427	31	28	86.4	0.07
12.5	0.591	0.056	1.65	749	91	87	672	28	421	30	30	82.6	0.21
14.5	0.546	0.057	1.64	777	89	19	642	19	429	29	29	84.4	0.17
16.5	0.545	0.065	1.69	793	90	19	649	20	448	31	30	84.7	0.41
18.5	0.575	0.062	1.66	765	93	31	695	22	427	30	28	84.9	0.14
19.5	0.672	0.063	1.79	688	88	65	723	63	394	31	25	81.1	0.27
20.5	0.748	0.065	1.72	602	71	113	718	85	323	29	19	78.7	n.d.
21.5	0.704	0.069	1.67	566	70	135	741	78	287	28	16	78.5	n.d.
22.5	0.700	0.070	1.41	546	55	139	678	51	247	27	14	82.2	-
23.5	0.669	0.071	1.26	514	47	54	672	45	217	27	12	83.6	0.09
25.5	0.708	0.067	1.13	449	37	53	749	47	172	28	9	84.1	0.32
26.5	0.719	0.064	1.29	436	38	58	822	65	164	26	9	81.2	0.28
27.5	0.743	0.063	1.32	451	40	87	929	73	175	30	10	83.8	n.d.
29.5	0.708	0.065	1.17	469	36	37	801	49	148	28	10	83.8	0.19
31.5	0.695	0.058	1.13	497	43	10	805	42	136	28	11	84.6	0.12
33.5	0.656	0.054	1.09	498	38	18	760	48	120	25	11	85.3	1.32
35.5	0.607	0.050	1.03	475	31	20	675	48	103	26	9	87.1	n.d.
37.5	0.568	0.046	0.95	491	32	12	458	29	87	23	10	86.6	0.54
38.5	0.623	0.049	1.06	487	37	14	404	33	73	24	12	85.8	-
39.5	0.613	0.047	1.07	524	36	12	325	32	87	24	13	87.4	n.d.
40.5	0.572	0.044	0.99	483	36	22	293	41	76	21	12	85.6	-

Rainbow core 316

cm	%	%	%	ppm	ppm	ppm	ppm	ppm	ppm	ppm	ppm	%	%
Depth	**Al**	**Ti**	**Fe**	**P**	**V**	**Cr**	**Mn**	**Ni**	**Cu**	**Zn**	**As**	**CaCO3**	**Corg**
0.5	0.532	0.050	1.53	755	92	21	685	18	334	30	25	86.2	n.d.
1.5	0.527	0.051	1.48	721	91	17	685	16	331	31	26	85.6	0.22
2.5	0.504	0.049	1.49	736	93	16	674	17	334	32	26	84.8	-
4.5	0.496	0.047	1.55	778	97	16	701	16	352	32	27	85.1	-
6.5	0.502	0.046	1.49	730	94	18	664	16	345	29	24	85.8	n.d.
8.5	0.502	0.049	1.51	727	86	14	702	15	346	29	25	85.2	-
10.5	0.520	0.049	1.53	710	93	12	700	17	330	29	25	84.6	-
12.5	0.563	0.056	1.52	699	89	25	760	18	334	31	24	85.5	n.d.
14.5	0.600	0.056	1.55	660	83	44	930	39	326	33	23	82.9	-
16.5	0.535	0.056	1.46	642	76	47	781	26	305	26	24	86.0	-
18.5	0.539	0.057	1.44	659	82	22	744	22	313	28	23	85.0	0.08
20.5	0.527	0.058	1.40	627	81	12	735	22	296	27	21	84.9	-
22.5	0.557	0.059	1.34	590	71	23	699	23	275	28	18	86.0	-
23.5	0.543	0.057	1.30	537	62	29	712	24	294	27	16	-	-
24.5	0.633	0.062	1.22	486	62	28	721	23	222	28	12	87.2	n.d.
25.5	0.574	0.057	1.09	390	42	40	714	34	166	31	7	85.1	-
26.5	0.633	0.058	1.06	363	36	39	723	45	179	31	7	-	-

Rainbow core 325

cm	%	%	%	ppm	ppm	ppm	ppm	ppm	ppm	ppm	ppm	%	%
Depth	**Al**	**Ti**	**Fe**	**P**	**V**	**Cr**	**Mn**	**Ni**	**Cu**	**Zn**	**As**	**CaCO3**	**Corg**
0.5	0.468	0.047	1.52	790	103	15	823	12	142	21	33	83.4	0.00
1.5	0.503	0.050	1.68	863	108	12	862	12	148	21	36	84.6	0.38
2.5	0.510	0.051	1.76	918	114	10	902	10	154	21	38	84.9	-
4.5	0.502	0.053	1.77	912	116	9	903	10	157	21	39	84.9	-
6.5	0.512	0.053	1.78	932	113	11	925	12	163	23	38	84.9	-
8.5	0.541	0.056	1.82	925	113	15	945	12	162	20	39	84.1	0.86
10.5	0.519	0.056	1.77	906	113	17	934	11	151	20	37	83.3	-
12.5	0.515	0.055	1.73	871	106	17	938	10	149	18	34	84.8	n.d.
14.5	0.529	0.057	1.67	823	103	13	944	13	151	20	36	87.2	-
16.5	0.558	0.061	1.58	778	90	12	921	12	144	21	30	85.2	-
17.5	0.566	0.063	1.55	764	94	15	863	13	135	26	27	82.3	0.47

Rainbow core 329

cm	%	%	%	ppm	ppm	ppm	ppm	ppm	ppm	ppm	ppm	%	%
Depth	**Al**	**Ti**	**Fe**	**P**	**V**	**Cr**	**Mn**	**Ni**	**Cu**	**Zn**	**As**	**CaCO3**	**Corg**
0.5	0.678	0.065	1.94	915	115	8	1063	14	110	22	39	80.7	n.d.
1.5	0.665	0.065	2.04	992	126	13	1048	13	113	20	40	81.9	0.03
2.5	0.648	0.065	2.03	996	121	13	1078	12	113	20	40	82.0	-
4.5	0.674	0.065	2.07	1005	122	15	1153	12	113	20	41	81.5	-
6.5	0.663	0.068	2.09	1015	129	20	1089	12	117	22	46	81.7	0.09
8.5	0.665	0.065	2.09	1019	120	14	1150	12	114	23	43	82.9	-
10.5	0.661	0.068	2.07	995	131	14	1129	14	111	21	42	82.5	-
12.5	0.816	0.077	2.12	954	124	19	1142	15	114	24	39	81.1	0.14
14.5	0.675	0.069	2.02	946	123	18	1255	16	114	23	36	83.7	-
16.5	0.679	0.069	2.02	898	106	17	1511	16	113	24	33	83.9	-
17.5	0.688	0.072	1.99	878	114	14	1337	13	114	25	35	81.5	0.26

BOFS core 22#6M/23#12M

cm	%	%	%	ppm	ppm	ppm	ppm	ppm	ppm	ppm	ppm	%	%
Depth	**Al**	**Ti**	**Fe**	**P**	**V**	**Cr**	**Mn**	**Ni**	**Cu**	**Zn**	**As**	**CaCO3**	**Corg**
6.5	1.31	0.130	0.913	347	32	26	469	13	47	20	<1	82.5	0.40
8.5	1.30	0.134	0.920	359	33	28	466	13	19	21	<1	83.2	0.40
5.5	1.38	0.112	0.871	301	31	19	532	13	45	21	<1	80.2	0.50
7.5	1.26	0.114	0.835	294	26	19	532	13	47	20	<1	81.5	0.50
Av.	1.31	0.123	0.885	325	31	23	500	13	40	21	<1	81.85	0.45

Serpentinite found in core 343

%	%	%	ppm	ppm	ppm	ppm	ppm	ppm	ppm	ppm
Al	**Ti**	**Fe**	**P**	**V**	**Cr**	**Mn**	**Ni**	**Cu**	**Zn**	**As**
0.328	0.016	8.80	77	54	977	1371	1490	116	45	13

Bulk data for sediment trap samples

N-F (l)	Mg %	Al %	Ti %	Fe %	V ppm	Mn ppm	Co ppm	Ni ppm	Cu ppm	Zn ppm
1	0.60	0.56	0.055	15.74	186	717	553	90	64226	7642
2	0.56	0.26	0.024	17.33	124	303	844	135	57754	5457
3	0.64	0.36	0.032	19.85	219	412	659	100	97304	4498
4	0.84	0.51	0.045	19.53	844	262	208	40	15301	1080
N-F (u)										
5	0.46	0.70	0.070	3.19	91	870	58	24	2757	554
6	0.58	0.57	0.048	5.90	111	582	185	52	14717	1445
7/8	0.40	0.59	0.048	5.17	90	365	49	68	2384	565
F-F (l)										
9	0.46	0.77	0.061	2.79	116	1111	27	47	1131	253
10	0.39	0.72	0.053	2.09	86	912	23	37	1021	324
11	0.47	0.43	0.035	1.43	60	721	16	57	474	123
12	0.37	0.65	0.054	1.90	96	606	20	57	279	109
F-F (u)										
13	0.42	0.74	0.088	1.33	58	824	11	34	100	100
14	0.43	0.66	0.050	1.18	55	789	9	50	93	124
15	0.48	0.51	0.043	0.80	37	548	7	36	59	72
16	0.36	0.79	0.067	1.27	91	543	11	63	76	68
R-T										
17/18	0.43	0.72	0.054	1.30	52	788	17	32	492	328
19/20	0.37	0.68	0.054	3.05	36	426	15	31	56	154

Hydrothermal contribution to sediment trap samples

N-F (l)	Mg%	Fe %	V ppm	Mn ppm	Co ppm	Ni ppm	Cu ppm	Zn ppm
1	0.43	15.40	177	575	551	82	64218	7632
2	0.49	17.17	120	238	843	132	57751	5453
3	0.54	19.63	213	321	657	95	97299	4492
4	0.68	19.21	836	133	206	33	15294	1071
N-F (u)								
5	0.25	2.76	80	692	55	14	2747	541
6	0.41	5.55	102	438	182	44	14710	1434
7/8	0.23	4.81	80	214	46	59	2376	555
F-F (l)								
9	0.22	2.32	103	915	24	36	1120	240
10	0.18	1.65	74	730	20	27	1011	311
11	0.34	1.16	53	612	15	51	468	115
12	0.18	1.50	85	441	17	48	270	97
F-F (u)								
13	0.20	0.87	45	635	8	23	89	87
14	0.24	0.78	44	623	6	41	84	112
15	0.33	0.49	29	419	5	29	52	63
16	0.12	0.79	78	343	8	52	65	54
R-T								
17/18	0.21	0.86	40	605	14	22	482	315
19/20	0.17	2.64	24	253	13	21	46	142

Bulk data for surficial sediment (core-top) samples

343	Mg %	Al %	Ti %	Fe %	V ppm	Mn ppm	Co ppm	Ni ppm	Cu ppm	Zn ppm
0-1cm	0.61	0.65	0.056	1.82	76	648	15	14	393	32
1-2cm	0.61	0.65	0.059	2.05	86	726	16	2	426	33
2-3cm	0.55	0.70	0.064	2.18	90	781	17	12	463	33
316										
0-1cm	0.56	0.62	0.059	2.00	83	889	18	37	413	40
1-2cm	0.51	0.63	0.058	1.93	81	872	18	19	419	33
2-3cm	0.52	0.60	0.055	1.90	81	857	18	27	419	38
325										
0-1cm	0.36	0.57	0.055	2.05	92	787	12	13	132	18
1-2cm	0.34	0.61	0.061	2.21	99	852	13	9	143	18
2-3cm	0.35	0.62	0.063	2.34	101	884	13	8	145	24
329										
0-1cm	0.43	0.82	0.079	2.62	108	1215	13	16	99	35
1-2cm	0.39	0.82	0.079	2.77	112	1243	13	21	108	22
2-3cm	0.40	0.83	0.081	2.81	115	1294	13	19	111	26
Average Background										
	0.54	1.80	0.16	1.10	30	456	7	26	25	32

Hydrothermal contribution to surficial sediment (core-top) samples

343	Mg %	Fe %	V ppm	Mn ppm	Co ppm	Ni ppm	Cu ppm	Zn ppm
0-1cm	0.41	1.42	65	482	13	5	384	20
1-2cm	0.41	1.65	75	560	14	0	417	21
2-3cm	0.34	1.76	78	604	15	2	453	21
316								
0-1cm	0.37	1.62	73	730	16	28	405	29
1-2cm	0.32	1.55	70	714	16	10	410	21
2-3cm	0.34	1.54	71	705	16	18	410	27
325								
0-1cm	0.19	1.70	83	642	10	5	124	8
1-2cm	0.15	1.84	89	696	10	0	135	7
2-3cm	0.16	1.96	90	726	10	0	136	13
329								
0-1cm	0.18	2.12	94	1006	10	4	88	20
1-2cm	0.15	2.27	98	1036	9	9	97	8
2-3cm	0.16	2.30	101	1084	10	7	99	11

Rainbow	Near-field lower, bulk				Hydrothermal contribution			
µg/g	1	2	3	4	1	2	3	4
La	15.69	22.99	21.74	13.57	12.35	21.46	19.58	10.53
Ce	18.75	23.85	23.09	13.78	12.79	21.10	19.24	8.35
Pr	2.37	2.33	2.46	2.97	1.49	1.92	1.89	2.17
Nd	9.14	7.99	8.90	12.72	5.41	6.27	6.49	9.32
Sm	1.85	1.39	1.74	2.82	1.19	1.09	1.32	2.22
Eu	1.39	1.99	1.86	1.20	1.21	1.91	1.74	1.04
Gd	1.97	1.21	1.57	3.53	1.50	0.99	1.27	3.10
Tb	0.29	0.22	0.28	0.49	0.20	0.18	0.22	0.40
Dy	1.73	1.35	1.67	3.21	1.20	1.11	1.33	2.72
Ho	0.34	0.24	0.32	0.65	0.24	0.19	0.25	0.56
Er	0.95	0.69	0.88	1.94	0.66	0.55	0.69	1.67
Tm	0.13	0.09	0.12	0.25	0.09	0.08	0.09	0.22
Yb	0.77	0.56	0.74	1.62	0.52	0.45	0.57	1.39
Lu	0.10	0.07	0.10	0.22	0.07	0.06	0.08	0.19

	Near-field upper, bulk			Hydrothermal contribution		
µg/g	5	6	7+8	5	6	7+8
La	7.86	10.57	6.08	3.67	7.19	2.52
Ce	13.55	15.86	9.52	6.06	9.82	3.18
Pr	1.99	2.07	1.39	0.88	1.18	0.46
Nd	8.30	8.53	5.68	3.61	4.74	1.70
Sm	1.83	1.84	1.19	1.00	1.17	0.49
Eu	0.51	0.79	0.36	0.29	0.61	0.17
Gd	1.94	1.82	1.12	1.35	1.34	0.62
Tb	0.28	0.28	0.18	0.16	0.19	0.08
Dy	1.67	1.69	1.07	1.00	1.15	0.51
Ho	0.33	0.30	0.22	0.20	0.20	0.10
Er	0.91	0.89	0.58	0.54	0.60	0.26
Tm	0.12	0.11	0.08	0.07	0.07	0.04
Yb	0.73	0.73	0.51	0.42	0.47	0.24
Lu	0.11	0.10	0.07	0.06	0.07	0.03

Rainbow	Far-field lower, bulk				Hydrothermal contribution			
µg/g	9	10	11	12	9	10	11	12
La	8.81	7.73	5.76	6.27	4.21	3.46	3.18	2.40
Ce	14.18	13.22	8.76	10.14	5.96	5.58	4.15	3.23
Pr	2.21	1.94	1.45	1.55	0.99	0.82	0.77	0.54
Nd	9.22	8.14	6.11	6.38	4.06	3.36	3.23	2.05
Sm	2.03	1.85	1.33	1.33	1.12	1.00	0.82	0.56
Eu	0.50	0.46	0.37	0.32	0.26	0.23	0.24	0.12
Gd	2.02	1.92	1.66	1.29	1.37	1.31	1.30	0.75
Tb	0.32	0.28	0.22	0.21	0.19	0.16	0.15	0.10
Dy	1.88	1.63	1.37	1.23	1.15	0.95	0.96	0.62
Ho	0.37	0.32	0.26	0.24	0.22	0.19	0.18	0.12
Er	1.05	0.91	0.75	0.70	0.64	0.54	0.52	0.36
Tm	0.14	0.12	0.10	0.10	0.09	0.08	0.07	0.05
Yb	0.85	0.78	0.64	0.57	0.50	0.45	0.44	0.28
Lu	0.12	0.10	0.09	0.09	0.07	0.06	0.06	0.05

	Far-field upper, bulk				Hydrothermal contribution			
µg/g	13	14	15	16	13	14	15	16
La	7.20	6.40	5.48	6.69	2.77	2.49	2.45	1.99
Ce	13.48	12.15	9.47	12.11	5.56	5.15	4.08	3.71
Pr	1.87	1.65	1.41	1.65	0.70	0.61	0.61	0.41
Nd	7.88	6.95	6.10	6.82	2.91	2.56	2.72	1.56
Sm	1.72	1.55	1.38	1.46	0.85	0.78	0.79	0.53
Eu	0.43	0.39	0.34	0.34	0.19	0.18	0.18	0.09
Gd	1.91	1.69	1.52	1.25	1.29	1.14	1.09	0.59
Tb	0.27	0.24	0.22	0.22	0.15	0.13	0.13	0.09
Dy	1.55	1.40	1.29	1.26	0.85	0.78	0.81	0.51
Ho	0.31	0.28	0.25	0.25	0.17	0.15	0.15	0.10
Er	0.86	0.77	0.69	0.69	0.47	0.42	0.42	0.27
Tm	0.12	0.11	0.09	0.09	0.06	0.06	0.06	0.04
Yb	0.68	0.62	0.59	0.58	0.35	0.32	0.37	0.23
Lu	0.10	0.09	0.08	0.08	0.05	0.05	0.05	0.04

	Ridge-top, bulk		Hydrothermal contribution	
µg/g	17+18	19+20	17+18	19+20
La	6.96	5.42	2.66	1.36
Ce	13.41	9.93	5.72	2.70
Pr	1.79	1.38	0.66	0.31
Nd	7.50	5.75	2.68	1.22
Sm	1.65	1.22	0.80	0.42
Eu	0.42	0.29	0.19	0.07
Gd	1.84	1.14	1.23	0.56
Tb	0.25	0.18	0.13	0.07
Dy	1.51	1.07	0.83	0.43
Ho	0.29	0.21	0.15	0.08
Er	0.80	0.57	0.41	0.21
Tm	0.11	0.08	0.06	0.03
Yb	0.66	0.49	0.34	0.19
Lu	0.09	0.07	0.04	0.03

Rainbow Core 343 - bulk sediment				Hydrothermal contribution		
µg/g	0-1cm	1-2cm	2-3cm	0-1cm	1-2cm	2-3cm
La	7.44	8.38	9.45	3.54	4.48	5.29
Ce	10.18	11.63	12.93	3.21	4.65	5.51
Pr	1.83	2.08	2.32	0.80	1.05	1.22
Nd	8.02	8.98	10.12	3.66	4.60	5.47
Sm	1.46	1.56	1.84	0.69	0.79	1.02
Eu	0.39	0.44	0.50	0.19	0.23	0.28
Gd	1.28	1.44	1.72	0.72	0.89	1.14
Tb	0.24	0.27	0.31	0.14	0.17	0.19
Dy	1.48	1.66	1.85	0.86	1.04	1.19
Ho	0.31	0.35	0.39	0.19	0.22	0.25
Er	0.89	0.97	1.10	0.55	0.63	0.73
Tm	0.12	0.13	0.15	0.07	0.08	0.10
Yb	0.72	0.79	0.89	0.42	0.49	0.58
Lu	0.10	0.12	0.13	0.06	0.07	0.09

Rainbow Core 316 - bulk sediment				Hydrothermal contribution		
µg/g	0-1cm	1-2cm	2-3cm	0-1cm	1-2cm	2-3cm
La	7.51	7.63	7.50	3.78	3.90	3.94
Ce	10.79	10.78	10.54	4.13	4.11	4.17
Pr	1.87	1.93	1.88	0.88	0.94	0.94
Nd	8.14	8.42	8.25	3.97	4.24	4.25
Sm	1.52	1.54	1.49	0.78	0.80	0.78
Eu	0.41	0.43	0.40	0.21	0.23	0.21
Gd	1.41	1.40	1.30	0.89	0.87	0.80
Tb	0.25	0.25	0.25	0.14	0.15	0.15
Dy	1.48	1.49	1.47	0.88	0.90	0.90
Ho	0.31	0.31	0.31	0.19	0.20	0.20
Er	0.90	0.88	0.87	0.57	0.55	0.56
Tm	0.12	0.12	0.11	0.07	0.07	0.07
Yb	0.73	0.75	0.74	0.45	0.47	0.47
Lu	0.11	0.11	0.11	0.07	0.07	0.07

Rainbow	Core 325 - bulk sediment			Hydrothermal contribution		
µg/g	0-1cm	1-2cm	2-3cm	0-1cm	1-2cm	2-3cm
La	8.00	8.37	8.73	4.59	4.72	5.02
Ce	10.90	11.58	12.20	4.80	5.05	5.57
Pr	2.02	2.16	2.28	1.12	1.20	1.31
Nd	8.97	9.58	10.17	5.15	5.49	6.01
Sm	1.63	1.77	1.86	0.96	1.05	1.13
Eu	0.45	0.49	0.50	0.26	0.29	0.31
Gd	1.56	1.68	1.72	1.08	1.16	1.19
Tb	0.27	0.30	0.30	0.18	0.20	0.20
Dy	1.60	1.77	1.83	1.06	1.19	1.24
Ho	0.33	0.37	0.38	0.22	0.26	0.26
Er	0.97	1.05	1.08	0.67	0.72	0.75
Tm	0.12	0.13	0.14	0.08	0.09	0.10
Yb	0.81	0.86	0.89	0.55	0.59	0.61
Lu	0.12	0.13	0.13	0.08	0.09	0.09

Rainbow	Core 329 - bulk sediment			Hydrothermal contribution		
µg/g	0-1cm	1-2cm	2-3cm	0-1cm	1-2cm	2-3cm
La	8.56	9.43	9.34	3.65	4.55	4.38
Ce	12.29	13.48	13.42	3.52	4.76	4.56
Pr	2.24	2.45	2.46	0.94	1.17	1.16
Nd	9.86	10.84	10.75	4.36	5.37	5.20
Sm	1.86	1.98	2.02	0.89	1.02	1.04
Eu	0.48	0.54	0.53	0.22	0.28	0.27
Gd	1.65	1.78	1.80	0.96	1.09	1.10
Tb	0.30	0.32	0.32	0.16	0.19	0.19
Dy	1.80	1.91	1.95	1.02	1.13	1.16
Ho	0.37	0.39	0.40	0.22	0.24	0.25
Er	1.06	1.11	1.15	0.63	0.68	0.72
Tm	0.13	0.14	0.15	0.08	0.09	0.09
Yb	0.89	0.94	0.99	0.52	0.58	0.61
Lu	0.13	0.14	0.14	0.08	0.09	0.09

	Core 23#112			Core 22#6		Core 343
µg/g	0-1cm	5-6cm	7-8cm	6-7cm	8-9cm	Serpentinite
La	11.74	11.13	10.48	10.05	10.21	0.39
Ce	20.72	19.97	19.58	17.80	17.68	2.01
Pr	3.04	2.92	2.81	2.67	2.69	0.09
Nd	12.87	12.26	11.69	11.51	11.68	0.35
Sm	2.28	2.13	2.06	2.03	2.08	0.08
Eu	0.59	0.56	0.54	0.56	0.59	0.03
Gd	1.40	1.29	1.34	1.71	1.84	0.14
Tb	0.31	0.30	0.29	0.28	0.30	0.02
Dy	1.81	1.71	1.66	1.66	1.71	0.12
Ho	0.36	0.34	0.34	0.32	0.33	0.03
Er	1.01	0.97	0.93	0.89	0.95	0.07
Tm	0.13	0.13	0.12	0.11	0.12	0.01
Yb	0.87	0.81	0.80	0.77	0.78	0.10
Lu	0.12	0.11	0.11	0.11	0.11	0.02

PGE and Os isotope data for bulk sediment core samples

Core 343	Ru ppb	Pd ppb	Pt ppb	Ir ppb	Os ppb	$^{187}Os/^{188}Os$	$^{187}Os/^{186}Os$
1-2cm	0.336	1.427	0.991	0.046	0.164	0.9975	8.288
2-3cm	0.503	1.489	0.963	0.082	0.162	1.0152	8.435
replicate	*0.314*	*1.549*	*1.311*	*0.043*	*0.157*	*1.0119*	8.408
4-5cm	0.528	1.456	0.822	0.103	0.142	0.9821	8.160
replicate	*0.439*	*1.471*	*0.947*	*0.046*	*0.154*	*1.0211*	8.484
replicate	*0.236*	*1.495*	*1.015*	*0.054*	*0.160*	*1.0187*	8.464
16-17cm	0.387	1.639	1.283	0.055	0.146	1.0014	8.321
23-24cm	0.560	1.218	1.051	0.107	0.124	0.5972	4.962
replicate	*0.426*	*1.278*	*1.139*	*0.122*	*0.129*	*0.6161*	5.119
25-26cm	2.604	1.214	1.217	0.092	0.111	0.6036	5.016
29-30cm	0.637	1.457	1.862	0.272	0.197	0.4191	3.483
31-32cm	0.785	1.046	0.866	0.048	0.096	0.8387	6.969
37-38cm	0.247	0.792	0.616	0.046	0.064	0.8542	7.098
replicate	*0.210*	*0.865*	*0.679*	*0.036*	*0.066*	*0.8973*	7.456
replicate	*0.233*	*0.727*	*0.643*	*0.042*	*0.072*	*0.8296*	6.894
39-40cm	0.414	1.076	0.873	0.059	0.085	0.7263	6.035

Core 316	Ru ppb	Pd ppb	Pt ppb	Ir ppb	Os ppb	$^{187}Os/^{188}Os$	$^{187}Os/^{186}Os$
0-1cm	5.038	1.597	0.891	0.032	0.141	1.0387	8.631
replicate	*0.669*	*1.700*	*6.541*	*0.440*	*0.315*	*0.5032*	4.181
2-3cm	0.357	1.624	0.958	0.040	0.147	0.9537	7.925
6-7cm	0.296	1.582	0.998	0.038	0.132	1.0078	8.374
20-21cm	0.688	1.681	1.184	0.221	0.265	0.5110	4.246
22-23cm	0.508	1.472	0.901	0.410	0.544	0.2719	2.259
25-26cm	0.142	1.163	0.663	0.032	0.074	0.9676	8.040

Core 325	Ru ppb	Pd ppb	Pt ppb	Ir ppb	Os ppb	$^{187}Os/^{188}Os$	$^{187}Os/^{186}Os$
0-1cm	0.372	1.442	0.851	0.030	0.142	1.0450	8.683
2-3cm	0.349	1.774	1.069	0.037	0.154	1.0390	8.632
8-9cm	0.365	1.856	1.106	0.064	0.163	1.0420	8.661
12-13cm	0.271	1.766	1.076	0.034	0.145	1.0678	8.873
16-17cm	0.280	1.785	1.040	0.036	0.141	1.0701	8.891

Core 329	Ru ppb	Pd ppb	Pt ppb	Ir ppb	Os ppb	$^{187}Os/^{188}Os$	$^{187}Os/^{186}Os$
0-1cm	0.353	1.583	0.961	0.033	0.157	1.0614	8.820
2-3cm	0.325	1.834	1.148	0.037	0.164	1.0600	8.807
4-5cm	0.275	1.889	1.246	0.038	0.165	1.0576	8.788
12-13cm	5.871	2.092	1.208	0.034	0.174	1.0578	8.790
16-17cm	0.571	1.861	1.138	0.037	0.147	1.0690	8.882

	Ru ppb	Pd ppb	Pt ppb	Ir ppb	Os ppb	$^{187}Os/^{188}Os$	$^{187}Os/^{186}Os$
343 Serpen	2.174	7.241	3.057	1.754	1.272	0.1255	1.042
316am-1	2.916	0.887	5.675	1.122	0.442	0.2791	2.319
316am-2	4.072	1.425	4.188	1.866	1.588	0.1635	1.359

Core 23#12	Ru ppb	Pd ppb	Pt ppb	Ir ppb	Os ppb	$^{187}Os/^{188}Os$	$^{187}Os/^{186}Os$
1-2cm	n.d.	0.824	0.051	0.030	-	-	-
6-7cm	n.d.	0.744	0.168	0.022	0.057	1.0185	8.463
replicate	n.d.	*0.835*	*0.109*	*0.016*	-	-	-
10-11cm	n.d.	0.668	0.074	0.020	0.040	1.0728	8.914
replicate	n.d.	*0.825*	*0.069*	*0.017*	-	-	-
14-15cm	n.d.	0.821	0.050	0.017	-	-	-
20-21cm	n.d.	0.601	0.045	0.018	0.033	1.0696	8.887
25-26cm	n.d.	0.652	0.066	0.022	0.037	0.9867	8.199
replicate	n.d.	*0.749*	*0.051*	*0.021*	-	-	-

Hydrothermal contribution of PGEs to core samples

	Bulk sed	hy Os	hy Pt	hy Pd	hy Ir
Core 343	$g.cm^{-2}.ky^{-1}$	ng/g	ng/g	ng/g	ng/g
1-2cm	1.91	0.152	0.966	1.245	0.041
2-3cm	1.97	0.149	1.113	1.347	0.057
4-5cm	1.98	0.141	0.904	1.302	0.063
16-17cm	2.10	0.135	1.258	1.463	0.050
Core 316					
0-1cm	1.81	0.130	0.891	1.597	0.032
6-7cm	1.95	0.122	0.998	1.582	0.038
Core 325					
0-1cm	1.48	0.132	0.851	1.442	0.030
2-3cm	1.70	0.143	1.069	1.774	0.037
8-9cm	1.74	0.152	1.106	1.856	0.064
12-13cm	1.94	0.134	1.076	1.766	0.034
16-17cm	2.44	0.129	1.040	1.785	0.036
Core 329					
0-1cm	2.32	0.143	0.961	1.583	0.033
2-3cm	2.39	0.151	1.148	1.834	0.037
8-9cm	2.89	0.151	1.246	1.889	0.038
12-13cm	2.58	0.157	1.208	2.092	0.034
16-17cm	3.06	0.133	1.138	1.861	0.037